1. Report No. 1303-F	2. Government Accession No.	3. Recipient's Catalog No.
4. Title and Subtitle Wind Load Effects on Signs, Luminaires, and Traffic Signal Structures		5. Report Date February 1995
		6. Performing Organization Code
7. Author(s) J.R. McDonald, K.C. Mehta, W. Oler and N. Pulipaka		8. Performing Organization Report No.
9. Performing Organization Name and Address Wind Engineering Research Center Texas Tech University Box 41023 Lubbock, TX 79409-1023		10. Work Unit No.
		11. Contract or Grant No. 11-5-92-1303
12. Sponsoring Agency Name and Address Texas Dept. of Transportation P.O. Box 5080 Austin, TX 78763-5080		13. Type of Report and Period Covered Final; 9/1/91 through 8/31/94
		14. Sponsoring Agency Code

15. Supplementary Notes

16. Abstract

The objectives of this study were: (1) to revise the wind load section of the TxDOT standard for highway signs, luminaires and traffic signal structures, and (2) to develop strategies to mitigate large vibrations in single-mast traffic signal structures subject to cross-wind vibrations. The first objective was accomplished by developing a new design wind speed map for the State of Texas. State-of-knowledge wind engineering technology is incorporated in the revised design standard. A better understanding of the cross-wind vibration problem, which takes place in steady winds in the range of 5 to 15 m/s, was obtained by conducting water table, tow tank and field studies. The vibrations are attributed to a galloping phenomenon, which primarily takes place when the wind is blowing normal to the mast arm from the back side of a traffic signal with backing plate. The most effective mitigation measure was found to be a horizontal wing attached above the signal light. TxDOT maintenance personnel should install a wing when mast arm tip vibrations exceed 40 cm.

17. Key Words wind, signs, traffic signals, standard, vibrations, wind speed, wind loads	18. Distribution Statement No restrictions.

19. Security Classif. (of this report) Unclassified	20. Security Classif. (of this page) Unclassified	21. No. of Pages 182	22. Price

Form DOT F 1700.7 (8-69)

WIND LOAD EFFECTS ON SIGNS, LUMINAIRES AND TRAFFIC SIGNAL STRUCTURES

by

James R. McDonald, Ph.D., P.E.
Kishor C. Mehta, Ph.D., P.E.
Walter W. Oler, Ph.D.
Narendra Pulipaka, R.A.

Report 1303-1F
Research Study 11-5-92-1303

Prepared for

Texas Department of Transportation
Austin, Texas

July 1995

Wind Engineering Research Center
Texas Tech University
Lubbock, Texas

The contents of this report reflect the views of the authors who are responsible for the facts and accuracy of the data presented herein. The contents do not necessarily reflect the official views or policies of the Federal Highway Administration or the Texas Department of Transportation. This report does not constitute a standard, specification, or regulation.

There was no invention or discovery conceived or first actually reduced to practice in the course of or under this contract, including any art, method, process, machine, manufacture, design or composition of matter, or any new and useful improvement thereof, or any variety of plant which is or may be patentable under the patent laws of the United States of America or any foreign country.

FOREWORD

The primary purposes of this study were to prepare revisions to the wind load section of the Texas Department of Transportation standard for design of signs, luminaires and traffic signal structures, and to develop strategies for mitigating certain large amplitude vibrations in single mast arm traffic signal structures. This final report documents the methodologies, assumptions, data, conclusions and recommendations for implementing the research results.

TABLE OF CONTENTS

TABLE OF CONTENTS (Continued)

LIST OF TABLES

LIST OF FIGURES

1. INTRODUCTION

Highway signs, luminaires, and traffic signal structures are exposed to a varied wind environment. When high winds occur in the form of tornadoes, hurricanes or other extreme winds, these structures are subjected to large wind loads. In addition, steady winds of 10 to 30 mph (4.5-1.34 m/s) may induce vibrations, large amplitude deflections and fatigue loadings.

Over the past twenty-five years, wind loading research has developed and matured to the point that practical applications can be achieved. The current standard specifications for design of structural supports for highway signs, luminaires, and traffic signal structures are published by the American Association of State Highways and Transportation Officials (AASHTO, 1985). The document is based on 17-year old wind technology. New technology is available today that is not reflected in the current AASHTO Standard. The gust response factor (GRF) approach would be an improvement over the current AASHTO Standard, because it accounts for spatial and time variation of wind gusts. Modern wind load standards also account for a variety of terrain roughnesses, which affect the wind flow.

Under certain conditions of wind speed and wind direction, some cantilevered traffic signal structures undergo large amplitude vibrations in wind speeds of 10 to 30 mph (4.5-13.4 m/s). These large amplitude vibrations deflections may lead to fatigue failures, in addition to being a distraction to passing motorists. One structure failed during the course of this study. A 48-ft (14.6-m) cantilever traffic signal structure failed in Dalhart, TX in November 1991. The cantilever arm fell to the ground when a crack developed at the connection between the horizontal arm and the vertical pole. Fortunately, no one was injured by the collapse.

1.1 Objectives and Scope

This project has two primary objectives:

(1)   to revise the wind load section of the TxDOT standard for highway signs, luminaires and traffic signal structures, and

(2)   to develop strategies to mitigate vibrations in single-mast traffic signal structures.

1

The first objective included revising design wind speeds for the State of Texas and incorporating state-of-knowledge wind engineering into the design standard. The second objective is accomplished by seeking a better understanding of wind-structure phenomena through a sequence of analytical studies, laboratory and field tests. Once the phenomena was understood, strategies for vibration mitigation were developed and tested in the field.

The scope of the field studies were limited to behavior of cantilever traffic signal structures. Highway signs and luminaires were not studied, because problems of wind-induced vibration are not perceived to be as great as those with the signal light structures.

1.2 Wind Effects on Traffic Signal Structures

Long cylindrical structures of circular, square or any other bluff cross-section may exhibit wind induced bending oscillations in a plane normal to the wind. Neglecting the effects of wind gusts and the wakes of other bodies, this behavior can be attributed to one of two aerodynamic mechanisms (Scruton, 1963): vortex shedding or galloping.

Vortex shedding in the wake behind a quasi two-dimensional object is the periodic formation of vorticity with alternating rotational directions caused by shear layers on opposite sides of the object. A wake which exhibits the generation and downstream convection of the alternating vortices is referred to as a von Karman vortex street. The formation of the wake vortices with axes approximately parallel to the axis of the body is a consequence of the inherent instability of a symmetric shear stress distribution in the wake. Although the coherence of the vortex street can be enhanced by synchronous motions, body motion is not necessary for the generation of the vortices. The frequency of vortex shedding is dependent primarily upon the cross-stream dimension of the body and the free stream velocity. There is also a secondary dependence on the viscosity of the fluid which can be characterized by Reynolds number of flow. The degree of coherence, periodicity, and two-dimensionality of the wake vortices depends on the aspect ratio of the body, the mean flow Reynolds number, and the background turbulence in the free stream flow. As a bluff body sheds vortices, the pressure on each side of the object is alternately reduced and increased. The result is a periodic forcing function normal to the freestream which can excite

2

motion of the body, particularly if the structure has a resonant frequency close to the vortex shedding frequency. These periodic forces associated with the vortex street are small relative to the mean drag forces.

Galloping occurs when the periodic vibrational motion of a structure normal to the freestream results in the generation of a periodic angle of attack of the relative vector with the corresponding generation of transverse aerodynamic forces in the same direction and frequency as the structural motion. Since the aerodynamic forces which sustain galloping are a direct result of structure motion, galloping requires an initial disturbance which can be caused by wake effects, wind gusts, or vortex shedding. For a given wind speed, the structural damping balances the aerodynamic excitation and limits the amplitude of the motion. Therefore, the galloping of an adequately damped structure in steady winds, is characterized by an oscillation that matches the natural frequency of the structure and is amplitude limited.

1.2.1 Vortex Shedding

The vortex shedding frequency is characterized by the non-dimensional Strouhal number

$$S_t = (fD)/V \tag{1.1}$$

where f is the shedding frequency of one complete pattern of wake vortices, D is the cross stream dimension of the object, and V is the freestream velocity. Figure 1.1 depicts Walshe and Wooten's (1970) summary of the variation of Strouhal number with Reynolds number for a stationary cylinder of circular cross-section. Over a large range of relatively low Reynolds numbers, two-dimensional wakes exhibit regular vortex shedding at an almost constant Strouhal number approximately equal to 0.2 At intermediate Reynolds numbers near 1×10^6, the vortex shedding process becomes random and irregular and occurs at a higher Strouhal number. At higher Reynolds numbers, the vortex shedding becomes regular again but the characteristic Strouhal number is slightly higher (approximately 0.27) than the low Reynolds number regime. These low, intermediate, and high Reynolds number regimes are referred to as the subcritical, critical or transcritical, and supercritical regimes, respectively.
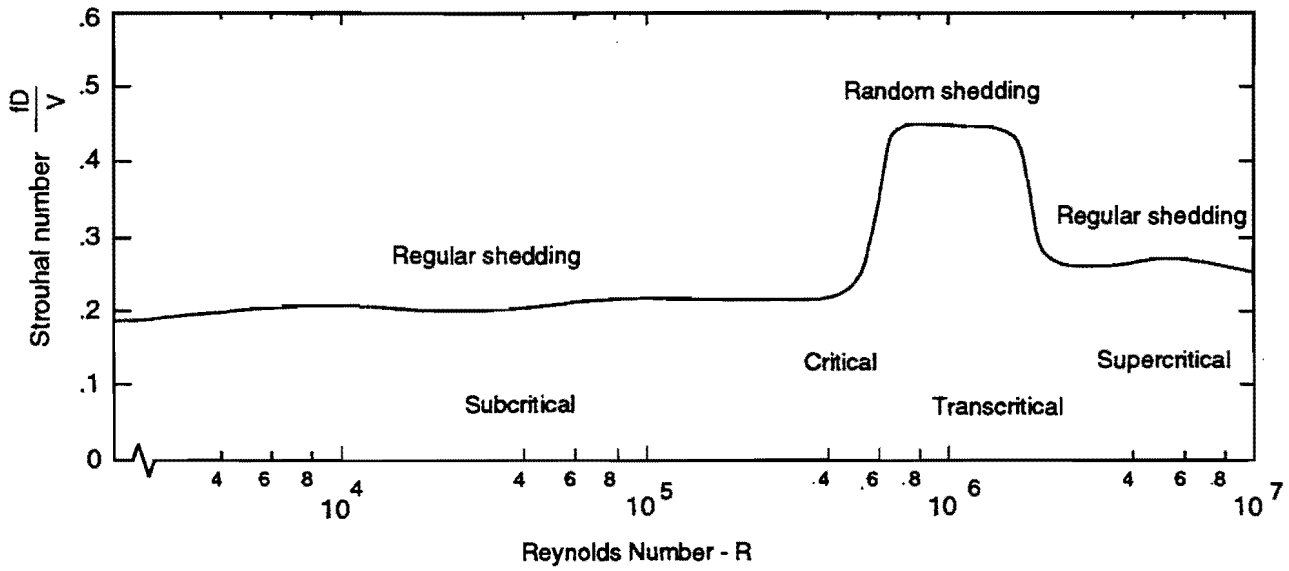
FIGURE 1.1. VARIATION OF STROUHAL NUMBER WITH REYNOLDS NUMBER (Walshe and Wooten, 1970)

Scruton (1963) dealt with practical methods of reducing wind effects on structures and tall stacks. In general, the effects of vortex excitation can be suppressed by reducing the periodicity of vortex formation or by reducing the spanwise cohesiveness of the flow, i.e., forcing the flow to be three-dimensional. Examples of devices meant to accomplish this goal are a perforated cylinder mounted outside a plain cylinder (Price 1956), triangular spoilers on a suspended pipe-line (Baird 1955), and helical strakes on vertical stacks, suggested by Scruton and Walshe (1957) for which Woodgate and Meybrey (1959) determined the optimal configuration.

Roshko (1955) studied flow past a circular cylinder at high Reynolds number. For Reynolds numbers from 3×10^6 to 1×10^7 regular vortex shedding from a simple cylinder occurred at a Strouhal number (S_t) of 0.27. Figure 1.1 depicts this result as the supercritical region where regular shedding has resumed. Roshko also noted that a splitter plate attached to the trailing edge of a circular cylinder tended to suppress the vortex shedding. It is possible that the splitter plate allows the flow to remain more nearly attached to the cylinder much in the same way that the trailing portions of an airfoil aid it in maintaining attached flow.

Achenbach and Heinecke (1981) evaluated the influence of surface roughness on the vortex-shedding frequency of circular cylinders in the Reynolds number regime of : $6 \times 10^3 < R < 5 \times 10^6$. Cylinder roughness was observed to delay the onset of the critical flow regime where vortex shedding becomes irregular. In addition, surface roughness reduced the Strouhal number in the critical flow regime. In the subcritical region the Strouhal number was nearly constant at $S_t = 0.205$, which is approximately equivalent to the smooth cylinder results. Therefore, variations in surface roughness cause a measurable, but not significant, variation from the general cylinder depicted in Figure 1.1.

Jones et al. (1969) studied the effect of forcing a circular cylinder to oscillate normal to the flow over a range of frequencies and amplitudes:

$$0.06 \leq (f_h D)/V \leq 0.5$$
$$0.014 \leq (h_o)/D \leq 0.083$$

In their nomenclature, f_h is the forcing frequency, h_o is the amplitude of the forced oscillation, D is the previously defined characteristic diameter, and V is the flow velocity. The results are summarized by them as follows:

> Oscillation of the cylinder in the lift direction has no significant effect on the mean drag coefficient. An unsteady lift due to cylinder motion, which increases with amplitude of motion, exists only when the cylinder is oscillated at or relatively near the aerodynamic Strouhal frequency for the stationary cylinder. This lift is a negative (destabilizing) aerodynamic damping force at cylinder frequencies below the stationary-cylinder Strouhal frequency. As the cylinder frequency is increased through and above the Strouhal frequency, there is an abrupt change to a positive (stabilizing) aerodynamic damping force.

In other words, cylinder motion does not significantly change the Strouhal frequency but tends to amplify the forces associated with vortex shedding and to facilitate a convergence of the cylinder's frequency of oscillation with the vortex shedding frequency for a given wind velocity. The resonance effects are strongest in a small bandwidth around the stationary Strouhal number with the greatest amplification of lift occurring when the ratio of forced frequency to Strouhal number is 0.99. Therefore, it can be concluded that an unconstrained cylinder will tend to experience vortex related aerodynamic forces at the same frequency as the stationary Strouhal frequency.

Szepessy and Bearman (1992) investigated the effect of using end plates on circular cylinders. By varying the ratio of cylinder span length between end plates (open length) to cylinder diameter, three-dimensional effects were controlled in an effort to observe their effect on fluctuating lift, drag and shedding frequency. At low open length ratios, the end plates effectively restricted cross-flows resulting in two-dimensional behavior whereas with high open length ratios, cylinders were subject to random three-dimensional flow.

Szepessy and Bearman observed that lower shedding frequencies were associated with an increased fluctuating lift. It is probable that the entire cylinder span was contributing to two-dimensional vortex shedding resulting in the lowest observed frequencies and largest observed forces. In contrast, three-dimensional flow along the span seemed to trigger more frequent but less

6

energetic vortex shedding. Even so, the minimum and maximum observed variation in Strouhal number were as follows:

$$S_t = 0.17 \qquad \text{at } R = 4.5 \text{x} 10^4 \text{ and } L/D = 1.0$$

$$S_t = 0.19 \qquad \text{at } R = 4.5 \text{x} 10^4 \text{ and } L/D = 6.7$$

Therefore, the variation in flow along a cylinder length does not have a significant effect on shedding frequency. Likewise, the three-dimensional flow that can be expected in a less controlled environment is not a significant factor when predicting the Strouhal number for a structure.

In addition to experiments on circular cross-sections, many researchers have published results for square or rectangular sections. Okajima (1982) obtained the Strouhal number for rectangular cylinders with side-to-height ratios (b/h) of 1.0 to 4.0 over a range of subcritical Reynolds numbers. For the square cylinder (b/h = 1.0), the Strouhal number was approximately constant at 0.13 for Reynolds numbers of $1 \text{x} 10^2$ to $2 \text{x} 10^4$. For rectangular cylinders (b/h of 2.0 and 3.0), Okajima observed a transitional Reynolds number where the flow separated at the leading edges with periodic reattachment on the lower or upper surfaces synchronized with the vortex shedding. At lower Reynolds numbers, the flow separated at the leading edges and did not reattach; at higher Reynolds numbers, the flow continuously reattached. The corresponding Strouhal numbers varied from 0.13 for the fully separated flow to 0.17 with the fully attached flow.

From the preceding discussion, it can be concluded that vortex shedding at subcritical Reynolds numbers occur at Strouhal numbers between 0.13 and 0.22. This range of Strouhal numbers encompasses the effects of cylinder cross-section shape, surface roughness, free-stream turbulence, and Reynolds number. The applicability of this observation to traffic light structures is reinforced by the observations in this study, where a Strouhal numbers for shapes characteristic of traffic signal lights were found to be in the range given above.

From this knowledge, the lock-in wind speed V_l at which the natural frequency of a traffic signal structure is in resonance with the excitation of vortex shedding can be computed from

$$V_l = (f_n D)/S_t \qquad\qquad (1.2)$$

Assuming that the natural frequency of the structure f_n is between 0.8 and 1.2 H_z and that the cross-stream dimension of the traffic light D is between 1.0 and 2.5 ft (30 and 76 cm), the corresponding range of expected lock-in wind speeds from Equation 1.2 is summarized in Table 1.1.

From the tabulated values, it is apparent that the maximum wind speed at which lock-in can occur is approximately 16 mph which occurs for the largest traffic light heads. For smaller heads of 1.0 ft (30 cm), the maximum lock-in wind speed is 6.3 mph (2.8 m/s). Since traffic signal vibrations have been observed at higher wind speeds, it follows that the source of the excitation force must be from some mechanism other than vortex shedding.

1.2.2 Galloping Oscillations

Den Hartog (1932) recognized that certain cross-sectional shapes exhibit galloping oscillations at near constant frequency over a wide range of wind speeds with oscillation amplitudes that increase as a function of wind speed. Simple vortex shedding could not account for this observed behavior. His study of that date dealt with transmission lines with non-circular cross-sections due to ice accumulation. Circular cross-sections do not develop steady lateral forces perpendicular to the freestream because of the symmetry at all angles of attack. However, non-circular shapes produce aerodynamic forces that are a function of angle of attack. Unlike the oscillations of circular cylinders which occur only in resonance with the periodic shedding of wake vortices, sections meeting the Den Hartog (1956) criterion exhibit a pure plunging motion perpendicular to the freestream at an amplitude that increases with wind speed. A cross-section meets this criterion if

$$(dC_{Fy})/d\alpha < 0 \qquad (1.3)$$

where y is perpendicular to the freestream and C_{FY} is the coefficient of aerodynamic force in that direction.

As illustrated in Figure 1.2, a square is an example of a cross-section which exhibits this behavior for $\alpha < 14$ degrees. Consider an initial disturbance of the cylinder which results in a

TABLE 1.1

BOUNDING VALUES OF LOCK-IN WIND SPEEDS
FOR TRAFFIC SIGNALS*

f_n (Hz)	D (ft)	S_t	V_1 (mph)
0.8	1.0	0.22	2.5
1.2	1.0	0.22	3.7
0.8	2.5	0.22	6.2
1.2	2.5	0.22	9.3
0.8	1.0	0.13	4.2
1.2	1.0	0.13	6.3
0.8	2.5	0.13	10.5
1.2	2.5	0.13	15.7

*Equation 1.2

1.0 ft = 30 cm

1.0 mph = 0.45 m/s

Angle of Attack α - Degrees
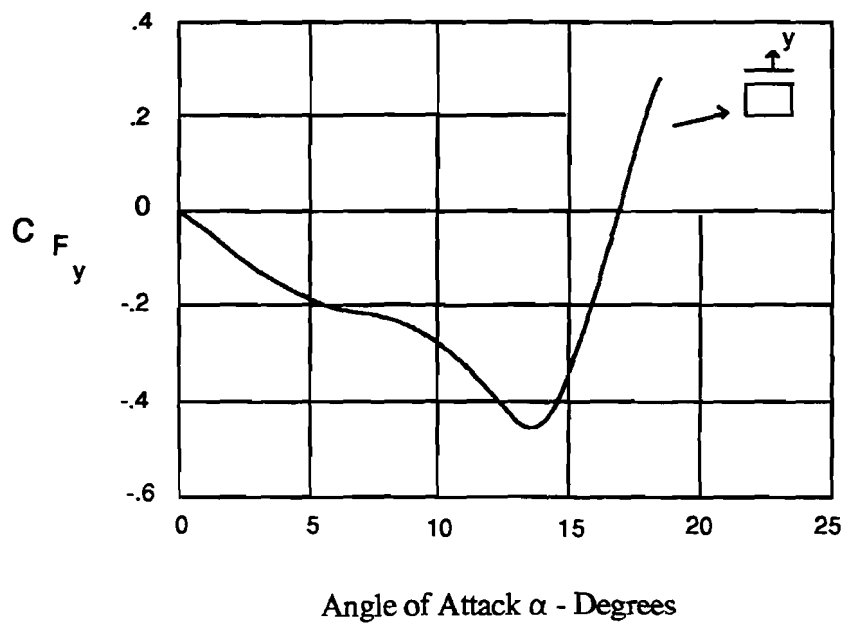
FIGURE 1.2. COEFFICIENT OF FORCE IN THE
Y-DIRECTION FOR A SQUARE SHAPE

10

downward motion or motion in the negative y direction. As a result of the cylinder motion, the relative velocity between the fluid and cylinder includes a cross-stream component giving a positive angle of attack. From Figure 1.2, it is noted that the aerodynamic force on the cylinder at a positive angle of attack is negative and most importantly, in the same direction as the cylinder motion. This characteristic is referred to as negative aerodynamic damping. As the structural stiffness decelerates the initial downward motion, the angle of attack and aerodynamic force return to zero. The deflected structure begins to move back towards neutral and an angle of attack opposite to the first is induced. Because the aerodynamic force is aligned with the motion, the structure will overshoot the neutral position and the motion will continue in a self-perpetuating manner. The extremes in angle of attack increase as vibration amplitude and translational velocity increase. The corresponding aerodynamic forces increase as well until the angle of attack exceeds approximately 15 degrees. At higher angles of attack the aerodynamic forces become stabilizing. Therefore, the amplitudes of galloping motions will be limited to the negatively damped angles of attack. Furthermore, the limit amplitude increases as the free-stream velocity increases.

Satisfaction of the Den Hartog criteria and exhibition of galloping behavior does not occur for all cylinder cross-sectional shapes. For example, a circular cylinder experiences a pure drag with respect to the relative velocity vector. Consequently, the transverse force is positive for positive angles of attack and is always in the opposite direction of the cylinder motion, thereby providing positive aerodynamic damping. Similarly, a symmetrical airfoil produces a lift force with respect to the relative velocity vector that is also positive for positive angles of attack. Any deviation from the statically neutral position always results in an aerodynamic force opposite to the disturbed motion.

Parkinson and Brooks (1961) presented a nonlinear analytical model using aerodynamic coefficients derived from Figure 1.2 to explain the galloping motion of cylinders. They refer to their model as "quasisteady" because of the assumption that steady-state aerodynamic data can be applied to a dynamic equation of motion. They start with the following general equation of motion:

$$m\ddot{y} + c\dot{y} + ky = F_y \tag{1.4}$$

where m , c, and k are constants characteristic of the structure, and

$$F_y = C_{Fy}\, 1/2\, \rho V^2 hs \tag{1.5}$$

where h and s are the cylinder height and span, respectively. Normal aerodynamic data for a section consists of lift and drag components or the aerodynamic force resolved into components parallel and perpendicular to the relative velocity vector. For application to galloping cylinders, the transverse force relative to the free-stream direction is required. This can be obtained from the standard lift and drag data using

$$C_{Fy} = C_L \cos\alpha + C_D \sin\alpha \tag{1.6}$$

where

$$\alpha = \tan^{-1}(-\dot{y}/V) \tag{1.7}$$

The experimental curves of C_L and C_D versus α are then approximated by polynomials and after some tedious manipulations, an analytical solution can be achieved that contains the galloping behavior.

In Parkinson and Brook's experiment, models of spring-mounted cylinders began plunging when resonance existed between the system's natural frequency and the stationary vortex-shedding frequency of the cylinder. Then, as predicted by their theory of galloping, sections which satisfied the Den Hartog criteria would oscillate at velocity dependent limit amplitudes. Parkinson & Smith (1962) improved the accuracy of the analytical model by using higher order polynomials to more closely approximate the aerodynamic coefficients of a square section. Parkinson & Wawjonek (1981) noted that the quasisteady theory of galloping did not adequately describe experimental results for cylinders at velocities near to the vortex shedding lock-in velocity. A nonlinear theoretical explanation of the interaction between vortex shedding and incipient galloping was presented by Obasaju (1983).

Whereas Parkinson and Wawjonek investigated the free vibration of cylinders in which only amplitudes were measured, Obasaju used a forced-vibration study of a square cylinder to determine the dependence of the mass-damping parameter on amplitude ratio and reduced velocity,

$$(2\varsigma M)/\rho D^2 L = f (A/D, V/f_F D)\qquad\qquad(1.8)$$

where the reduced velocity is noted to be equivalent to the inverse of the Strouhal number. He determined that the reduced velocity where vortex shedding is amplified by the cylinder's motion occurs at 7.7. As expected, the inverse of this number corresponds to the Strouhal number for a square or 0.13. In addition, Obasaju found that the band of resonance effects is broadened by an increase in amplitude. As detailed by Bearman and Obasaju (1982), the vortex lock-in region was

$$7.0 \leq V/ f D \leq 8.0 \quad \text{for } A/D = 0.05,$$

$$6.9 \leq V/ f D \leq 8.7 \quad \text{for } A/D = 0.10,$$

$$\text{and} \quad 5.5 \leq V/ f D \leq 12 \quad \text{for } A/D = 0.25.$$

All of these results are similar to those of Jones et al. (1969) for a circular cylinder. Furthermore, Obasaju linearized the forcing function used in the quasisteady theory of galloping by making an assumption of small amplitude oscillations, and compared the resulting behavior to that predicted by vortex shedding alone. He concluded that near the resonant reduced velocity, a spring-mounted cylinder can perform either a high amplitude oscillation at the vortex shedding frequency or small-amplitude galloping. Furthermore, for certain mass-damping parameters, this response can continue somewhat above the resonant velocity. Finally, although galloping is never observed below the resonant velocity for vortex shedding, the quasisteady theory of galloping by itself fails to make this prediction. In Parkinson and Brooks' (1961) non-linear quasisteady theory, the minimum speed for galloping onset is a function of structural damping and negative aerodynamic damping but doesn't take into account the critical or lock-in velocity due to vortex shedding. Therefore, an advantage of incorporating Obasaju's forced-vibration results is that it correctly predicts that galloping cannot occur below vortex resonance. Also, the seemingly chaotic behavior

of cylinders having an incipient galloping velocity greater than but <u>very</u> near to the vortex lock-in velocity is explained.

Novak (1969, 1972) has provided the most mathematically detailed and comprehensive development of the quasisteady theory of galloping. Using early theoretical and experimental results as a foundation, he has successfully provided a rigorous and complete description of the quasisteady theory of galloping. With the exception of Obasaju's more recent linearization refinement, Novak's theoretical development parallels and is inclusive of all published work and at the same time more detailed. Even more refined are his closed-form equations generalized for any aerodynamic cross-section and many degrees of freedom.

1.2.3 Conclusion

Although vortex shedding is a factor in the oscillations of traffic signals at low wind speeds and as the excitation mechanism for galloping, it is the theory of quasisteady galloping which best explains their behavior in a wide range of winds. The nonlinear nature of the aerodynamic forces on most shapes results in a limit to the amplitude of galloping oscillation at a given wind speed. However, as velocity increases, so does the limit-amplitude until in the instance of the square at $\alpha \approx 15$ degrees, the aerodynamic forces resulting from displacement become stabilizing.

1.3   Research Plan

A research plan was developed to attain the objectives of the project as outlined in Section 1.1. The plan for this comprehensive research project was divided into four phases to provide a logical sequence of work. The phases were as follows:

Phase 1:	Literature search, revisions of design wind speeds in State of Texas, and planning of experimental studies
Phase II:	Update of wind load specifications and laboratory experiments
Phase III:	Full-scale experiments at the Texas Tech field site
Phase IV:	Coalescence of results and final report.

Phase I: Literature, Wind Speeds and Planning

The work in this phase involved assembly of previously published work on the subject and analysis of existing wind data to obtain updated design wind speeds for the State of Texas. In addition, after reviewing the literature, plans were formulated for the experimental research in the laboratory.

The literature search concentrated in two areas: (1) wind effects on highway signs, luminaires and traffic signal structures, (2) analysis and testing of traffic signal structures. Wind effects on structures involve research related to wind speed, direction, and gustiness of the wind structural dynamics, aerodynamics, fatigue loading and extreme value wind loading. A very limited number of publications are available on analysis and testing of traffic signal structures subjected to wind loads.

Wind engineering has evolved over the last thirty years into a mature discipline of research and application. During this period there have been eight international conferences and seven U.S. National Conferences on wind engineering research. A number of prestigious journals report the efforts of researches around the world. Data bases were searched specifically to find wind effects related to highway structures.

Data bases available to Texas Tech University and TxDOT were searched for publications on analysis and testing of traffic signal structures. In addition to published literature, the search turned up video tapes of traffic signal structures responding to wind. Incidents of wind damage from both extreme winds and steady winds were sought in the search.

The American Society of Civil Engineers standard, *Minimum Design Loads for Buildings and Other Structures,* ASCE 7-88, gives a design wind speed map that is used in the current wind standard in Texas (AASHTO, 1985). The ASCE 7-88 map was assembled in 1978 using data collected at only nine weather stations within the State of Texas (Mehta, 1988). Since 1978, there are ten or more additional years of wind speed records. Also, there are a total of 52 stations that possibly have records suitable for a wind speed hazard assessment in the State. When the data was

evaluated for quality and consistency, the number of useable stations in the state was reduced to 26.

As the literature survey progressed, plans were formulated for conducting the laboratory experiments. Two phenomena appeared to be the potential course of the large amplitude vibration of cantilevered signal structures: vortex shedding and galloping. Wind tunnel studies, although possible, were eliminated from consideration because of problems with scaling the structures and Reynolds numbers in the fluid flow.

Plans were developed for using a water table to study the vortex shedding phenomena. The approach appealed to the researchers because vortex shedding is a 2-dimensional process. The Texas Tech University tow tank was used to study the galloping phenomena. The advantages of the tow tank greatly outweighed the use of a wind tunnel. The tow tank accommodated full-scale sections of signal arms and traffic lights. Use of water instead of air as the flow medium permitted flow velocities 10 times smaller than air. The relatively slow velocities [1-5 mph (0.4-2.2 m/s)] enhanced flow visualization by the use of a red dye. Use of the tow tank allowed us to measure forces on the signal structure produced by galloping. Results from the water table and tow tank experiments lead to a clear understanding of the aerodynamic phenomena affecting the structure. Design of the field experiments were based on these results. The field research plans developed in this phase of the project are described in Section 8.

Phase II: Specification Update and Laboratory Studies

The work in this phase, which extended over the first two years, consisted of two tasks: (1) updating wind load specifications, and (2) conducting laboratory experiments.

The current specifications for structural supports for highway signs, luminaires and traffic signal structures use a gust factor (GF) approach to determine wind pressures. The ASCE 7-88 standard specifies wind loading criteria using a gust response factor (GRF) approach (ASCE, 1990). The GF approach of AASHTO assumes that peak wind loads are directly proportional to peak gusts. In reality, this assumption is not valid, because peak wind load effects depend on both time and spatial variation of wind gusts. The GRF approach is based on response of structures to

wind gustiness, thus taking into account variations in wind gusts, as well as structure size and flexibility. The GRF approach gives more realistic wind loads.

The ASCE 7-88 approach also recognizes velocity pressure exposure coefficients for open, suburban, and urban terrain. The force (drag) coefficient values for various structure shapes remain the same, since better values are not available in the literature.

The laboratory studies were conducted to obtain a better understanding of the vortex shedding and galloping phenomena. A water table was used for the vortex shedding studies, since the fluid flow is two-dimensional. The galloping phenomenon was studied in the tow tank, because the flow is essentially three-dimensional. Full-size signal arm and traffic signal heads were used in the tow-tank experiments.

Phase III: Field Studies

The third phase of the project involved experiments in the field on full-size traffic signal structures. The water table and tow tank studies confirmed that galloping was the cause of large amplitude vibrations. The field studies were designed to (1) reproduce the galloping phenomena, and (2) to explore various concepts for mitigating the vibrations. From observations of the galloping, it was clear that the phenomena is very sensitive to wind direction. For this reason, we developed a foundation structure that allowed the signal structure to be rotated. The challenge to the design was to have the ability to rotate and yet have the same stiffness and rigidity as a normal installation. Tests, which are described later, were conducted to verify the similarity of the rotatable structure and standard installation.

The full-scale tests were conducted at the WERFL because the wind measuring instrumentation and data acquisition system were in place. Two different signal structures were tested. The first was one readily available early in the study. The second one represents the nominal upper limit [48 ft (14.6 m) cantilevered arm] used in Texas. The larger structure was expected to be more susceptible to the galloping phenomenon.

17

A series of tests were designed to measure the response of the two structures to various conditions of signal light arrangements and mitigation measures. The structures were tested bare, with signal lights in place and with devices designed to mitigate the vibration.

Phase IV: Coalescence of Results

This phase of the project pulls everything together to reach final conclusions and recommendations. Results of literature surveys, analytical studies, laboratory tests and the field tests play a role in the final conclusion.

2. WIND HAZARD ASSESSMENT

As part of the update of the wind load specifications for highway signs, luminaries, and traffic signal structures (AASHTO, 1985), a new design wind speed map was developed for the State of Texas. This section describes the assumptions, data and methodology used in developing the new map.

The design wind speeds map in the current AASHTO Specification (1985) for Texas is taken from the ASCE 7-88 design load standard (ASCE, 1990). The ASCE 7-88 map was developed in 1981 and first appeared in the ANSI A58.1-1982 design standard (ANSI, 1982), which was the predecessor to ASCE 7. Shown in Figure 2.1, the map presents wind speed contours for a 50-year mean recurrence interval. Figure 2.2 is a blowup of the contours for Texas. The wind speeds are expressed in terms of fastest mile winds at 33 feet (10 m) above ground in flat, open terrain.

Different methods were used to obtain the wind speed contours in Figure 2.1 at inland and coastal locations. The probability distributions of wind speeds away from the coast are based on records measured at weather stations around the state. Hurricane winds dominate the wind risks near the coastline, but the periods of records at coastal weather stations are not long enough to accurately reflect hurricane probabilities. To overcome this problem, the ASCE 7 Standard relies on Monte Carlo simulations to generate hurricane records near the coastline. A study by Batts et al. (1980) generated sufficient hurricane data to establish hurricane wind speed probability distributions analogous to those obtained at inland stations. The influence of hurricane winds diminishes as the storms move inland. At about 100 miles (160 km) from the coastline, the hurricane winds have little influence compared to straight wide.

A new design wind speed map was developed for inland locations in this study for the following reasons:

(1)   Availability of 11 additional years of wind speed data

(2)   Quality data from 26 weather stations in the state, as opposed to nine stations used for the ASCE 7 map.

19
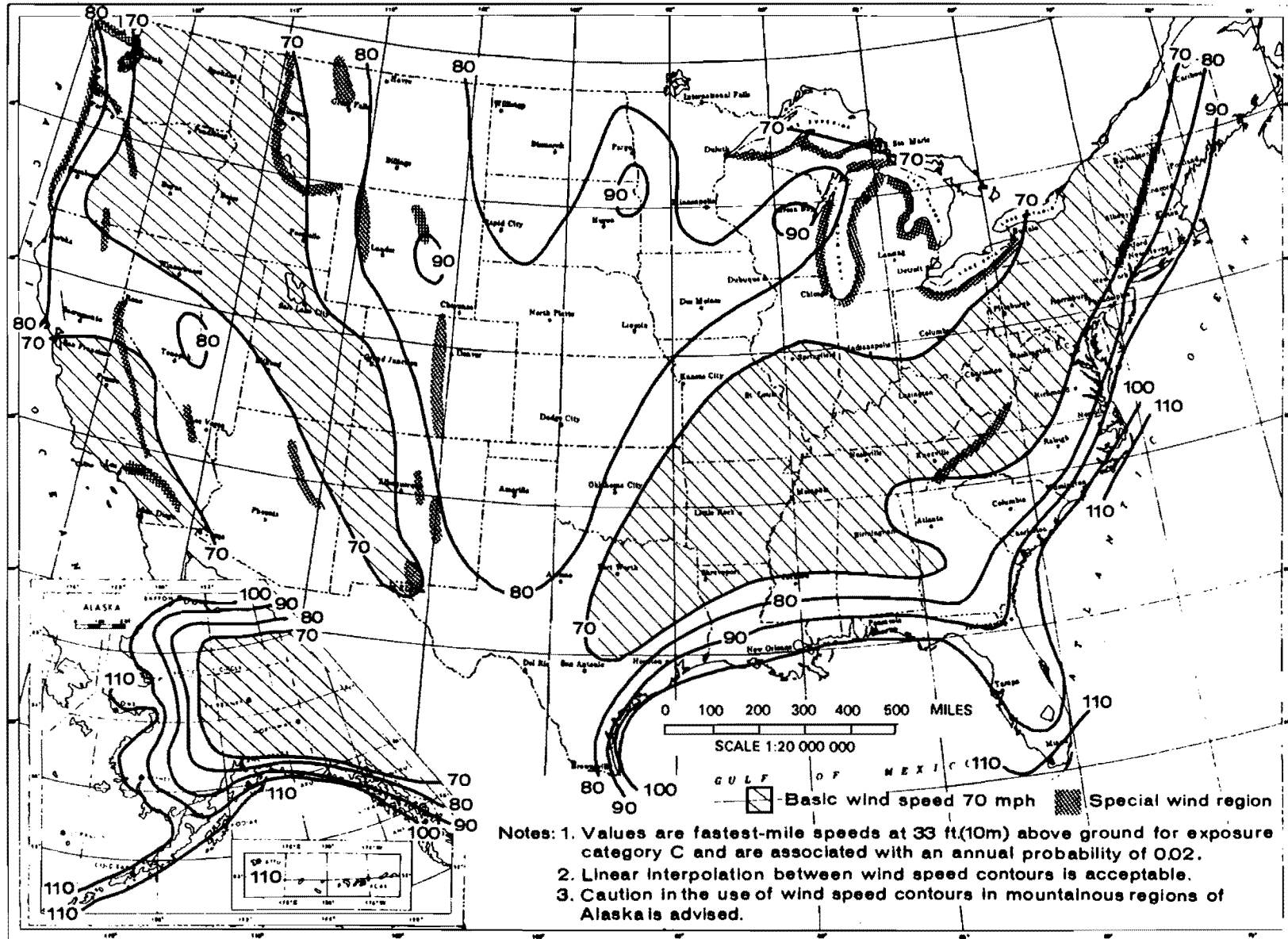
FIGURE 2.1. BASIC WIND SPEED MAP FROM ASCE 7-88 (ASCE, 1990)

1 mph = 0.45 m/s
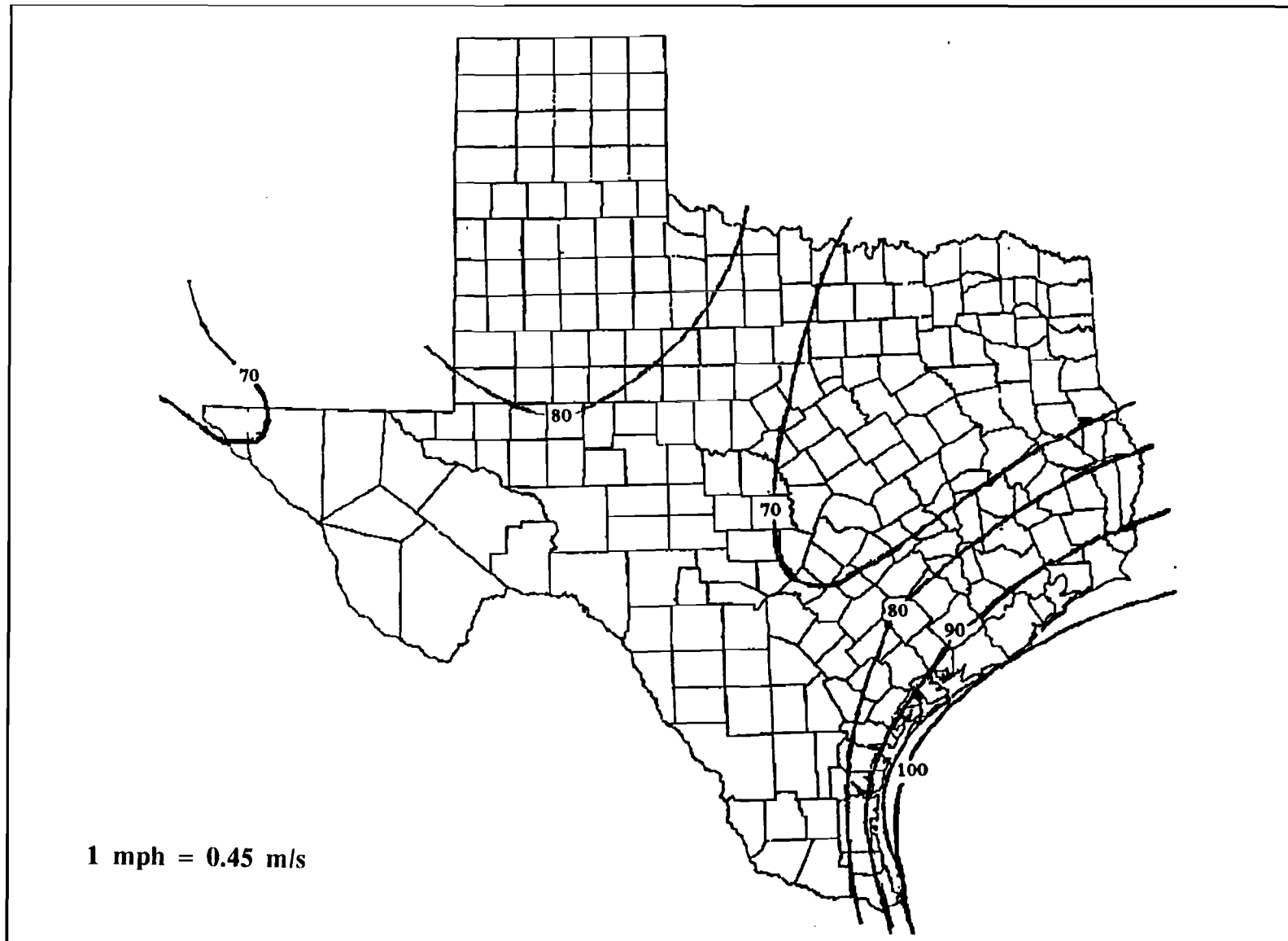
FIGURE 2.2. BASIC WIND SPEED CONTOURS FROM ASCE 7-88 FOR STATE OF TEXAS (ASCE, 1990)

The hurricane design wind speeds in ASCE 7 are used in the new map with only slight modifications. Additional years of data would have no effect on the simulated hurricane data. A similar approach was taken by the ASCE 7 Wind Load Subcommittee in proposing 1995 revisions to the standard. The subcommittee elected to revise the wind speed contours at inland stations, but retained the ones along the coastline with only slight modifications (Peterka, 1992).

2.1 Methodology

A Type I extreme value distribution represents a well-behaved inland wind climate (Simiu et al., 1979). The methodology for determining the parameters of the Type I distribution at each weather station is described in this section. An estimate of the wind speed associated with a mean recurrence interval (MRI) N is given by Simiu and Scanlan (1986):

$$\overline{V}_N = \overline{x} + s\,(y - 0.5772)\frac{\sqrt{6}}{\pi} \tag{2.1}$$

where

$\overline{x}$ = sample mean of the set of annual extreme fastest-mile wind speeds at a particular weather station, mph

s = standard deviation of the wind speed sample

N = mean recurrence interval, yr

y = variate
    = $-Ln\,[-Ln\,(1-1/N)]$ \qquad (2.2)

Wind speeds corresponding to MRIs of 10, 25, 50, and 100 years were calculated for each weather station. Rather than plot wind speed maps for each MRI, the wind speeds at all the stations within the state are averaged to obtain an importance coefficient I that gives the relationship between the 50-year and any other N-year MRI.

$$V_N = IV_{50} \tag{2.3}$$

where

V_N = average N-year MRI wind speed for all 26 stations in Texas

V_{50} = average 50-year MRI wind speed for all 26 stations in Texas

Thus, only one wind speed contour map is needed for the 50-year MRI. Wind speeds for other MRIs are obtained using an appropriate importance coefficient.

2.2 Wind Speed Records

Wind speed records are archived at the National Climatic Data Center in Asheville, North Carolina. Records were found for 52 recording stations in Texas. However, after reviewing each one for consistency, quality, and length of record, only 26 stations were judged acceptable for this study.

The records generally contain annual maximum gust speeds for 16 wind directions. This study did not elect to determine design wind speeds by direction. Instead, the data sets consist of the largest annual gust speeds, independent of direction. The gust speeds are assumed to be 3 second gusts, because three seconds is the response time of the 3-cup anemometer used by the weather service. The data files also contain the date on which the maximum gust speed occurred. This information is needed to correct the wind speed data when the anemometer is not set at the standard height of 33 feet (10 m) above ground.

The wind speed data at each station was carefully screened. Of particular concern was: (1) missing data, (2) non-standard anemometer height, (3) anemometer located on a rooftop, and (4) length of data record. Some stations recorded wind speeds at zero mph, indicating the data was not recorded, or was lost. Those years with zero wind speeds were eliminated from the data set. Another important factor is the history of the anemometer height above ground over the years of record. Changery (1978) compiled the history of anemometer heights for all official weather stations in the United States. Wind speeds recorded at anemometer heights other than 33 feet (10 m) were corrected to 33 feet (10 m) using the power law equation:

$$U_{33} = U_z(33/z)^\alpha \qquad (2.4)$$

where

U_z = wind speed recorded at anemometer height z, mph

z = anemometer height above ground, ft

α = power law exponent
   = 0.11

The exponent α represents flat, open terrain as found at airports. If records indicated an anemometer was mounted on a rooftop, the data were disqualified during that period of time. Air flow over a roof can give erroneous anemometer readings, because the free-field flow is modified as the air passes over and around a building. Finally, the number of years of record was considered. Ten years is thought to be the minimum to obtain a reasonable estimation of the distribution function. To be conservative and yet not loose too many potential stations, a minimum length of 19 years was adopted. Applying all of the above criteria, a total of 26 stations in the state qualified for the study. Table 2.1 shows the number of stations and their various lengths of records.

In order to obtain better information near state borders, several weather stations in neighboring states were used. The data at these stations had to meet the same criteria for quality and consistency as the stations in Texas. Table 2.2 lists the out of state stations used in the study. A total of 26 in-state and six out-of-state stations were used in preparing the proposed wind speed map for inland locations.

2.3   Hazard Assessment

After completing the screening process, the sets of annual maximum gust wind speeds for the stations were converted to fastest-mile wind speeds using gust factors developed by Durst (1960). The sample mean and standard deviation were calculated. Then, using Eq. (2.1), the wind speeds corresponding to 10-, 25-, 50-, and 100-year MRIs were calculated for each of the 32 weather stations. Table 2.3 presents the results of these calculations.

24

TABLE 2.1

NUMBER OF STATIONS VERSUS YEARS OF RECORD

Years of Record	Number of Stations
19-20	6
21-25	9
26-30	4
>30	7
Total Stations	26

TABLE 2.2

STATIONS FROM NEIGHBORING STATES

State	Stations Used
Oklahoma	Altus
Oklahoma	Fort Sill
Louisiana	Shreveport
Arkansas	Little Rock
New Mexico	Holloman AFB
New Mexico	Cannon AFB

Note: Total "out of Texas" stations used: 6

TABLE 2.3

SUMMARY OF WIND HAZARD ASSESSMENT
FOR THE STATE OF TEXAS

Station Number	Station Name	Symbol	Location Lat.	Location Long.	Wind Speed, mph) Mean Recurrence Interval, yr 10	25	50	100
03902	Robert Gray	RBG	3104	9749	57	63	67	71
03927	Dallas	DAL	3254	9702	62	69	74	80
12906	Ellington AFB	ELL	2936	9510	59	65	68	73
12909	Kelly AFB	KEL	2923	9834	56	62	66	71
12911	Randolph AFB	RDF	2932	9817	56	61	65	69
12912	Victoria	VIC	2851	9655	52	55	58	60
12917	Port Arthur	PTA	2952	9356	55	60	63	67
12919	Brownsville	BSV	2554	9726	53	59	63	67
12921	San Antonio	SAO	2932	9828	55	61	65	69
12924	Corpus Christi	CCI	2741	9717	80	97	110	122
12925	Beeville	BVL	2822	9740	59	66	71	77
12926	Corpus Christi NAS	CCN	2741	9717	72	84	92	101
12928	Kingsville NAS	KSV	2730	9748	62	71	79	86
12960	Houston Intercontinental	HOU	2959	9521	63	71	78	84
13904	Bergstrom AFB	BSM	3012	9740	56	61	65	70
13910	Dyess AFB	DYS	3226	9951	62	68	73	78
13911	Carswell AFB	CWL	3247	9740	61	67	71	75
13958	Austin	AUS	3018	9742	56	61	65	69
13959	Waco	WAC	3133	9711	58	64	69	73
13962	Abilene	ABL	3226	9641	60	65	69	73
13966	Wichita Falls	WFL	3359	9831	62	67	71	76
22001	Laughlin AFB	LLG	2922	10047	72	83	91	99
23023	Midland	MID	3156	10212	67	73	78	83
23042	Lubbock	LBK	3338	10150	66	73	78	83
23047	Amarillo	AMA	3514	10142	62	66	69	73
93901	Hensley Field	HEN	3244	9658	58	64	68	73
13957	Shreveport, LA	SHP	3228	9349	61	67	73	78
03930	Little Rock, AR	LRK	3455	9209	63	70	77	83
13902	Altus, OK	ALT	3439	9916	69	77	82	88
13945	Fort Sill, OK	FTS	3439	9824	68	75	81	87
23002	Holloman AFB, NM	HOL	3251	10605	60	65	69	74
23008	Cannon AFB, NM	CAN	3423	10319	64	71	75	77

1 mph = 0.45 m/s

Hurricane wind speeds near the Texas coastline at the 50-year MRI were obtained from the ASCE 7-88 wind speed map (see Figure 2.1). According to the ASCE 7-88 procedure, the wind speeds at the coastline should be multiplied by a hurricane importance factor of 1.05. This step was implemented, because the wind load subcommittee felt the results from the Batts et al., (1980) study were slightly unconservative. The importance factor may be reduced in proportion to the distance inland from the coastline. At 100 miles (160 km) inland, the coefficient reduces to 1.0.

2.4   Wind Speed Hazard Map

In order to avoid interpolation between contour lines, design wind speeds for the 50-year MRI are specified by county. After calculating wind speed values at the weather stations and determining the hurricane wind speeds from ASCE 7-88, four distinct wind speed regions were defined. The counties in the regions have 50-year MRI wind speeds of 70, 80, 90, and 100 mph (31, 36, 40, 45 m/s) (fastest-mile).

Figure 2.3 shows the location of the weather stations and the 50-year MRI wind speeds. The records of stations located within 100 miles (160 km) of the coastline are not sufficient to determine the hurricane hazards. Looking at the rest of the state, stations in the Central Texas have 50-year MRI wind speeds less than 70 mph (31 m/s). Stations in the rest of the state and in neighboring states have 50-year MRI wind speeds less than 80 mph (36 m/s) (with one exception). The gradation of wind speeds from the coastline reflects the decay of hurricane wind speeds as the storms move inland. The 100 mph (45 m/s) contour, which is increased to 105 mph (47 m/s) after applying the importance coefficient, generally lies a few miles off-shore (See Figure 2.2), so a 100 mph (45 m/s) wind speed was judged appropriate for the first tier of counties along the coastline. The wind speed are reduced to 90 mph (40 m/s) in the second tier of counties. An 80 mph (36 m/s) transition zone is located between the hurricane zone and the hill country zone of 70 mph (31 m/s) winds. Figure 2.4, then, represents the final proposed regions of the 50-year MRI design wind speed map for the State of Texas.

Importance factors for converting wind speeds to other MRIs are obtained from Eq (2), using the average wind speed values for the Texas stations as given in Table 2.4.
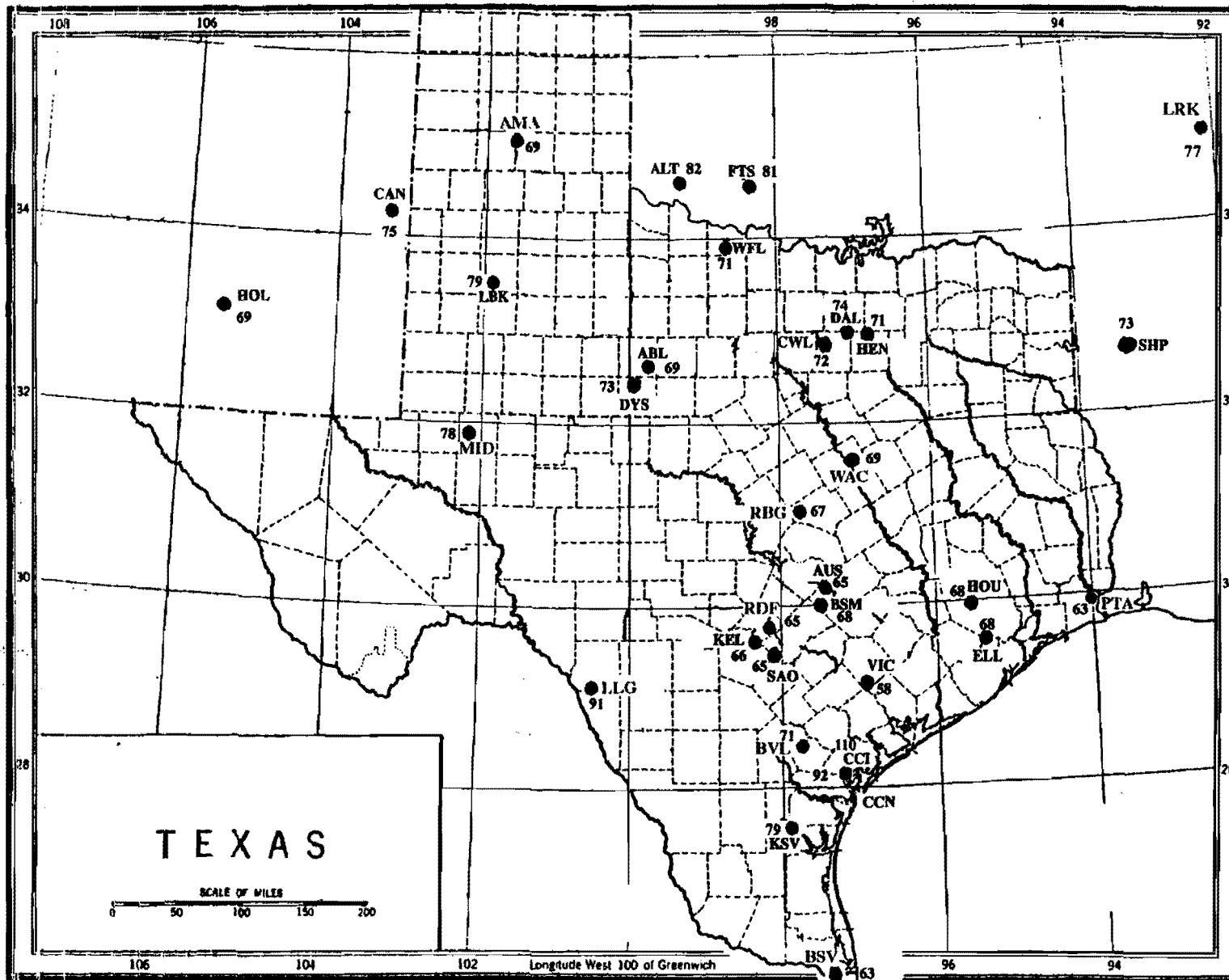
FIGURE 2.3. FIFTY-YEAR MRI FOR WIND SPEEDS FOR REPORTING STATIONS IN TEXAS

28

Legend

speed, mph.

▦	70
☐	80
▤	90
▥	100

0   50   100

miles

NOTE: Values indicated are fastest-mile speeds at
33 ft (10 m) above ground for Exposure
Category 3, and are associated with a
50-year mean recurrence interval (annual
probability of 0.02).

1.0 mi   =   1.6 km
1.0 mph =   0.45 m/s
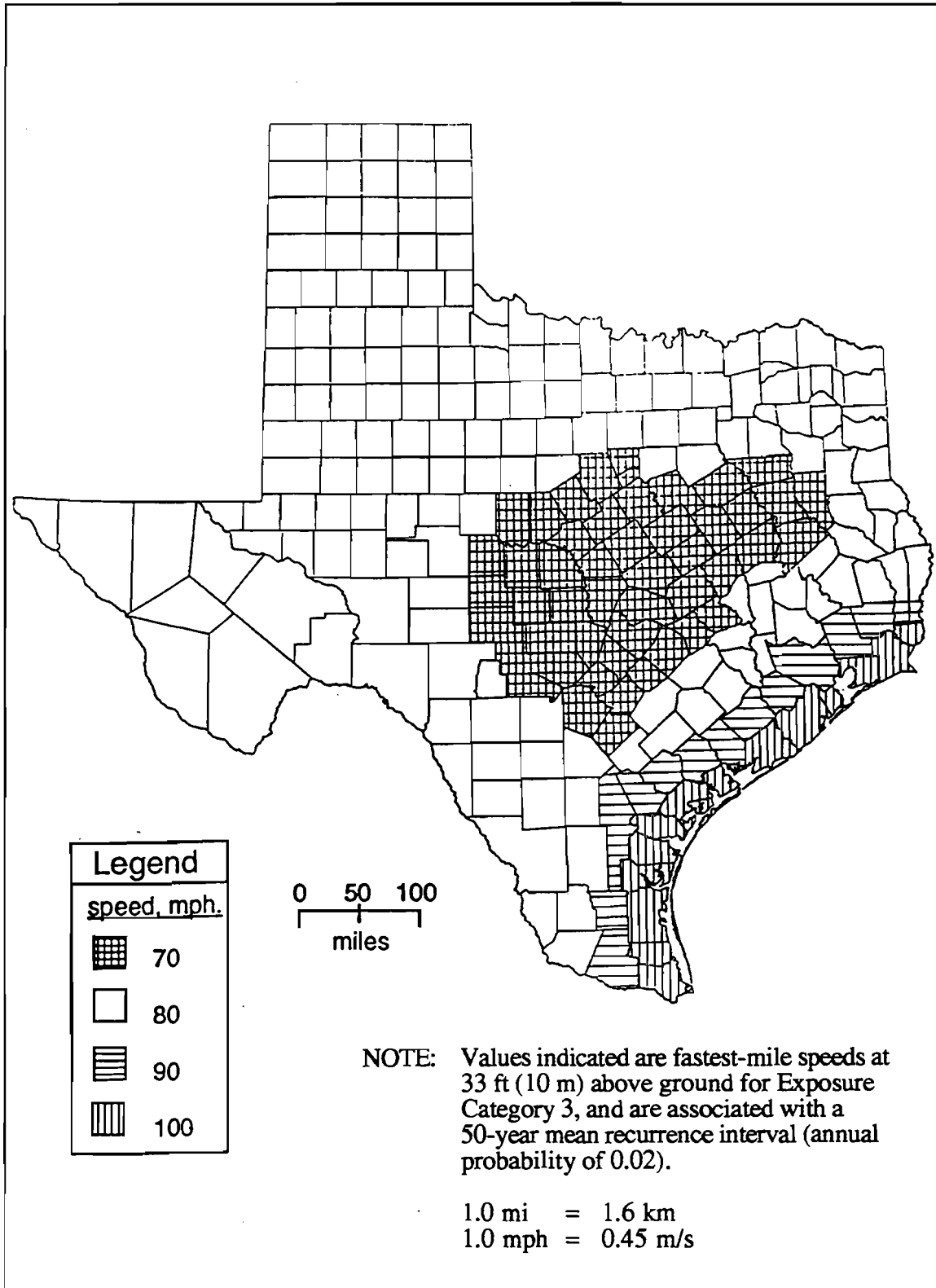
**FIGURE 2.4. RECOMMENDED BASIC 50-YEAR WIND
SPEEDS FOR COUNTIES IN TEXAS**

TABLE 2.4

IMPORTANCE FACTOR FOR VARIOUS MEAN RECURRENCE INTERVALS

| | Mean Recurrence Intervals | | | |
	10	25	50	100
Mean wind speed, V_N	63.8	68.9	72.5	77.8
Inland, I	0.88	0.95	1.00	1.07
Coastline, I	0.88	0.95	1.05	1.11

1 mph = 0.45 m/s

3. REVISIONS OF WIND DESIGN STANDARD

3.1 Introduction

The wind load provisions for design of structural supports for highway signs, luminaires and traffic signals published by AASHTO in 1985 were reviewed and revised. The revisions follow two basic concepts: (1) the revisions conform to the current consensus standard ASCE 7-88, and (2) design wind speeds are updated as indicated in Section 2.

The revised wind load provisions are based on the gust response factor concept as presented in ASCE 7-88. The gust response factors, given in tabular form, reflect response of structures that are not dynamically excited by the wind. The gust response factor approach is more realistic than the current gust factor approach in the AASHTO standard. It also is less conservative and leads to more economical designs than the provisions of the AASHTO standard.

Some sections of the AASHTO standard related to application of wind loads are revised, while the remaining sections are unchanged. A brief explanation of revised sections of the standard and design examples for comparison of AASHTO 1985 and the revised standard are presented below. The text of the revised sections of the standard and associated commentary are given in Appendices A and B, respectively.

3.2 Summary of Revisions

The AASHTO 1985 specification articles 1.2.4 - Wind Load, and 1.2.5 - Application of Wind Load: Part 1 are revised. The AASHTO 1985 articles 1.2.1, 1.2.2, 1.2.3, 1.2.5C, 1.2.5D and 1.2.6 are not affected. Design factors that are revised are discussed below; revisions to the specification are given in Appendix A. Revisions to the commentary, which explain new concepts, are given in Appendix B.

Wind Pressure: The equation for wind pressure incorporates wind speed, importance factor, exposure and height coefficient, gust response factor, and drag coefficient. The wind pressure equation gives horizontal pressures, which are to be applied on projected surfaces normal to wind.

Wind Speed: Revised design wind speeds for the State of Texas are shown in Figure 2.4, as well as in the wind speed map of the specifications (Appendix A). The methodology used in developing the new wind speed map is described in Section 2.

Importance Factor: The importance factor is based on the expected life of the structure, the probability of wind speed occurrence (MRI), and the importance of the structure. Recommended mean recurrence intervals for different structures are shown in Table 1.2.5A of the Specifications (Appendix A). The values of importance factor, Table 1.2.5B of the Specifications (Appendix A) are developed from wind hazard assessment analysis discussed in Section 2. Two sets of importance factor values are given; one related to hurricane winds and the other are related to non-hurricane winds.

Exposure and Height Factor: Velocity pressure exposure coefficients shown in Table 1.2.5C of Specifications (Appendix A) are the same as the ones in ASCE 7-88. Exposure Categories 1, 3 and 4 are equivalent to Exposure Categories B, C and D of ASCE 7-88, respectively. Category 2 represents outskirts of town, countryside with scattered buildings, and areas with clumps of trees or bushes, and falls between Exposure Categories B and C of ASCE 7-88. The velocity pressure for exposure coefficient and expanded explanations of exposures are given in the Commentary, Appendix B.

Gust Response Factor: The gust response factor values shown in Table 1.2.5E of the revised specifications (Appendix A) are the same as the ones in ASCE 7-88. Gust response factor accounts for the additional loading effects of wind gusts above the fastest-mile wind speed. It also depends on the gustiness in wind and on the size of the structure. Gust response factors in the revised specifications reflect response of structures that are not dynamically excited. If the fundamental frequency of the structure is judged to be smaller than 1 H_z, additional dynamic analysis is necessary. Gust response factor values shown in Table 1.2.5E of the revised specifications can be determined using the equation given in the Commentary (Appendix B).

Drag Coefficient: A literature search did not reveal new information on drag coefficients. Thus, the drag coefficients for various shapes in the revised specifications are the same as the ones

in AASHTO (1985). Table 1.2.5C of AASHTO (1985) will be Table 1.2.5D in the revised standard.

In the revised specifications (Appendix A), articles 1.2.4, 1.2.5A, B, C, D and E are given. In addition, Figure 1.2.4 and Tables 1.2.5A, 1.2.5B and 1.2.5D, which are updated, are shown. It is suggested that these revisions and unchanged articles of AASHTO (1985) be combined to produce a stand-alone specification. Articles, figures and tables in Appendices A and B follow the numbering system of the AASHTO specifications to avoid confusion with other tables and figures of this report.

3.3 Revised Standard

The text of proposed revisions to the AASHTO (1985) Standard Specification for Structural Supports for Highway Signs, Luminaires and Traffic Signal Structures are presented in Appendix A. Only those sections with proposed changes are written out.

3.4 Revised Commentary to Standard

Appendix B contains text of the revised commentary to the Standard Specifications for Structural Supports for Highway Signs, Luminaires and Traffic Signals for the State of Texas. Commentary is presented only on those sections where changes are proposed. The remainder of the Commentary is the same as for AASHTO (1985). Both the proposed revisions and the Commentary were submitted to the Texas Department of Transportation in 1993.

3.5 Comparison of Existing and Updated Standard

This section contains five example problems worked out using the 1985 AASHTO Specifications and the revised specifications. Table 3.1 summarizes the features of each example problem. Explanations are presented for selecting parameters for the new procedure. Only the wind loadings to be applied to the structure are calculated; structural analysis is not carried out. Results of each problem are summarized in Tables 3.2 to 3.6.

The first example problem is worked twice: Once using an Exposure Category 1 and once with Exposure Category 2. The results point out that Exposure Category 1 gives extremely small

TABLE 3.1

EXAMPLE PROBLEM CONDITIONS

	Structure	Location	County	Basic Wind Speed, mph	Exposure	Distance to Coastline, mi
1.	Traffic Signal Structure	San Antonio	Bexar	70	1	>100
1A.	Traffic Signal Structure	San Antonio	Bexar	70	2	>100
2.	Overhead Bridge Sign	Lubbock	Lubbock	80	3	>100
3.	Break-Away Roadside Sign	Woodville	Tyler	90	2	83
4.	High Mast Luminaire	Corpus Christi	Nueces	100	4	0
5.	Roadway Illumination Assembly	Corpus Christi	Nueces	100	4	0

1 mi = 1.6 km

1 mph = 0.45 m/s

loads that may not be appropriate for practical design. The loads based on Category 2 are approximately 33% larger than those based on Category 1. As a practical matter, Exposure Category 1 should not be used.

The figures and tables referred to in the examples are in the revised specifications given in Appendix A and in the AASHTO (1985) specifications.

3.5.1 Example Problem #1: Traffic Signal Structure

Determine the wind loads on a cantilever traffic signal structure to be located in downtown San Antonio. The signal structure has a single arm with two signal heads and a standard illumination mast. One signal head has three lights; the other has four.

Analysis of New Parameters

San Antonio is located in Bexar County, which, from Figure 1.2.4, has a basic design wind speed of 70 mph (31 mph). According to Table 1.2.5A, design of the signal support structure should be based on a 25-year mean recurrence interval. Since the location is more than 100 miles (160 km) from the coastline, the Importance Factor is 0.95 according to Table 1.2.5B. Because the signal structure is located in the downtown area of a large city, one could us Exposure Category 1. The example should also be solved using Exposure Category 2. Compare results holding all other parameter constant. From Table 1.2.5C, select values of C_h for Exposure 1 and 2, and various heights above ground. The Gust Response Factor is C_h obtained from Table 1.2.5E for Exposure 1 and 2, respectfully and a structure height of 35 feet (11 m). The Drag Coefficients C_d is obtained from Table 1.2.5.D.

TABLE 3.2

Example 1: Design Wind Loads on a Traffic Signal Structure in Downtown San Antonio (Bexar County), Texas, Exposure Category 1

Parameters	AASHTO 1985	New Specifications
Exposure	****	1
V (mph)	70	70
MRI (yrs)	25	25
I	****	0.95
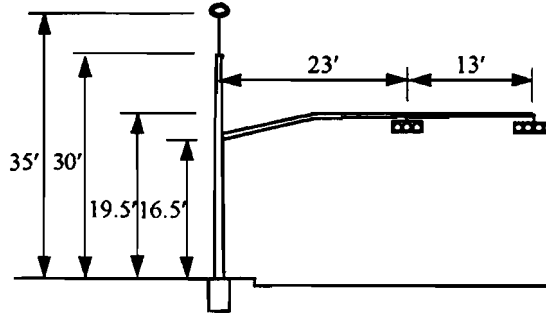
Design Wind Loads	AASHTO 1985 C_h	C_d	Wind Load	New Specifications C_h	C_d	C_g	Wind Load
Vertical Support							
$0 < H \le 7$	0.8	0.45	7.6 plf	0.37	0.45	1.50	2.8 plf
$7 < H \le 14$	0.8	0.45	7.0 plf	0.37	0.45	1.50	2.6 plf
$14 < H \le 22$	1.0	0.51	9.0 plf	0.43	0.51	1.50	3.2 plf
$22 < H \le 30$	1.0	0.59	9.3 plf	0.50	0.59	1.50	3.7 plf
$30 < H \le 35$	1.1	1.10	11.6 plf	0.53	1.10	1.50	4.5 plf
Horizontal Support							
$0 < L \le 9$	1.0	0.59	9.3 plf	0.40	0.59	1.50	3.0 plf
$9 < L \le 18$	1.0	0.71	9.6 plf	0.42	0.71	1.50	3.2 plf
$18 < L \le 27$	1.0	0.89	10.2 plf	0.42	0.89	1.50	3.4 plf
$27 < L \le 36$	1.0	1.10	10.0 plf	0.42	1.10	1.50	3.4 plf
Signals							
Three Lights	1.0	1.20	119.6 lbs	0.39	1.20	1.65	41.1 lbs
Four Lights	1.0	1.20	161.1 lbs	0.39	1.20	1.65	55.4 lbs
Luminaire	1.1	0.50	13.2 lbs	0.53	0.50	1.50	5.1 lbs

AASHTO 1985 CRITERIA

$P = 0.00256 \, (1.3 \, V)^2 C_h C_d$

P = Wind pressure in psf.

V = Wind speed in mph. From Fig.1.2.4 C, for 25 year mean recurrence interval,
V = 70 mph.

C_h = Coefficient for height above ground measured to the centroid of the corresponding limits of the loaded area, from Table 1.2.5 B.

C_d = Drag coefficient, from Table 1.2.5 C.

Vertical Pole

Height (ft)	C_h	C_d	Pressure P (psf)	Diameter (ft)	Load w (plf)
0 < H ≤ 7	0.80	0.45	7.6	1.00	7.6
7 < H ≤ 14	0.80	0.45	7.6	0.92	7.0
14 < H ≤ 22	1.00	0.51	10.8	0.83	9.0
22 < H ≤ 30	1.00	0.59	12.5	0.74	9.3
30 < H ≤ 35	1.10	1.10	25.7	0.45	11.6

Horizontal Support

Horizontal Distance from Pole (ft)	C_h	C_d	Pressure P (psf)	Diameter (ft)	Load w (plf)
0 < L ≤ 9	1.00	0.59	12.5	0.74	9.3
9 < L ≤ 18	1.00	0.71	15.1	0.64	9.6
18 < L ≤ 27	1.00	0.89	18.9	0.54	10.2
27 < L ≤ 36	1.00	1.10	23.3	0.43	10.0

Luminaire

$W_L = 0.00256 \, (1.3 \, V)^2 C_h C_d A_L$
$= 0.00256 \times (1.3 \times 70)^2 \times 1.10 \times 0.50 \times 1.13$
$= 13.2 \, lbs$

Signals

$$W_{S1} = 0.00256 \, (1.3V)^2 \, C_h \, (C_d \, A_{S1})$$
$$= 0.00256 \times (1.3 \times 70)^2 \times 1.00 \times 5.64$$
$$= 119.6 \text{ lbs}$$

$$W_{S2} = 0.00256 \, (1.3V)^2 \, C_h \, (C_d \, A_{S2})$$
$$= 0.00256 \times (1.3 \times 70)^2 \times 1.00 \times 7.6$$
$$= 161.1 \text{ lbs}$$

NEW SPECIFICATIONS

$$P = 0.00256 \, (I \, V)^2 \, C_h \, C_g \, C_d$$

P = Wind pressure in psf.

V = Wind speed in mph. From Fig.1.2.4 C, V = 70 mph.

I = Importance factor. From Table 1.2.5 B, for 25 year mean recurrence interval, I = 0.95.

C_h = Coefficient for height above ground and Exposure Category 1, from Table 1.2.5 C.

C_g = Gust response factor at 35 ft, from Table 1.2.5 E

C_d = Drag coefficient, from Table 1.2.5 D.

Vertical Pole

Height (ft)	C_h	C_g	C_d	Pressure P (psf)	Diameter (ft)	Load w (plf)
$0 < H \le 7$	0.37	1.50	0.45	2.83	1.00	2.8
$7 < H \le 14$	0.37	1.50	0.45	2.83	0.92	2.6
$14 < H \le 22$	0.44	1.50	0.51	3.81	0.83	3.2
$22 < H \le 30$	0.50	1.50	0.59	5.01	0.74	3.7
$30 < H \le 35$	0.53	1.50	1.10	9.90	0.45	4.5

Horizontal Support

Horizontal Distance From Pole (ft)	C_h	C_g	C_d	Pressure P (psf)	Diameter (ft)	Load w (plf)
$0 < L \leq 9$	0.40	1.50	0.59	4.00	0.74	3.0
$9 < L \leq 18$	0.42	1.50	0.71	5.07	0.64	3.2
$18 < L \leq 27$	0.42	1.50	0.89	6.34	0.54	3.4
$27 < L \leq 36$	0.42	1.50	1.10	7.84	0.43	3.4

Luminaire

$$W_L = 0.00256 \, (I \, V)^2 \, C_h \, C_g \, C_d \, A_L$$
$$= 0.00256 \times (0.95 \times 70)^2 \times 0.53 \times 1.50 \times 0.5 \times 1.13$$
$$= 5.09 \text{ lbs}$$

Signals

$$W_{S1} = 0.00256 \, (I \, V)^2 \, C_h \, C_g \, (C_d \, A_{S1})$$
$$= 0.00256 \times (0.95 \times 70)^2 \times 0.39 \times 1.65 \times 5.64$$
$$= 41.1 \text{ lbs}$$

$$W_{S2} = 0.00256 \, (I \, V)^2 \, C_h \, C_g \, (C_d \, A_{S2})$$
$$= 0.00256 \times (0.95 \times 70)^2 \times 0.39 \times 1.65 \times 7.6$$
$$= 55.4 \text{ lbs}$$

TABLE 3.3

Example 1A: Design Wind Loads on a Traffic Signal Structure in San Antonio (Bexar County), Texas, Exposure Category 2

Parameters	AASHTO 1985	New Specifications
Exposure	****	2
V (mph)	70	70
MRI (yrs)	25	25
I	****	0.95
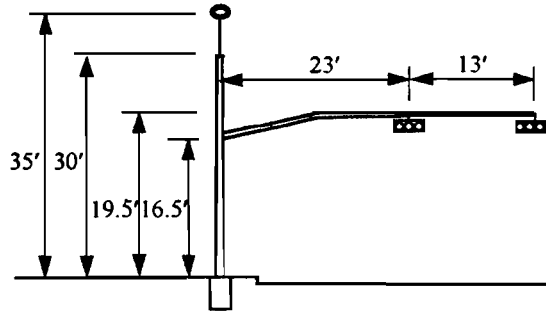
Design Wind Loads	AASHTO 1985			New Specifications			
	C_h	C_d	Wind Load	C_h	C_d	C_g	Wind Load
Vertical Support							
$0 < H \leq 7$	0.8	0.45	7.6 plf	0.55	0.45	1.38	3.9 plf
$7 < H \leq 14$	0.8	0.45	7.0 plf	0.55	0.45	1.38	3.6 plf
$14 < H \leq 22$	1.0	0.51	9.0 plf	0.63	0.51	1.38	4.2 plf
$22 < H \leq 30$	1.0	0.59	9.3 plf	0.71	0.59	1.38	4.8 plf
$30 < H \leq 35$	1.1	1.10	11.6 plf	0.75	1.10	1.38	5.8 plf
Horizontal Support							
$0 < L \leq 9$	1.0	0.59	9.3 plf	0.59	0.59	1.38	4.0 plf
$9 < L \leq 18$	1.0	0.71	9.6 plf	0.61	0.71	1.38	4.3 plf
$18 < L \leq 27$	1.0	0.89	10.2 plf	0.61	0.89	1.38	4.6 plf
$27 < L \leq 36$	1.0	1.10	10.0 plf	0.61	1.10	1.38	4.5 plf
Signals							
Three Lights	1.0	1.20	119.6 lbs	0.58	1.20	1.49	55.2 lbs
Four Lights	1.0	1.20	161.1 lbs	0.58	1.20	1.49	74.4 lbs
Luminaire	1.1	0.50	13.2 lbs	0.75	0.50	1.38	6.6 lbs

AASHTO 1985 CRITERIA

$P = 0.00256 \, (1.3 \, V)^2 \, C_h \, C_d$

P = Wind pressure in psf.

V = Wind speed in mph. From Fig.1.2.4 C, for 25 years mean recurrence interval,
V = 70 mph.

C_h = Coefficient for height above ground measured to the centroid of the corresponding limits of the loaded area, from Table 1.2.5 B.

C_d = Drag coefficient, from Table 1.2.5 C.

Vertical Pole

Height (ft)	C_h	C_d	Pressure P (psf)	Diameter (ft)	Load w (plf)
0 < H ≤ 7	0.80	0.45	7.6	1.00	7.6
7 < H ≤ 14	0.80	0.45	7.6	0.92	7.0
14 < H ≤ 22	1.00	0.51	10.8	0.83	9.0
22 < H ≤ 30	1.00	0.59	12.5	0.74	9.3
30 < H ≤ 35	1.10	1.10	25.7	0.45	11.6

Horizontal Support

Horizontal Distance from Pole (ft)	C_h	C_d	Pressure P (psf)	Diameter (ft)	Load w (plf)
0 < L ≤ 9	1.00	0.59	12.5	0.74	9.3
9 < L ≤ 18	1.00	0.71	15.1	0.64	9.6
18 < L ≤ 27	1.00	0.89	18.9	0.54	10.2
27 < L ≤ 36	1.00	1.10	23.3	0.43	10.0

Luminaire

$W_L = 0.00256 \, (1.3 \, V)^2 \, C_h \, C_d \, A_L$
$\quad = 0.00256 \times (1.3 \times 70)^2 \times 1.10 \times 0.50 \times 1.13$

$= 13.2 \text{ lbs}$

Signals

$W_{S1} = 0.00256 \, (1.3V)^2 \, C_h \, (C_d \, A_{Sr})$
$\quad = 0.00256 \times (1.3 \times 70)^2 \times 1.00 \times 5.64$
$\quad = 119.6 \text{ lbs}$

$W_{S2} = 0.00256 \, (1.3V)^2 \, C_h \, (C_d \, A_{S2})$
$\quad = 0.00256 \times (1.3 \times 70)^2 \times 1.00 \times 7.6$
$\quad = 161.1 \text{ lbs}$

NEW SPECIFICATIONS

$P = 0.00256 \, (I \, V)^2 \, C_h \, C_g \, C_d$

P = Wind pressure in psf.

V = Wind speed in mph. From Fig. 1.2.4 C, $V = 70$ mph.

I = Important factor. From Table 1.2.5 B, for 25 years mean reccurence interval, $I = 0.95$.

C_h = Coefficient for height above ground and exposure category: Exp.2, from Table 1.2.5 C.

C_g = Gust responce factor, from Table 1.2.5 E

C_d = Drag coefficient, from Table 1.2.5 D.

Vertical Pole

Height (ft)	C_h	C_g	C_d	Pressure P (psf)	Diameter (ft)	Load w (plf)
$0 < H \le 7$	0.55	1.38	0.45	3.87	1.00	3.9
$7 < H \le 14$	0.55	1.38	0.45	3.87	0.92	3.6
$14 < H \le 22$	0.63	1.38	0.51	5.02	0.83	4.2
$22 < H \le 30$	0.71	1.38	0.59	6.54	0.74	4.8
$30 < H \le 35$	0.75	1.38	1.10	12.89	0.45	5.8

Horizontal Support

Horizontal Distance From Pole (ft)	C_h	C_g	C_d	Pressure P (psf)	Diameter (ft)	Load w (plf)
$0 < L \leq 9$	0.59	1.38	0.59	5.44	0.74	4.0
$9 < L \leq 18$	0.61	1.38	0.71	6.77	0.64	4.3
$18 < L \leq 27$	0.61	1.38	0.89	8.48	0.54	4.6
$27 < L \leq 36$	0.61	1.38	1.10	10.48	0.43	4.5

Luminaire

$$W_L = 0.00256 \, (I\,V)^2 \, C_h \, C_g \, C_d \, A_L$$
$$= 0.00256 \times (0.95 \times 70)^2 \times 0.75 \times 1.38 \times 0.5 \times 1.13$$
$$= 6.62 \text{ lbs}$$

Signals

$$W_{S1} = 0.00256 \, (I\,V)^2 \, C_h \, C_g \, (C_d \, A_{S1})$$
$$= 0.00256 \times (0.95 \times 70)^2 \times 0.58 \times 1.49 \times 5.64$$
$$= 55.2 \text{ lbs}$$

$$W_{S2} = 0.00256 \, (I\,V)^2 \, C_h \, C_g \, (C_d \, A_{S2})$$
$$= 0.00256 \times (0.95 \times 70)^2 \times 0.58 \times 1.49 \times 7.6$$
$$= 74.4 \text{ lbs}$$

3.5.2   Example Problem #2:   Overhead Sign Bridge

Determine the wind loads on an overhead sign bridge on I-27 on the outskirts of Lubbock, Texas. The sign bridge is located over the north bound lane. At this location, the freeway is elevated over the natural ground by a 41 ft (12.5 m) high embankment.

Analysis of New Parameters

The City of Lubbock is located in Lubbock County and has a basic design wind speed of 80 mph (36 m/s). The structure is located over the roadway surface and thus should be designed for a 50-year mean recurrence interval. The Importance Factor is 1.0. Since the bridge is located on the outskirts of Lubbock, Exposure Category 3 is appropriate in this case. The Gust Response Factor C_h should be based on the total height above ground, which in this case should include the 27-ft (9-m) berm for a total of 68 feet (21 m). The Drag Coefficient C_d is obtained from Table 1.2.5.D. The structure has two horizontal trusses spaced 5.5 ft (1.7 m) apart and is supported on four vertical columns. Use a Drag Coefficient 1.7 for each truss to obtain the total load on the two trusses. In order to obtain the wind load per foot on the horizontal bridge truss, the projected area per unit length can be calculated. Multiplying this factor by the design wind pressure gives a wind load per ft on the bridge structure.

Example Problem No. 2: Overhead Sign Bridge

30 @ 5' = 150'

5.5'

$L\ 4 \times 4 \times \dfrac{1}{4}$ $L\ 4 \times 4 \times \dfrac{1}{4}$

PLAN

5.5'

$L\ 6 \times 6 \times \dfrac{5}{16}$ $L\ 6 \times 6 \times \dfrac{5}{16}$

$L\ 3\dfrac{1}{2} \times 3\dfrac{1}{2} \times \dfrac{5}{16}$ $L\ 3\dfrac{1}{2} \times 3\dfrac{1}{2} \times \dfrac{5}{16}$

W 21×68

27'

ELEVATION

11'×7'

27'

41'
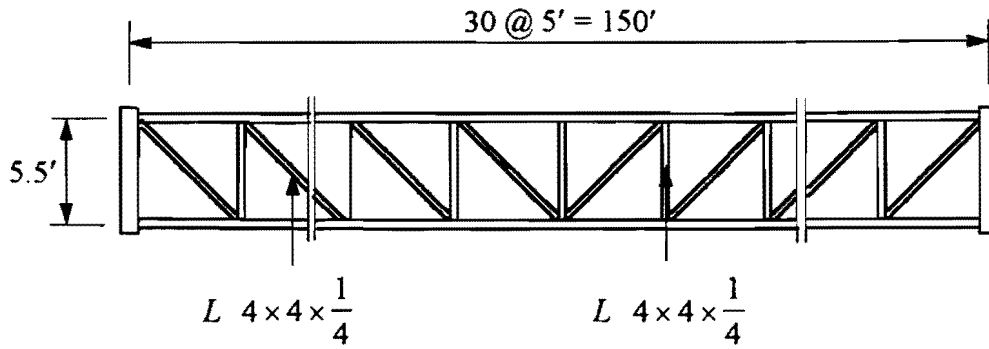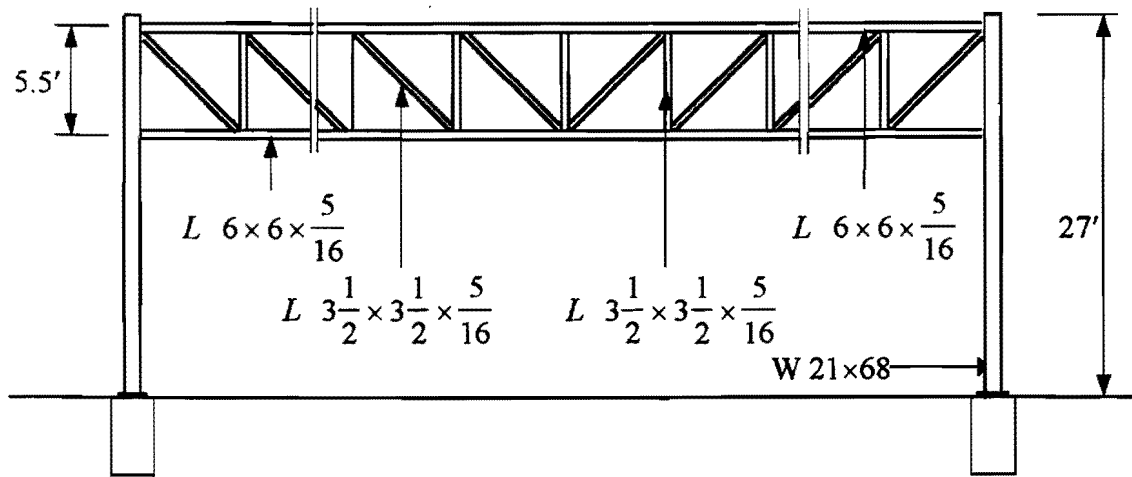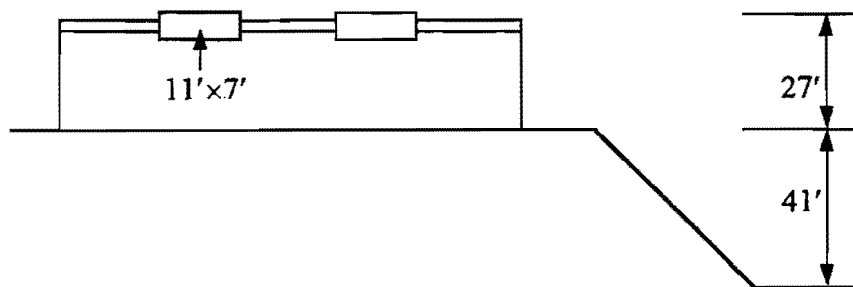
Location: Lubbcck, Texas
Lubbock County
Outskirts of City

45

TABLE 3.4

Example 2: Design Wind Loads on an Overhead Sign Bridge on I-27 near Lubbock (Lubbock County), Texas

Parameters	AASHTO 1985	New Specifications
Exposure	****	3
V (mph)	80	80
MRI (yrs)	50	50
I	****	1.0
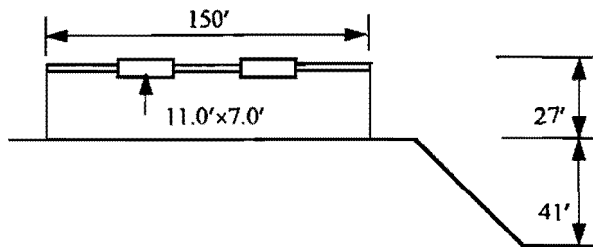
150'

11.0'×7.0'

27'

41'

Design Wind Loads	AASHTO 1985			New Specifications			
	C_h	C_d	Wind Load	C_h	C_d	C_g	Wind Load
Vertical Support 41 < H ≤ 49	1.10	3.4	181.2 plf	1.13	3.4	1.22	134.4 plf
Vertical Support 49 < H ≤ 68	1.25	3.4	206.0 plf	1.23	3.4	1.19	142.7 plf
Horizontal Support	1.25	3.4	195.2 plf	1.22	3.4	1.20	135.4 plf
Sign Panel	1.25	1.16	3091.6 lbs	1.22	1.16	1.20	2142.4 lbs

AASHTO 1985 Criteria

$P = 0.00256(1.3V)^2 C_h C_d$

P = Wind pressure in psf.

V = Wind speed in mph. From Fig.1.2.4 C, for 50 year mean recurrence interval, V= 80 mph.

C_h = Coefficient for height above ground measured to the centroid of the corresponding limits of the loaded area, from Table 1.2.5 B.

C_d = Drag coefficient, from Table 1.2.5 C.

Vertical Supports (Two Trusses)

Height (ft)	C_h	C_d	Pressure P (psf)	Width (ft)	Load w (plf)
27 < H ≤ 29	1.00	2 × 1.7	94.2	1.75	164.8
29 < H ≤ 49	1.10	2 × 1.7	103.6	1.75	181.2
49 < H ≤ 68	1.25	2 × 1.7	117.6	1.75	206.0

Horizontal Bridge (Two Trusses)

Projected Area Per Ft.   A / L = 1.66 ft.

$w_H = 0.00256 (1.3V)^2 C_h C_d (A / L)$
   $= 0.00256 \times (1.3 \times 80)^2 \times 1.25 \times (2 \times 1.7) \times 1.66$
   $= 195.2$ plf

Sign Panel

$A_P = 11.0 \times 7.0 = 77.0$ sq. ft.

$W_P = 0.00256 (1.3V)^2 C_h C_d A_P$
   $= 0.00256 \times (1.3 \times 80)^2 \times 1.25 \times 1.16 \times 77.0$
   $= 3091.6$ lbs

NEW SPECIFICATIONS

$P = 0.00256 \, (I \, V)^2 \, C_h \, C_g \, C_d$

P = Wind pressure in psf.

V = Wind speed in mph. From Fig.1.2.4 C, V = 80 mph.

I = Importance factor. From Table 1.2.5 B, for 50 year mean recurrence interval, I = 1.00.

C_h = Coefficient for height above ground and Exposure Category3, from Table 1.2.5 C.

C_g = Gust response factor at 68 ft from Table 1.2.5 E

C_d = Drag coefficient, from Table 1.2.5 D.

Vertical Supports (Two Trusses)

Height (ft)	C_h	C_g	C_d	Pressure P (psf)	Width (ft)	Load w (plf)
27 < H ≤ 29	0.98	1.19	2 × 1.7	64.97	1.75	113.7
29 < H ≤ 49	1.13	1.19	2 × 1.7	74.91	1.75	131.1
49 < H ≤ 68	1.23	1.19	2 × 1.7	81.54	1.75	142.7

Horizontal Bridge (Two Trusses)

$w_H = 0.00256 \, (IV)^2 \, C_h \, C_g \, C_d \, (A \, / \, L)$
$= 0.00256 \times (1.00 \times 80)^2 \times 1.22 \times 1.19 \times (2 \times 1.7) \times 1.66$
$= 134.2 \, plf$

Sign Panel

$W_P = 0.00256 \, (I \, V)^2 \, C_h \, C_g \, C_d \, A_P$
$= 0.00256 \times (1.00 \times 80)^2 \times 1.22 \times 1.20 \times 1.16 \times 77.0$
$= 2124.6 \, lbs$

3.5.3 Example Problem # 3: Break-a-way Road Side Sign

Determine the wind loads on a break-a-way road side sign that is located near Woodville, Texas in Tyler County. The sign is 16-ft (4.9-m) wide by 8-ft (2.4 m) high. Top of sign stands 15 ft (4.6 m) above ground. The sign is located on the roadway shoulder in an rural area with scattered trees and bushes, meadows and grassland.

Analysis of New Parameters

The basic design wind speed for Tyler County is 90 mph (40 m/s). The sign is clear of the roadway, which allows use of a 10-year mean recurrence interval. The location is 83 miles (134 km) from the nearest coastline. Taking into account the Mean Recurrence Interval and distance from coastline leads to an Importance Factor of 0.88. The surrounding terrain is typical of Exposure Category 2. Based on Exposure Category 2 and a total sign height of 15 feet, (4.6 m) the Gust Response Factor is 1.51. The Velocity Pressure Exposure Coefficient C_h is 0.55 since the sign is 15 feet (4.6 m) tall. Drag Coefficients for the sign columns and the sign itself are obtained from Table 1.2.5D.

Example Problem No. 3: Break-a-way Road Side Sign
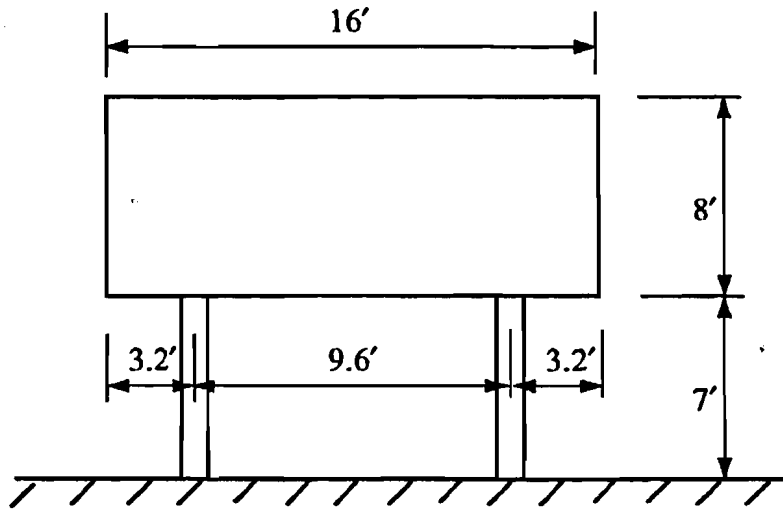
Location: Woodville, Texas
Tyler County
Rural Setting

Dimension: Sign Panel: 16' × 8'
Poles: W 8×18

TABLE 3.5

Example 3: Design Wind Loads on a Road Side Break-away Sign in Rural Setting near Woodville (Tyler County), Texas

Parameters	AASHTO 1985	New Specifications
Exposure	****	2
V (mph)	60	60
MRI (yrs)	10	10
I	****	0.88
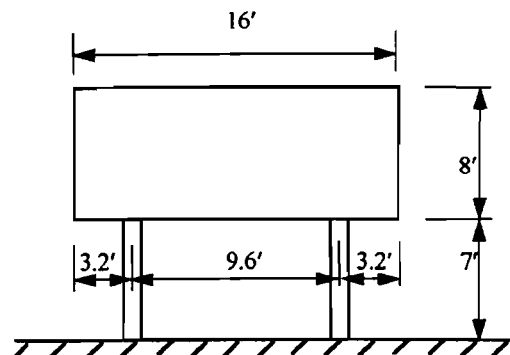
Design Wind Loads	AASHTO 1985 C_h	C_d	Wind Load	New Specifications C_h	C_d	C_g	Wind Load
Columns	0.8	1.7	9.3 plf	0.55	1.7	1.51	9.9 plf
Sign panels $0 < H \leq 14$	0.8	1.19	14.8 psf	0.55	1.19	1.51	15.9 plf
$14 < H \leq 15$	1.0	1.19	18.5 psf	0.55	1.19	1.51	15.9 plf

AASHTO 1985

$$P = 0.00256 \, (1.3V)^2 C_h C_d$$

P = Wind pressure in psf.

V = Wind speed in mph. From Fig.1.2.4 C, for 10 year mean recurrence interval,
    V = 60 mph.

C_h = Coefficient for height above ground measured to the centroid of the corresponding
    limits of the loaded area, from Table 1.2.5 B.

C_d = Drag coefficient, from Table 1.2.5 C.

Columns

Height (ft)	C_h	C_d	Pressure P (psf)	Width (ft)	Load w (plf)
0 < H ≤ 7	0.80	1.70	21.2	0.44	9.3

Sign Panel

Height (ft)	C_h	C_d	Pressure P (psf)
7 < H ≤ 14	0.80	1.19	14.8
14 < H ≤ 15	1.00	1.19	18.5

NEW SPECIFICATIONS

$$P = 0.00256 \, (I \, V)^2 C_h C_g C_d$$

P = Wind pressure in psf.

V = Wind speed in mph. From Fig.1.2.4 C, V = 90 mph.

I = Importance factor. From Table 1.2.5 B, for 10 year mean recurrence interval,
    I = 0.88.

C_h = Coefficient for height above ground and Exposure Category 2, from Table 1.2.5 C.

C_g = Gust response factor at 15 ft, from Table 1.2.5 E

C_d = Drag coefficient, from Table 1.2.5 D.

<u>Columns</u>

Height (ft)	C_h	C_g	C_d	Pressure P (psf)	Width (ft)	Load w (plf)
0 < H ≤ 7	0.55	1.51	1.7	22.67	0.44	10.0

<u>Sign Panel</u>

Height (ft)	C_h	C_g	C_d	Pressure P (psf)
7 < H ≤ 15	0.55	1.51	1.19	15.87

3.5.4 Example Problem #4: High Mast Luminaire

Determine the wind loads on a 100-ft (30-m) high luminaire located at the terminus of I-37 in Corpus Christi, Texas. This location in Nueces County is adjacent to the open water of Corpus Christi Bay.

Analysis of New Parameters

The basic design wind speed for Nueces County is 100 mph (45 m/s). The Mean Recurrence Interval for a 100-ft (30 m) high luminaire is 50 years. Thus, the Importance Factor should be 1.05. The Gust Response Factor for a structure height of 100 feet (30 m) and Exposure Category 4 is 1.07. Drag Coefficients are obtained from Table 1.2.5D.

3.5.5 Example Problem #5: Roadway Illumination Assembly

Determine the wind loads on a 45-ft (13.5-m) high roadway illumination assembly placed at Corpus Christi at the same location as the high mast luminaire in Example #4.

Example Problem No.4:   Luminaire (High Mast)
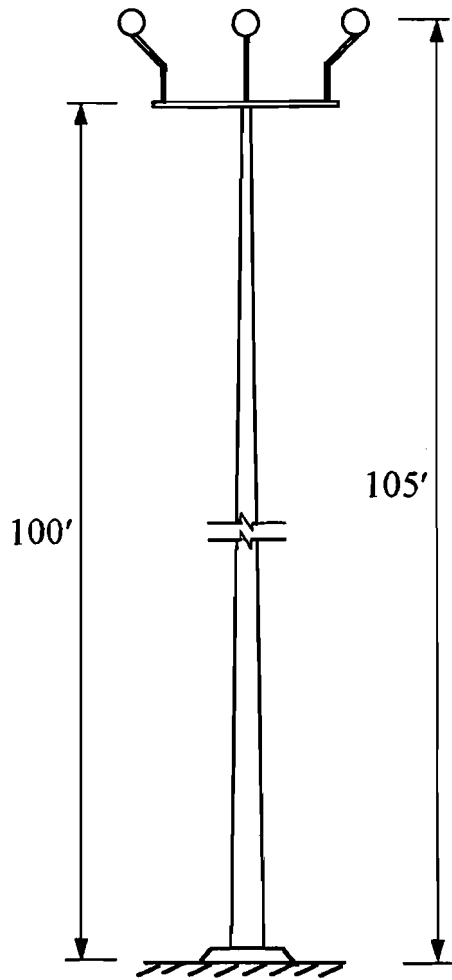
Location: Corpus Christi, Texas
            Nueces County
            Corpus Christi Bay

Dimension: Circular Tapered Pole

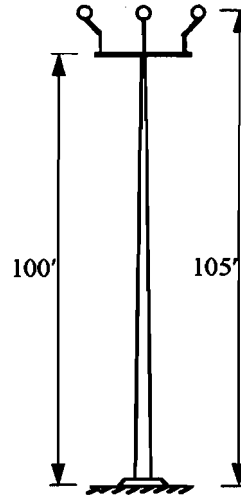|	Base	Top
Outside Diameter:	18″	12″

Luminaire Support: A_S = 7.5 sq. ft.

Luminaire: A_L = 4.52 sq ft

TABLE 3.6

Example 4: Design Wind Loads on a 100-ft High Mast Luminaire near Corpus Christi Bay in Corpus Christi (Nueces County), Texas

Parameters	AASHTO 1985	New Specifications
Exposure	****	4
V (mph)	90	100
MRI (yrs)	50	50
I	****	1.05

100' 105'

Design Wind Loads	AASHTO 1985			New Specifications			
	C_h	C_d	Wind Load	C_h	C_d	C_g	Wind Load
Vertical Support $0 < H \le 14$	0.80	0.45	18.6 plf	1.20	0.45	1.16	26.0 plf
$14 < H \le 29$	1.00	0.45	21.9 plf	1.36	0.45	1.12	26.9 plf
$29 < H \le 49$	1.10	0.45	22.5 plf	1.51	0.45	1.10	27.4 plf
$49 < H \le 100$	1.40	0.45	24.7 plf	1.75	0.45	1.07	26.6 plf
Luminaire Support	1.40	1.45	533.5 lbs	1.77	1.45	1.07	581.3 lbs
Luminaire	1.40	0.50	110.9 lbs	1.77	0.50	1.07	120.8 lbs

AASHTO 1985

$$P = 0.00256 \, (1.3 \, V)^2 \, C_h \, C_d$$

P = Wind pressure in psf.

V = Wind speed in mph. From Fig.1.2.4 C, for 50 year mean recurrence interval, $V = 90$ mph.

C_h = Coefficient for height above ground measured to the centroid of the corresponding limits of the loaded area, from Table 1.2.5 B.

C_d = Drag coefficient, from Table 1.2.5 C.

Pole

Height (ft)	C_h	C_d	Pressure P (psf)	Diameter (ft)	Load w (plf)
$0 < H \le 14$	0.80	0.45	12.62	1.47	18.6
$14 < H \le 29$	1.00	0.45	15.77	1.39	21.9
$29 < H \le 49$	1.10	0.45	17.35	1.30	22.5
$49 < H \le 95$	1.25	0.45	19.72	1.12	22.0

Luminaire Support

$$W_S = 0.00256 \, (1.3 \, V)^2 \, C_h \, C_d \, A_S$$
$$= 0.00256 \times (1.3 \times 90)^2 \times 1.25 \times 1.45 \times 7.5$$
$$= 476.4 \text{ lbs}$$

Luminaire

$$W_L = 0.00256 \, (1.3 \, V)^2 \, C_h \, C_d \, A_L$$
$$= 0.00256 \times (1.3 \times 90)^2 \times 1.40 \times 0.50 \times 4.52$$
$$= 110.9 \text{ lbs}$$

NEW SPECIFICATIONS

$P = 0.00256 \, (I \, V)^2 \, C_h \, C_g \, C_d$

P = Wind pressure in psf.

V = Wind speed in mph. From Fig.1.2.4, $V = 100$ mph.

I = Importance factor. From Table 1.2.5 B, for 50 year mean recurrence interval and hurricane zone, $I = 1.05$.

C_h = Coefficient for height above ground and Exposure Category 4, from Table 1.2.5 C.

C_g = Gust response factor at 100ft, from Table 1.2.5 E

C_d = Drag coefficient, from Table 1.2.5 D.

Pole

Height (ft)	C_h	C_g	C_d	Pressure P (psf)	Diameter (ft)	Load w (plf)
$0 < H \leq 14$	1.20	1.07	0.45	16.31	1.47	24.0
$14 < H \leq 29$	1.36	1.07	0.45	18.49	1.39	25.7
$29 < H \leq 49$	1.51	1.07	0.45	20.52	1.30	26.7
$49 < H \leq 95$	1.73	1.07	0.45	23.51	1.12	26.3

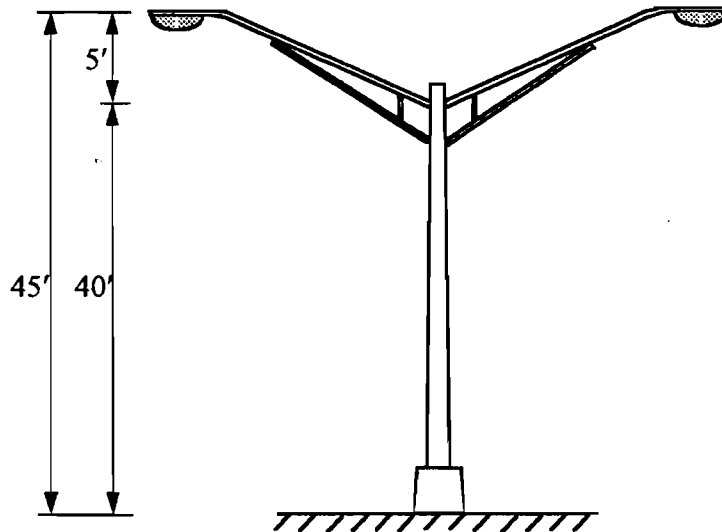## Luminaire Support

$W_s = 0.00256 \, (I \, V)^2 \, C_h \, C_g \, C_d \, A_s$
$= 0.00256 \times (1.05 \times 100)^2 \times 1.74 \times 1.07 \times 1.45 \times 7.5$
$= 571.5$ lbs

Luminaire

$W_L = 0.00256 \, (I \, V)^2 \, C_h \, C_g \, C_d \, A_L$
$= 0.00256 \times (1.05 \times 100)^2 \times 1.75 \times 1.07 \times 0.50 \times 4.52$
$= 119.4$ lbs

Example Problem No. 5: Roadway Illumination Assembly

Location: Corpus Christi, Texas
                Nueces County
                Corpus Christi Bay

Dimension: Circular Tapered Pole :

	Base	Top
Outside Diameter:	10″	4.75″

Arm Diameter:

Upper Arm:	2″
Lower Arm:	1.5″

Luminaire: $A_L = 3.0$ sq ft

Transformer Base:

Height:	17″
Top:	15″ × 15″
Bottom:	17.375″ × 17.375″

59

TABLE 3.7

Example 5: Design Wind Loads on a Roadway Illumination Assembly near Corpus Christi Bay in Corpus Christi (Nueces County), Texas

Parameters	AASHTO 1985	New Specifications
Exposure	****	4
V (mph)	90	100
MRI (yrs)	25	25
I	****	1.00
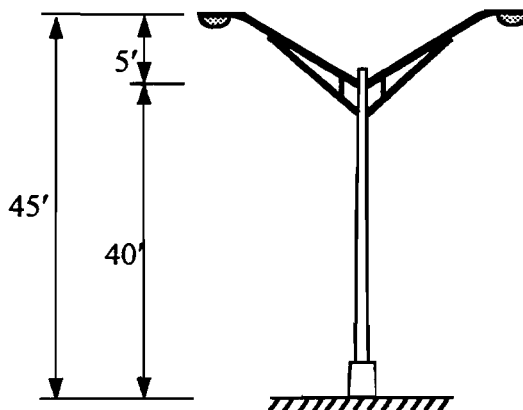
5'

45'

40'

Design Wind Loads	AASHTO 1985			New Specifications			
	C_h	C_d	Wind Load	C_h	C_d	C_g	Wind Load
Vertical Support $0 < H \le 1.4$	0.80	1.45	54.9 plf	1.20	1.45	1.11	66.7 plf
$1.4 < H \le 14$	0.80	0.45	9.6 plf	1.20	0.45	1.11	11.7 plf
$14 < H \le 29$	1.00	0.55	11.4 plf	1.36	0.55	1.11	13.0 plf
$29 < H \le 40.5$	1.10	0.79	14.0 plf	1.46	0.79	1.11	15.1 plf
Horizontal Support Upper Arm	1.10	1.10	7.1 plf	1.49	1.10	1.11	7.8 plf
Lower Arm	1.10	1.10	5.3 plf	1.49	1.10	1.11	5.8 plf
Luminaire	1.10	0.50	57.8 lbs	1.49	0.50	1.11	63.5 lbs

AASHTO 1985 CRITERIA

$$P = 0.00256 \, (1.3 \, V)^2 \, C_h \, C_d$$

P = Wind pressure in psf.

V = Wind speed in mph. From Fig.1.2.4 C, for 25 years mean recurrence interval, V = 90 mph.

C_h = Coefficient for height above ground measured to the centroid of the corresponding limits of the loaded area, from Table 1.2.5 B.

C_d = Drag coefficient, from Table 1.2.5 C.

Pole

Height (ft)	C_h	C_d	Pressure P (psf)	Diameter (ft)	Load w (plf)
0 < H ≤ 1.4	0.80	1.45	40.7	1.35	54.9
1.4 < H ≤ 14	0.80	0.45	12.6	0.76	9.6
14 < H ≤ 29	1.00	0.55	18.7	0.61	11.4
29 < H ≤ 40.5	1.00	0.79	30.5	0.46	14.0

Arms

	C_h	C_d	Pressure P (psf)	Diameter (ft)	Load w (plf)
Upper Arm	1.10	1.10	42.4	0.167	7.1
Lower Arm	1.10	1.10	42.4	0.125	5.3

Luminaire

$$\begin{aligned}
W_L &= 0.00256 \, (1.3 \, V)^2 \, C_h \, C_d \, A_L \\
&= 0.00256 \times (1.3 \times 90)^2 \times 1.10 \times 0.50 \times 3.0 \\
&= 57.8 \text{ lbs}
\end{aligned}$$

NEW SPECIFICATIONS

$$P = 0.00256 \, (I \, V)^2 \, C_h \, C_g \, C_d$$

P = Wind pressure in psf.

V = Wind speed in mph. From Fig.1.2.4 C, V = 100 mph.

I = Important factor. From Table 1.2.5 B, for 25 years mean reccurence interval, I = 1.00.

C_h = Coefficient for height above ground and exposure category: Exp.4, from Table 1.2.5 C.

C_g = Gust responce factor at 45ft height, from Table 1.2.5 E

C_d = Drag coefficient, from Table 1.2.5 D.

Pole

Height (ft)	C_h	C_g	C_d	Pressure P (psf)	Diameter (ft)	Load w (plf)
$0 < H \le 1.4$	1.20	1.11	1.45	49.4	1.35	66.7
$1.4 < H \le 14$	1.20	1.11	0.45	15.3	0.76	11.7
$14 < H \le 29$	1.36	1.11	0.55	21.3	0.61	13.0
$29 < H \le 40.5$	1.46	1.11	0.79	32.8	0.46	15.1

Arms

	C_h	C_g	C_d	Pressure P (psf)	Diameter (ft)	Load w (plf)
Upper Arm	1.49	1.11	1.10	46.6	0.167	7.8
Lower Arm	1.49	1.11	1.10	46.6	0.125	5.8

Luminaire

$$W_L = 0.00256 \, (I \, V)^2 \, C_h \, C_g \, C_d \, A_L$$
$$= 0.00256 \times (1.00 \times 100)^2 \times 1.49 \times 1.11 \times 0.5 \times 3.0$$
$$= 63.5 \text{ lbs}$$

4. FINITE ELEMENT ANALYSIS OF TRAFFIC SIGNAL STRUCTURES

Finite element method (FEM) models of the cantilever traffic signal structure tested in the field were formulated. The primary purpose of these analyses were

(1) To estimate natural frequencies of vibration of the structure

(2) To obtain a relationship between a static load at some location on the cantilever arm and the strain at the gage location

(3) To obtain a theoretical relationship between arm tip displacement and the maximum stress on the signal structure for the purpose of evaluating fatigue effects.

4.1 Finite Element Model

The cantilever traffic signal structure, which is a statically determinate structure, can be modeled with beam elements. Because both the vertical pole and the cantilever arm are tapered, a relatively fine mesh is needed to represent the mass and stiffness of the structure. A commercially available FEM software package, Stardyne for Windows, Version 4.0 (Titan Corp., 1993) was used to perform the static and dynamic analyses. Figures 4.1 and 4.2 show models of the 40-ft (12.2-m) and 48-ft (14.6-m) signal structures, respectively.

The models were first formulated using the sizes and dimensions of standard SMA-80 structures. However, when the results of selected analyses were compared with corresponding tests in the field (see Section 8), the agreement was not very good. When we resorted to field measurements and actual weights of the structures, the agreement between calculated and measured parameters (e.g., natural frequencies of vibrations) were much better. This study provided an excellent opportunity to compare theoretical calculations with full-scale field measurements.

4.2 Fundamental Frequencies of Vibration

The two signal structures tested in the field were first analyzed by the FEM using the Stardyne software. The purpose was to determine the natural frequencies of vibrations and mode shapes. Models were also developed and analyzed for the SMA-80 standard TxDOT signal

63

structures with different cantilever arm lengths. The models were based on published geometry and weights.

Table 4.1 summarizes the results of the FEM analyses. The table gives the calculated fundamental frequencies (first mode) for standard signal structures with different cantilever arm lengths. The fundamental frequencies for the two structures tested in the field were compared with the values measured in the field. Using the measured dimensions and actual weights of the structures, the field and calculated values agree very well. Estimating natural frequencies from the standard dimensions using a commercial software package may not always give correct results.

4.3   Load Versus Strain

The purpose of this exercise was to validate the FEM model with field measurements. Static concentrated load increments were applied at a location near the free end of the cantilever arm. The FEM analysis was then used to determined the strains at gage locations on the structure where strain gages were mounted for the field tests. If the FEM model gives reasonable agreement between load and strain, then the model can be used with confidence in calculating other parameters, such as stress and displacement. Table 4.2 presents the results of the load versus strain calculations. Calculated values can be compared with measured values in Table 8.1. Agreement is good.

4.4   Arm Tip Displacement Versus Maximum Stress

The relationship between arm tip displacement and maximum stress in the vertical pole and the cantilever arm was needed to study fatigue effects from cycle loading. The endurance limit is a function of mean stress, range of stress and number of cycles of load. The amplitude of tip displacement is a good indicator of the galloping phenomena. Hence, if we have a relationship between tip displacement and maximum stress in the signal structure, conclusions regarding potential fatigue during galloping damage can be drawn.

Table 4.3 presents the relationship between tip displacement of the cantilever arm versus maximum stress in the cantilever arm and the vertical pole.
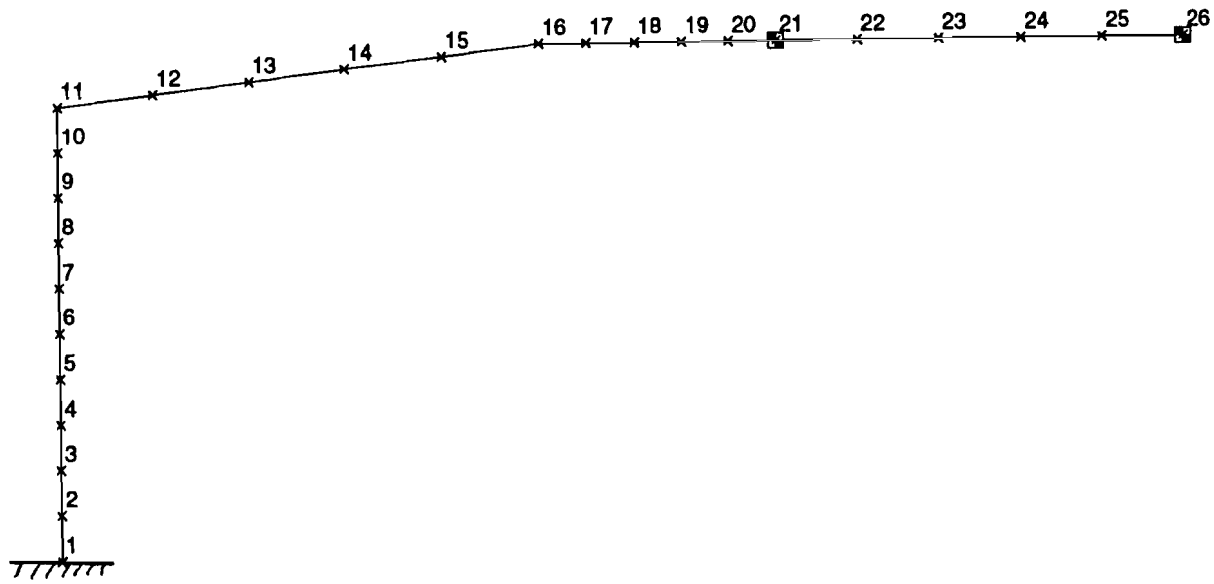
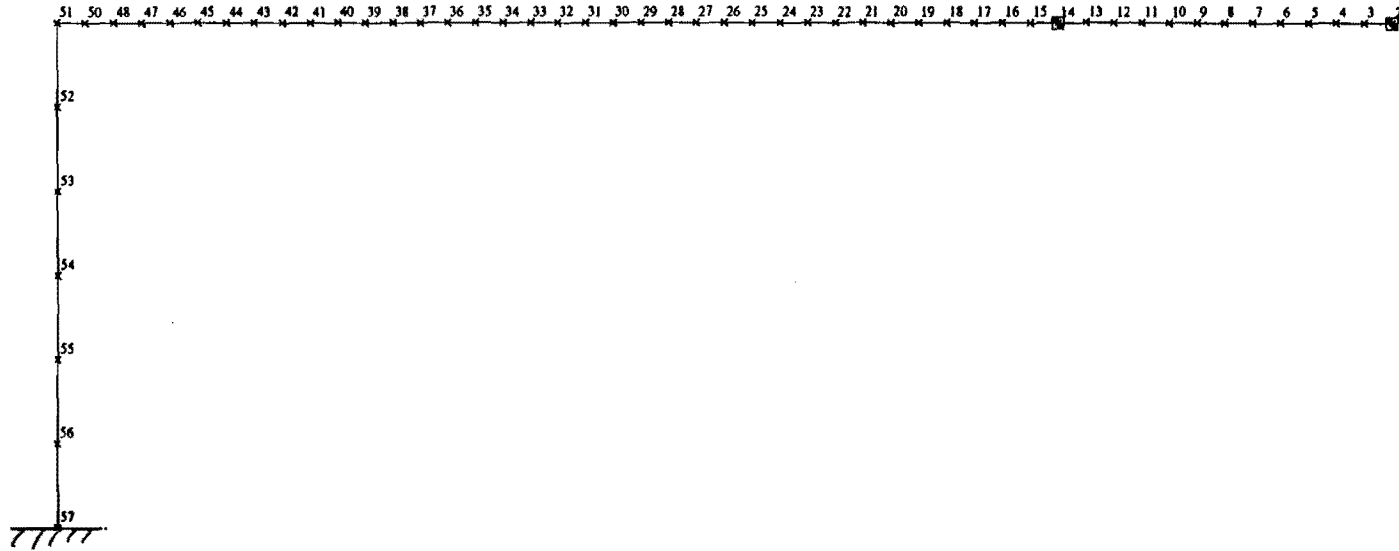**FIGURE 4.1. FEM MODEL OF 40-FT (12.2-m) SIGNAL STRUCTURE**

51 50 48 47 46 45 44 43 42 41 40 39 38 37 36 35 34 33 32 31 30 29 28 27 26 25 24 23 22 21 20 19 18 17 16 15 14 13 12 11 10 9 8 7 6 5 4 3 2

52

53

54

55

56

57

FIGURE 4.2.   FEM MODEL OF 48-FT (14.6-m) SIGNAL STRUCTURE

TABLE 4.1

CALCULATED FREQUENCIES OF SIGNAL STRUCTURES
WITH DIFFERENT LENGTH CANTILEVER ARMS

Arm length, ft	Fundamental Frequency, Hz
20	1.70
24	1.56
28	1.35
32	1.23
36	1.10
40	0.96
44	0.88
48	0.81

SMA-80 TxDOT Standard

1.0 ft = 0.30 m

TABLE 4.2

CALCULATED LOAD VERSUS STRAIN

	Strain on Vertical Pole - µstrain	
Load, lbs[1]	40-ft Structure[2]	48-ft Structure[2]
0	0	0
50	49.6	31.5
60	59.3	37.8
70	69.4	44.1
80	79.4	50.4
90	89.3	56.7

[1]Load applied 3 feet (1 m) from tip of arm.

[2]Strains located 13 in. (33 cm) above base plate.

$$1.0 \text{ ft} = 0.30 \text{ m}$$
$$1.0 \text{ lbm} = 0.45 \text{ kg}$$

TABLE 4.3

CALCULATED ARM TIP DEFLECTIONS, MOMENTS
AND STRESSES FOR VARIOUS LOAD CASES[1]

Case	Load	Arm Tip Defl. (in.)	Moment at Pole Base and Arm Connection (in.-lb x 10^{-5})	Stress at Pole Base (ksi)	Stress at Arm Connection (ksi)
1	Dead load of pole and arm only	15.4	2.142	7.28	11.09
2	Case 1 + two signal[2] lights (80 lb and 50 lb)	21.7	1.811	9.52	14.55
3	Case 2 with forced arm tip deflection of	25	3.131	10.60	16.21
4	Case 2 with forced arm tip deflection of	28	3.42	11.58	17.73
5	Case 2 with forced arm tip deflection of	31	3.72	12.56	19.26

[1]Values are calculated for 48-ft (14.6-m) SMA-80 signal structure.

[2] Case 2 is reference stage where stresses and deflection are due to wieght of the structure and signal lights.

1.0 in	=	2.5 cm
1.0 x 10^5 in.lb	=	0.113 x 10^5 Nm
1.0 ksi	=	6.9 MPa

5. DEVELOPMENT OF EXPERIMENTAL PLAN

5.1 Experimental Approach

The experimental plan for this project involved the use of three testing environments. The three testing environments provided a logical sequence of experiments for a more complete understanding of the mechanism involved in the vibration of traffic signal structures and the development of vibration mitigation strategies. The three testing environments were: (1) water table, (2) tow tank and (3) field site. Specific experiments were planned for each of the three test environments.

The water table (WT) provides a scaled model, two-dimensional testing environment. Scale models of the signal structure arm and traffic signal light cross sections were placed in the water flow; the interaction of the flow and the objects was observed and recorded. The signal arm and signal light models were arranged in various typical relative positions and the resulting vortex shedding phenomena were observed by injecting dye into the water. Both qualitative and quantitative data were obtained.

The tow tank permitted the testing of full-scale signal arm and traffic light. Using water instead of air as the fluid has the advantage of working with flow speeds less than 10-ft per second (3.0 m/s). Actual traffic signal lights along with a portion of the arm were towed through the tank to simulate wind speeds in the range of 10 to 30 mph (4.5 to 13.4 m/s). The resulting flow patterns were observed by injecting dye into the flow pattern and were recorded on video tape. Experiments were designed to visualize vortex shedding and/or galloping. A load transducer capable of measuring forces in three coordinate directions determined equivalent wind forces on the signal light arm assembly as it was towed through the tank.

The field site tests were conducted at the Wind Engineering Research Field Laboratory (WERFL). During the course of study, two full-size traffic signal structures were erected on a foundation that permitted rotation of the signal structure to the desired wind angle of attack. The foundation otherwise reproduced foundation stiffness and response similar to a standard field installation. Various meteorological instrumentation measured wind characteristics during the

71

testing. Strain gages displacement and tilt transducers were used to measure the signal structure's response to the wind. The experiments involved (1) measurement of the structural dynamic properties, (2) replicating the galloping phenomena in the field, and (3) testing several strategies for mitigation of wind induced vibrations (galloping).

5.2 Experimental Research Plan

A series of water table, tow tank and field experiments were designed to obtain a clear understanding of the behavior of traffic signal structures. From a search of the literature and theoretical studies, a hypothesis was developed, tested and ultimately proved. The hypothesis was as follows:

(1) Vortex shedding from flow around traffic lights and signal arms occur at wind speeds less than about 6-7 mph (2.7 - 3.1 m/s) and cannot be used to explain the large amplitude displacements observed in the field.

(2) Galloping, with large amplitude deflection, can occur under precise conditions of wind direction, wind speed and traffic light/signal arm orientation.

(3) Galloping can be induced in the field; certain measures can be employed to mitigate the vibrations associated with galloping.

The water table experiments were designed to test part (1) of the hypothesis: the tow tank was used to test part (2); and part (3) was tested in the field.

Table 5.1 summarizes the specific experiments conducted during the course of this project to verify the stated hypothesis. These tests and the results are described in Section 8.

TABLE 5.1
WATER TABLE, TOW TANK AND FIELD EXPERIMENTS

Test No.	Specimen or Configuration	Purpose or Comment
WT1	Circular and Octagonal Shapes	Flow visualization, Video, Strouhal number
WT2	Signal arm and traffic light (various arrangements)	Flow visualization, Video, Strouhal number
WT3	Signal arm and traffic signal with back plate (various arrangements)	Flow visualization, Video, Strouhal number
TT1	Circular cylinder [8-in. (20.3-cm)] diameter	Flow visualization, Video Strouhal number
TT2	Octagonal cylinder [8-in. (20.3-cm)] diameter	Flow visualization, Video Strouhal number
TT3	Circular signal arm, traffic light and damping plate (wing). Current mitigation practice	Flow visualization, Video Strouhal number
TT4	Octagonal signal arm, traffic light and damping plate. Current mitigation practice	Flow visualization, Video Strouhal number
TT5	Circular arm/traffic light and damping plate (various arrangements)	Flow visualization, Video Strouhal number
TT6	Octagonal arm/traffic light and damping plate (various arrangements)	Flow visualization, Video Strouhal number
TT7	Circular arm/traffic light with and without back plate, (various arrangements; see Figure 7.2	Force measurements versus angle of attack
FS1	Bare signal structure [40-ft and 48-ft (12.2-m and 14.6-m] arm	Frequency and damping measurements
FS2	Both signal structures (various arrangements of traffic lights)	Parameters that contribute to galloping
FS3	Signal structure with 48-ft (14.6-m) arm. Various vibration mitigation devices	Mitigation of galloping vibration

6. WATER TABLE EXPERIMENTS

The experimental plan developed in Section 5 provides for a study of vortex shedding by means of a water table experiment. A water table experiment is a study of two-dimensional flow. A layer of water under conditions of laminar flow is provided over a flat illuminated surface. Models of the signal arm and traffic light shapes are cut out and placed in the water flow. Vortices shed by the water flowing around the models can be visualized using red dye in the water. A video camera placed above the water table records the flow visualization of the vortex shedding phenomena.

6.1 Objectives

The primary objective of the water table experiment was to observe the two-dimensional fluid flow around models of the signal arm and traffic signal light. Specific objectives include:

(1) Observe the vortex shedding phenomena for various arrangements of the signal light and cantilever arm

(2) Obtain quantitative data for calculating Strouhal numbers

(3) Estimate vortex shedding frequencies as a function of wind speed for the full-scale traffic signal structure.

By knowing the vortex shedding frequencies as a function of wind speed, and the fundamental frequency of vibration of the signal structure, conclusions regarding cross wind behavior at resonance frequency can be drawn.

6.2 Test Facilities and Procedures

The water table apparatus is shown in Figure 6.1. It consists of two rectangular tanks, a 37 x 72 in. (94 x 183 cm) translucent table top and a circulating pump. Water is pumped into the first tank until it overflows onto the table top. To achieve a uniform and laminar flow across the water table top, a grid of dense padding is fitted to the tank overflow. The water is approximately 1 in. (2.5 cm) deep and travels at 7 in. (18 cm) per second. After crossing the table top, the water drains into the second tank where it is recirculated to the first tank. A non-glare light fixture under the translucent table top enhances visualization and makes video taping of the flow patterns
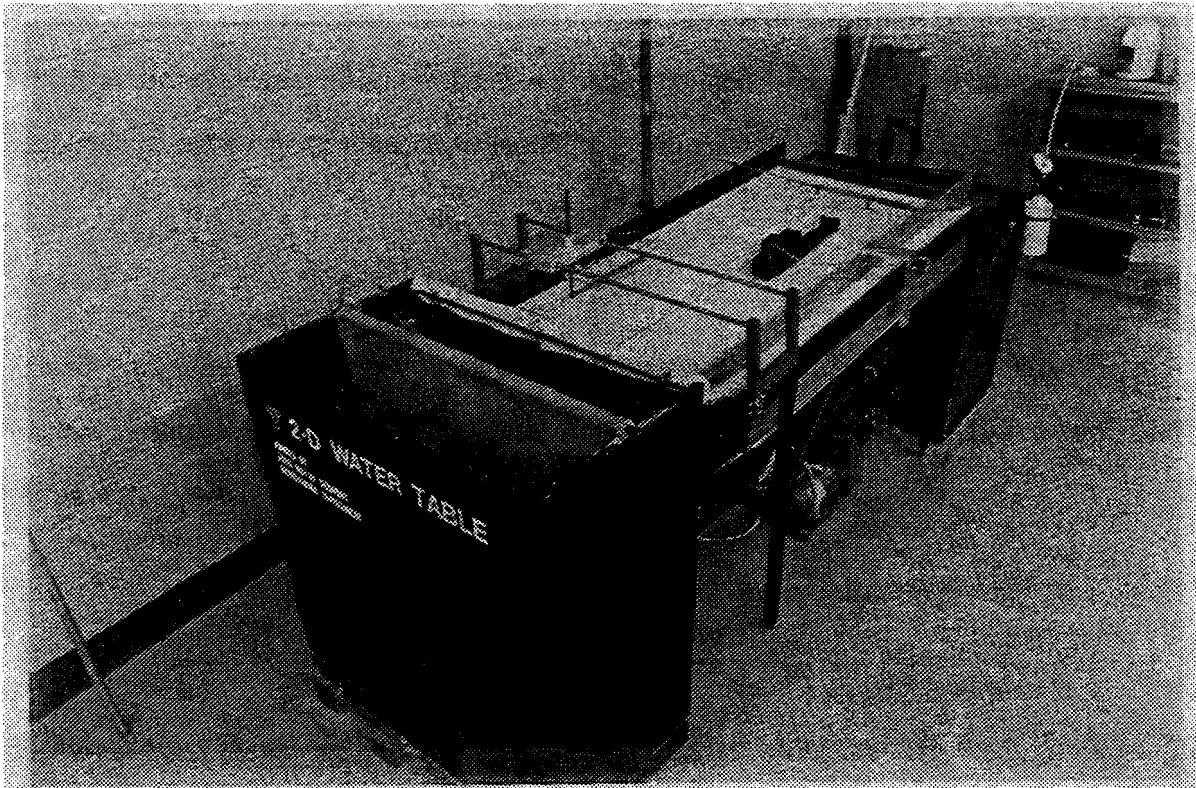
75

FIGURE 6.1 WATER TABLE APPARATUS FOR VISUALIZATION OF TWO-DIMENSIONAL FLOW

possible. Red food coloring is injected into the flow with a portable wand. A VHS video camera installed directly above the water table records the flow patterns.

The vortex shedding frequencies were determined using a video editing set up. By viewing the video tape of the flow visualization one frame at a time, and knowing the frame speed, the vortex shedding frequencies could be attained with reasonable accuracy.

Two-dimensional, quarter-scale models of the traffic signal head and signal arm cross section were cut from wood. Figure 6.2 shows one-quarter scale models of the octagon and circular signal arm cross sections. Dimensions perpendicular to flow directions are given in the figure. Figure 6.3 shows the cross section of the traffic signal light that was used in the water table, tow tank and field experiments.

The water table experiments consisted of various tests of individual model shapes and combinations of signal arm and traffic signal shape positioned relative to each other.

The test procedure consisted of the following steps:

(1)   Turned on circulating pump and allowed water flow to stabilize

(2)   Measured water flow velocity

(3)   Placed models on the water table top in the desired arrangement

(4)   Injected red dye into the water to enhance flow visualization

(5)   Turned on video camera and recorded flow patterns

(6)   Counted number of shed vortices in a selected length of time (usually one minute)

(7)   Repeated process for other model configurations

The video tapes were analyzed to obtain vortex shedding frequencies more accurately.

6.3   Experimental Plan and Results

The octagon and circular cross sections, as well as other arrangements of signal arm and signal light configurations were tested on the water table. Figures 6.4 through 6.7 show four arrangements of signal light and arm that have been observed in the field. Flow was directed from both front and back side of signal. In two cases, the signal light was equipped with a back plate. Table 6.1 summarizes the various configurations tested and the results obtained from the
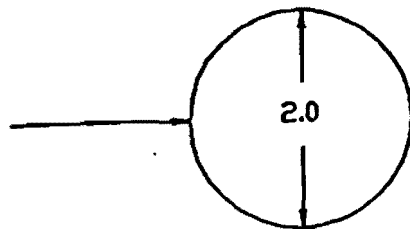
Octagonal Section
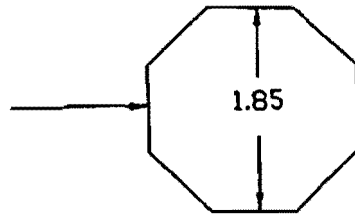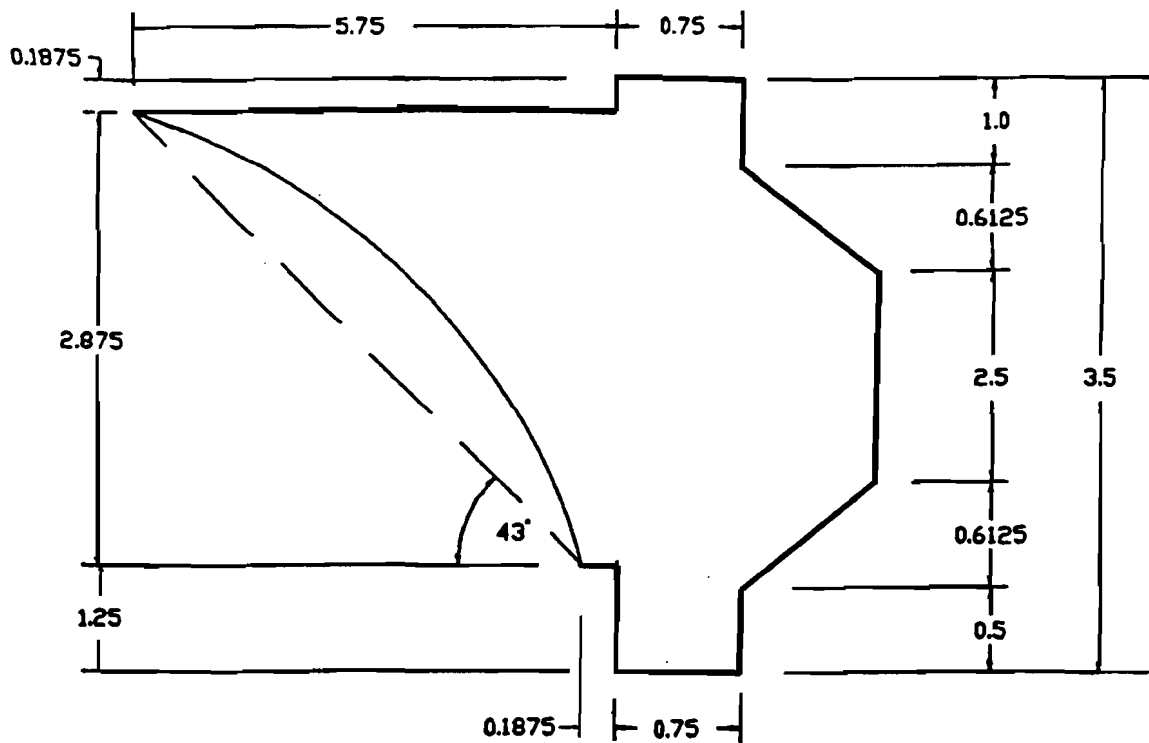

(a)   Flow Across Flat
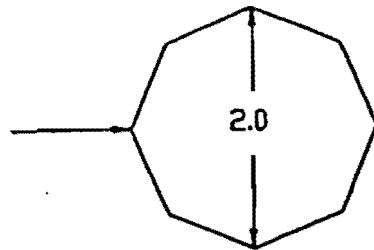
(b)   Flow Across Corner

Circular Section

(c)   Flow Across Cylinder

FIGURE 6.2   SIGNAL ARM SHAPES AND FLOW DIRECTIONS

78

Dimensions in inches (1.0 in. = 2.5 cm)
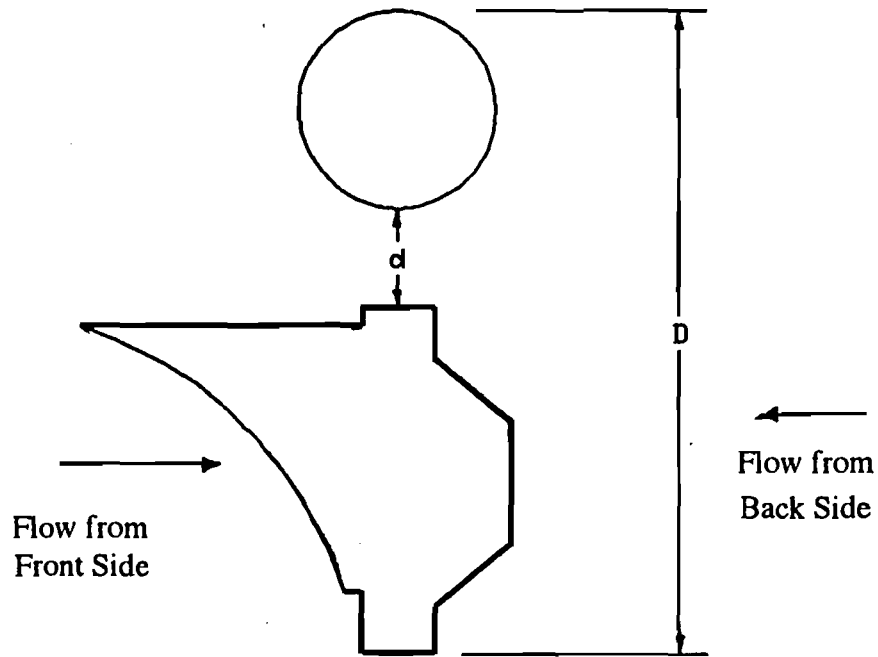
FIGURE 6.3. SIGNAL LIGHT MODEL FOR WATER TABLE EXPERIMENT
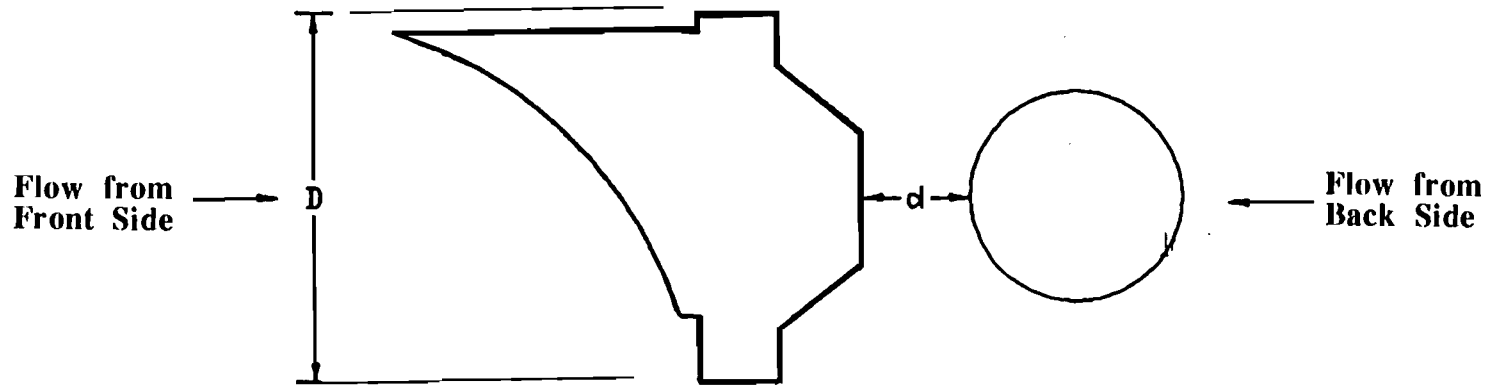
FIGURE 6.4   SIGNAL LIGHT HANGING BELOW SIGNAL ARM

Flow from Front Side → D

← d →

← **Flow from Back Side**

FIGURE 6.5 SIGNAL LIGHT AT SAME LEVEL AS SIGNAL ARM

Flow from
Front Side →

D

← Flow from
Back Side
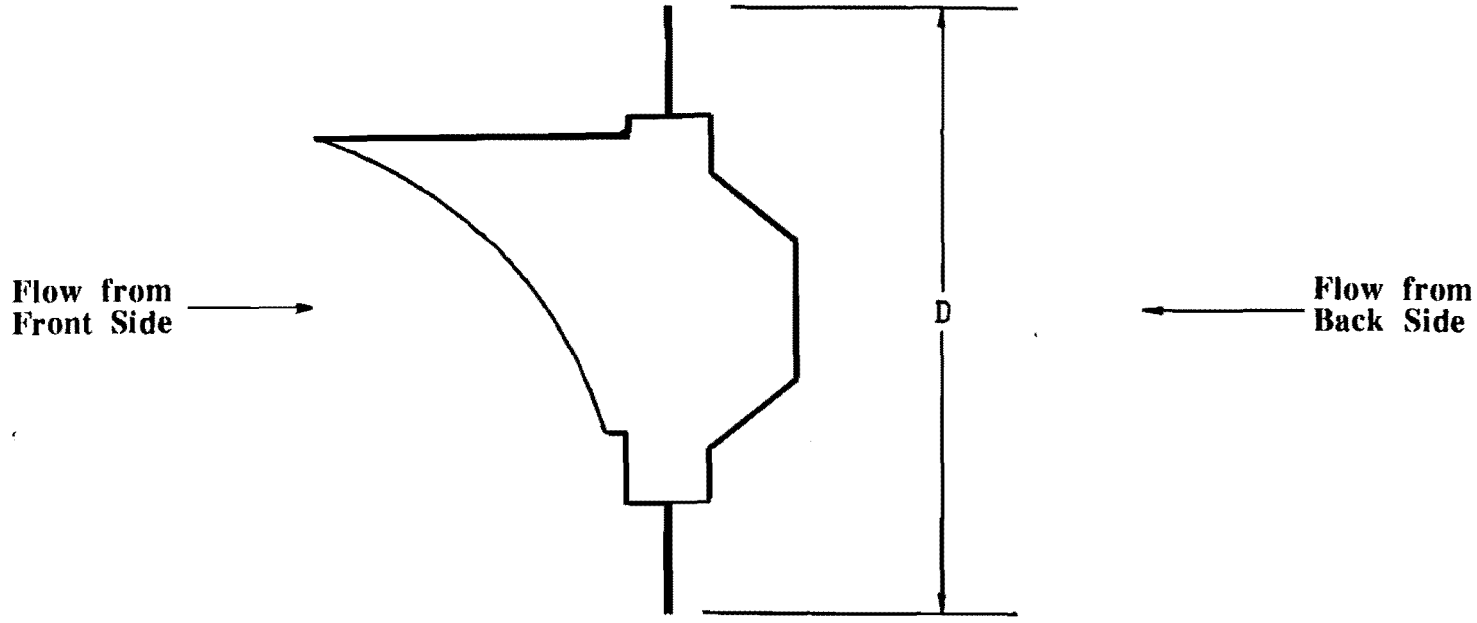
FIGURE 6.6. SIGNAL LIGHT WITH BACK PLATE

Flow from
Front Side

Flow from
Back Side

d

D
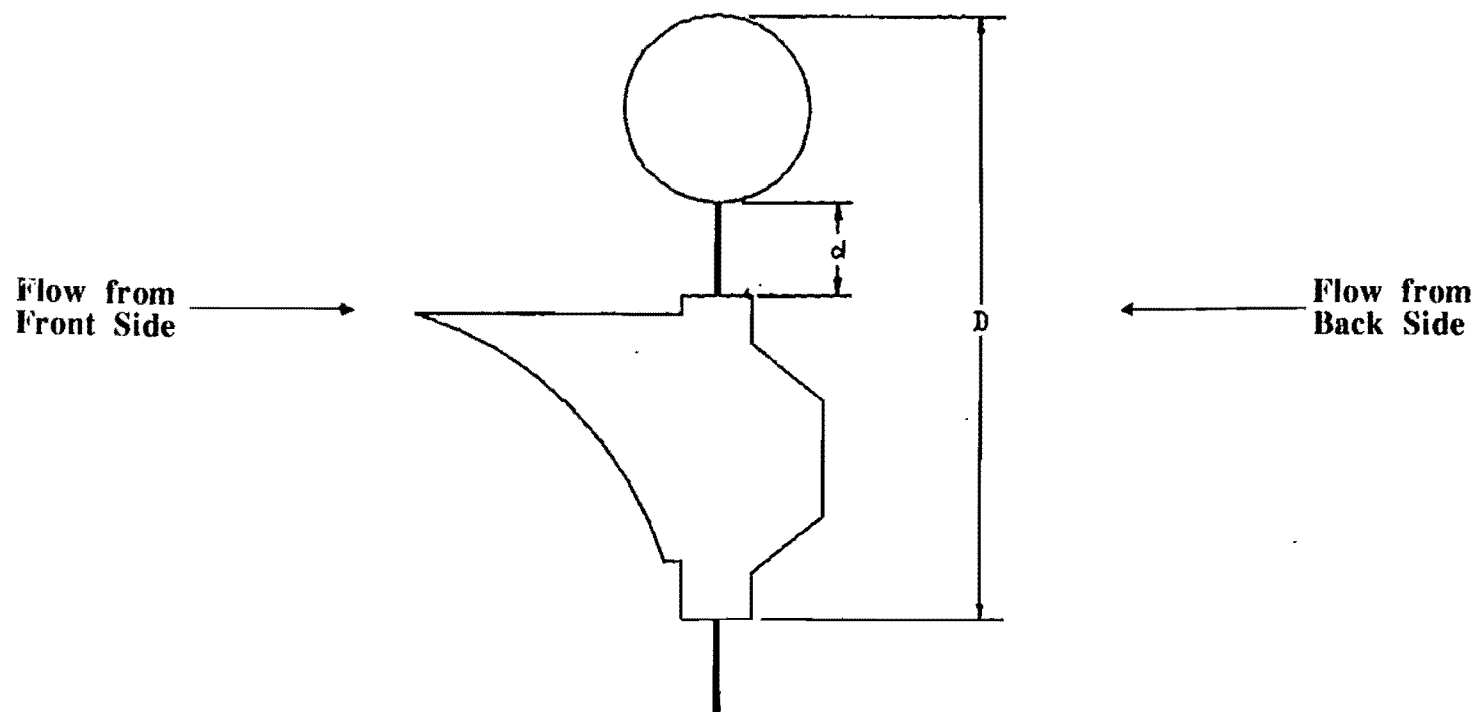
**FIGURE 6.7. SIGNAL LIGHT WITH BACK PLATE
HANGING BELOW SIGNAL ARM**

experiment. The Strouhal number for the circular cylinder alone from Table 6.1 is 0.202, which matches value obtained by Walshe and Wooten (1970) in the subcritical Reynolds number range (See Figure 7.1).

Figures 6.8 through 6.11 are reproduced from the video to give an idea of the vortex shedding phenomena. The data in Table 6.1 is used to calculate the equivalent vortex shedding frequency in air for wind speeds of 10 mph (4.5 m/s) and 20 mph (9.0 m/s).

The dimensionless Strouhal number for flow on the water table (model) is equal to the value in air (prototype), if scaling of the linear dimensions are taken into account. The Strouhal number, S_t, is given by

$$S_t = [(fD)/V]_{model} = [(f_a(4D))/V_a]_{prototype} \qquad (6.1)$$

Thus, the vortex shedding frequency in air is given by

$$f_a = (S_tV_a)/4D \qquad (6.2)$$

where

V_a = wind speed, in./sec

D = characteristic dimension, in.

The vortex shedding frequencies for each configuration tested are calculated for wind speeds of 10 mph (4.5 m/s) and 20 mph (9.0 m/s), as tabulated in Table 6.1 For the 10 mph (4.5 m/s) wind speed, the vortex shedding frequencies vary from 1.2 H_z to 4.5 H_z. For the 20 mph (9.0 m/s) wind speed, they range from 2.4 H_z to 8.9 H_z. Comparing these values with fundamental frequencies calculated for various cantilever signal structures in Table 4.1, it is clear that for a resonance condition, the vortex shedding frequencies need to be approximately equal to 1.0 H_z. Vortex shedding frequencies of 1.0 H_z occur at wind speeds less than 10 mph (4.5 m/s), which is not consistent with observations of vibrating signal structures in the field (see description of signal structure vibration characteristics in Section 1.2). Thus, the configurations tested could reach a resonance condition only if the wind speeds are 10 mph (4.5 m/s) or less.

TABLE 6.1
WATER TABLE EXPERIMENT RESULTS

Configuration	Separation d (in)	Reference Figure	Flow Direction	Velocity v (in/sec)	Frequency f (Hz)	Distance D (in)	Strouhal Number fD/v	Vortex shedding frequency in wind of 10 mph	Vortex shedding frequency in wind of 20 mph
Octagonal		2a	Face	7.7	0.67	1.92	0.167	3.8	7.7
Arm alone		2b	Corner	7.7	0.71	2	0.184	4.0	8.1
Circular Arm alone		2c	NA	7.52	0.76	2	0.202	4.5	8.9
Traffic Signal		3	Front	7.7	0.38	3.5	0.173	2.2	4.4
Alone			Back	7.7	0.30	3.5	0.135	1.7	3.4
Arm and Signal	1 in.	4	Front	7.65	0.37	6.5	0.314	2.1	4.3
	Vertical		Back	7.52	0.31	6.5	0.268	1.8	3.6
Arm and Signal	2 in.	4	Front	7.65	0.44	7.5	0.431	2.5	5.1
	Vertical		Back	7.65	0.30	7.5	0.294	1.7	3.5
Arm and Signal	3 in.	4	Front	7.53	0.43	8.5	0.485	2.5	5.0
	Vertical		Back	7.53	0.29	8.5	0.327	1.7	3.4
Arm and Signal	1 in.	5	Front	7.77	0.38	3.5	0.169	2.1	4.2
	Horizontal		Back	7.77	0.39	3.5	0.177	2.2	4.4
Arm and Signal	2 in.	5	Front	7.77	0.38	3.5	0.169	2.1	4.3
	Horizontal		Back	7.77	0.40	3.5	0.179	2.2	4.5
Arm and Signal	3 in.	5	Front	7.77	0.31	3.5	0.138	1.7	3.5
	Horizontal		Back	7.77	0.44	3.5	0.198	2.5	5.0
Signal Light Alone		6	Front	7.59	0.23	5.5	0.167	1.3	2.7
with back plate			Back	7.59	0.25	5.5	0.181	1.4	2.9
Signal with back plate	1 in.	7	Front	7.59	0.21	7.5	0.207	1.2	2.4
and arm	Vertical		Back	7.59	0.22	7.5	0.215	1.3	2.5

1.0 in. = 2.5 cm   1.0 mph = 0.45 m/s

Flow

→
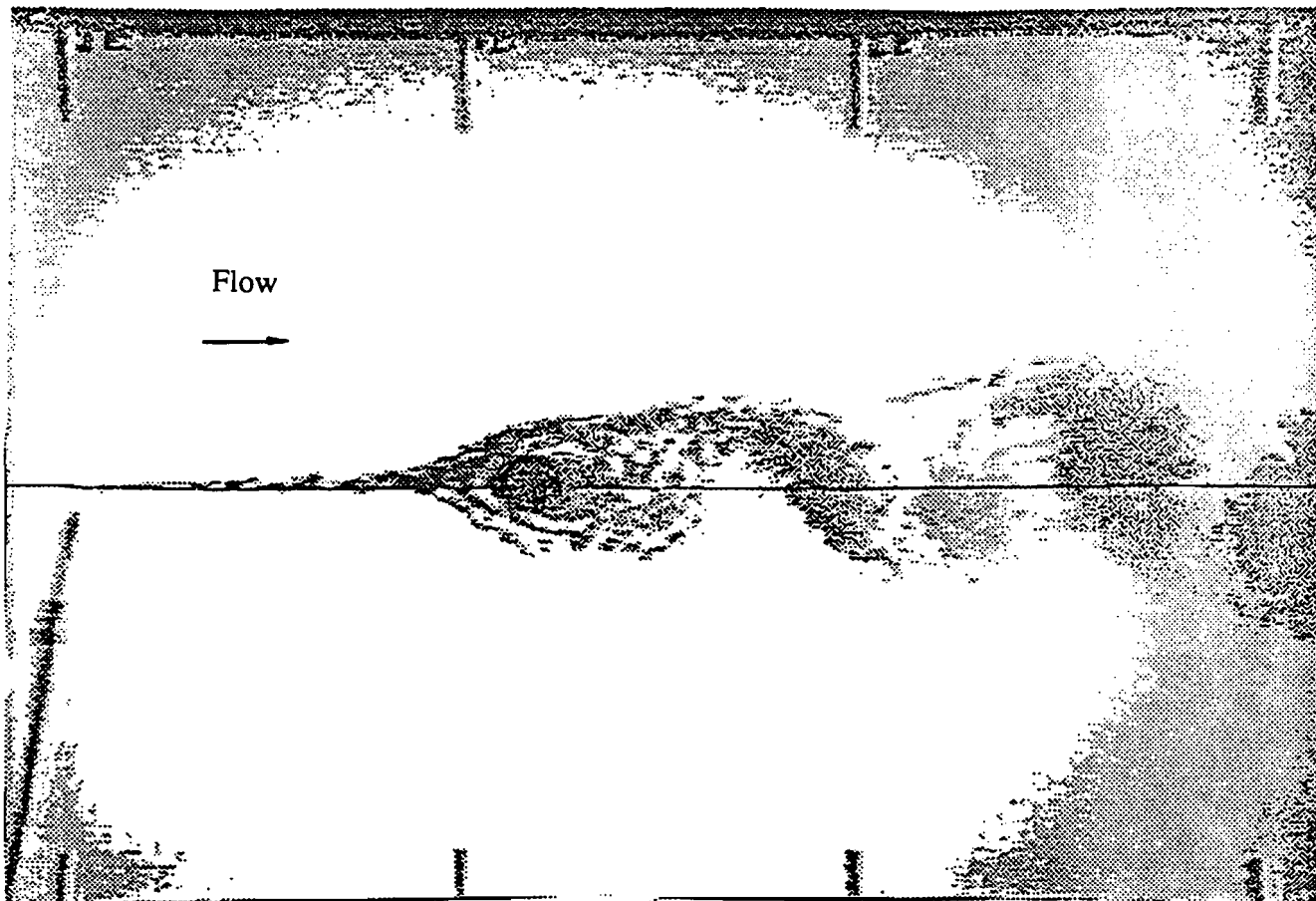
**FIGURE 6.8. FLOW VISUALIZATION: VORTEX SHEDDING
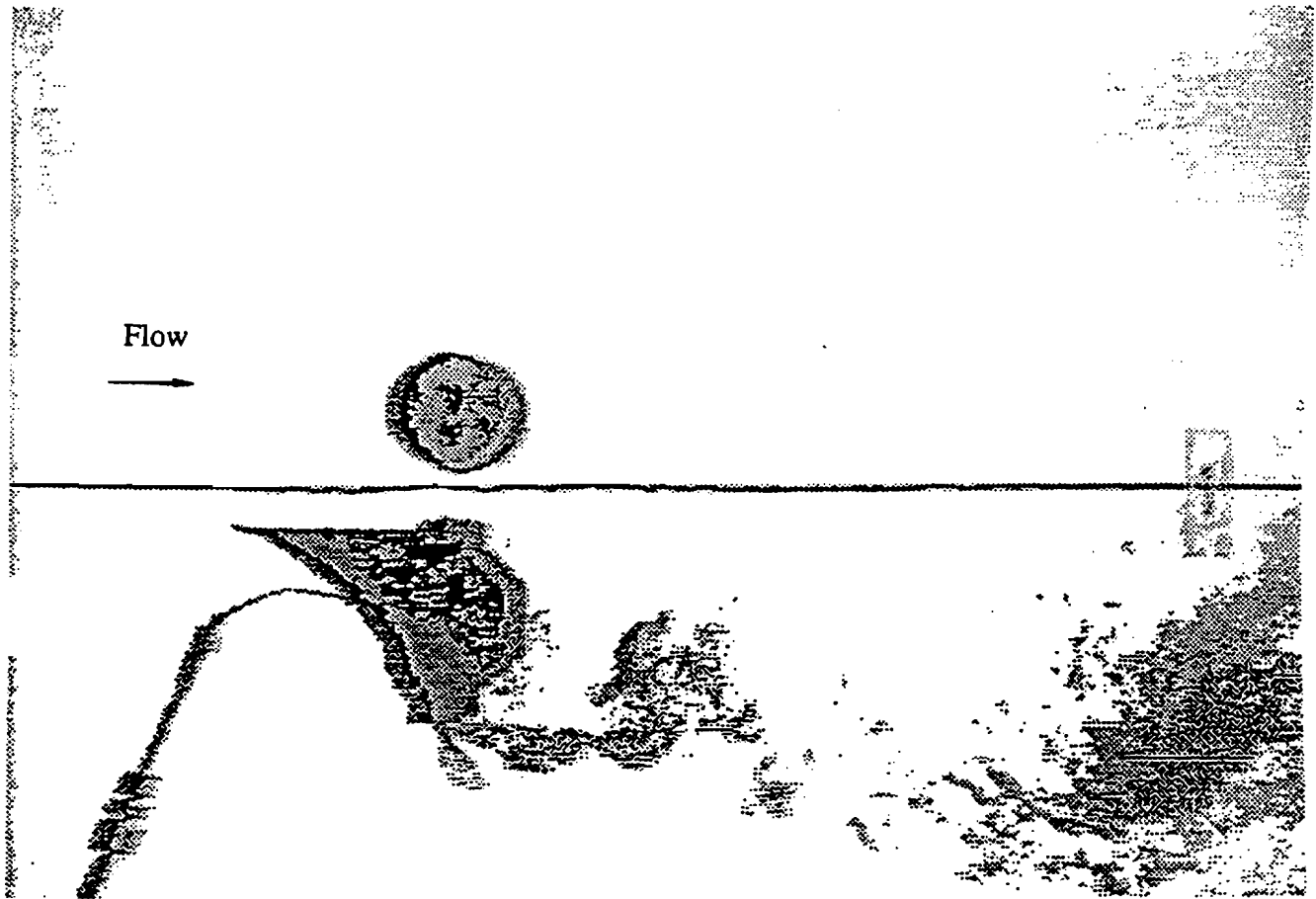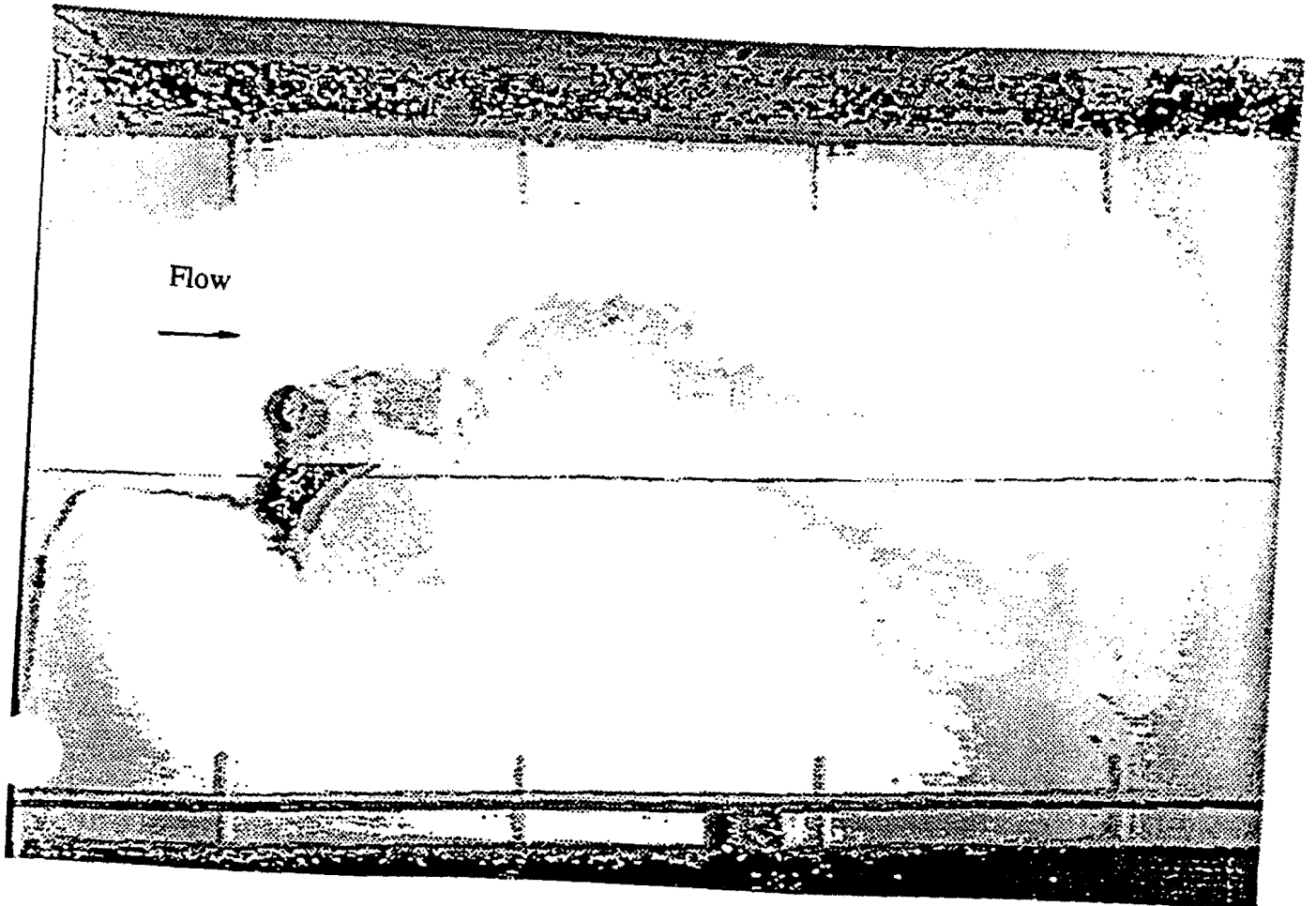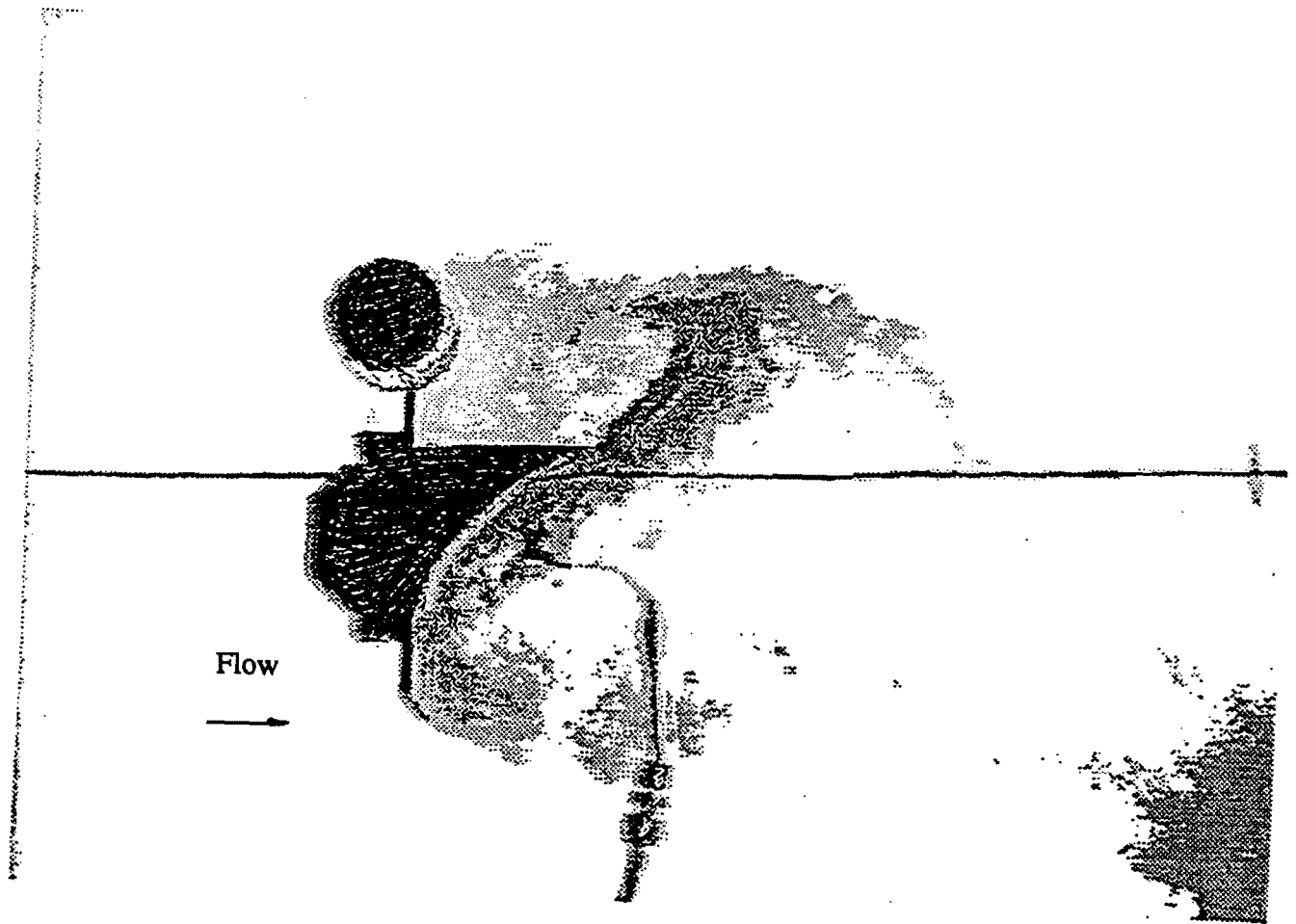AROUND A CIRCULAR ARM**

Flow →

FIGURE 6.9. FLOW VISUALIZATION: SIGNAL LIGHT BELOW ARM WITH FLOW FROM FRONT SIDE

Flow
→

FIGURE 6.10. FLOW VISUALIZATION: SIGNAL LIGHT BELOW ARM WITH FLOW FROM BACK SIDE

Flow →

FIGURE 6.11. FLOW VISUALIZATION: SIGNAL LIGHT WITH BACK PLATE BELOW ARM AND FLOW FROM BACK SIDE

6.4 Conclusions

The water table experiment yielded both qualitative and quantitative results. The flow visualizations gave a clear indication of how vortices are alternately shed from the signal arm and traffic light arrangements. The following conclusions can be stated:

(1) Strouhal numbers for circular cross sections obtained in this study match values in published literature.

(2) Strouhal numbers depend on the traffic signal and signal arm configurations and on the direction of flow.

(3) Traffic signal and signal arm configurations yielded vortex shedding frequencies greater than 1.0 H_z at wind speeds of 10 mph (4.5 m/s) or greater.

(4) The water table experiments demonstrated that vortex shedding is not the cause of large amplitude vibrations of cantilevered traffic signal structures.

Results from the water table experiments were then used to design the tow tank experiments.

7. TOW TANK EXPERIMENTS

7.1 Objectives

The primary objective of the tow tank experiments was to determine the source of the aerodynamic forcing which has been observed in field applications of traffic signals on cantilevered support arms. The two most likely candidates are vortex shedding and galloping. Separate experimental programs were developed to evaluate the significance of each of these phenomena. A flow visualization experiment was utilized to detect the occurrence of vortex shedding into the wake and to identify the shedding frequency. The potential for galloping of the traffic signals was evaluated by making steady state aerodynamic lift and drag measurements and applying the Den Hartog [1956] criteria for negative aerodynamic damping. Both the flow visualization and force measurements were performed for a variety of geometries of traffic signal heads with wind directions into the face and into the rear of the signals.

7.2 Tow Tank Facilities and Capabilities

Shown in Figure 7.1, the Texas Tech Tow Tank consists of a below-ground, water filled tank with overall dimensions of 80 ft (24 m) by 15 ft (4.6 m) and a 10 ft (3.0 m) water depth. Steel rails mounted above the water on either side of the tank support a motorized towing carriage which is used to propel a variety of models through the tank. The carriage also supports the computerized motion control and data acquisition systems and has adequate space for the operator and several observers. The carriage and supported models can be tested at preprogrammed speeds of 0-5 ft/s (0-1.5 m/s) with the capacity for accelerations of up to ± 2 ft/s^2 (± 0.6 m/s^2). Data acquisition systems include a high speed pressure measurement system, load cells for force and moment measurements, and several options for video taped flow visualization both above and below the water surface.

In general, the tow tank can be used for any incompressible aerodynamic study which might more typically be conducted in a wind tunnel. The 16:1 ratio of kinematic viscosity of air to
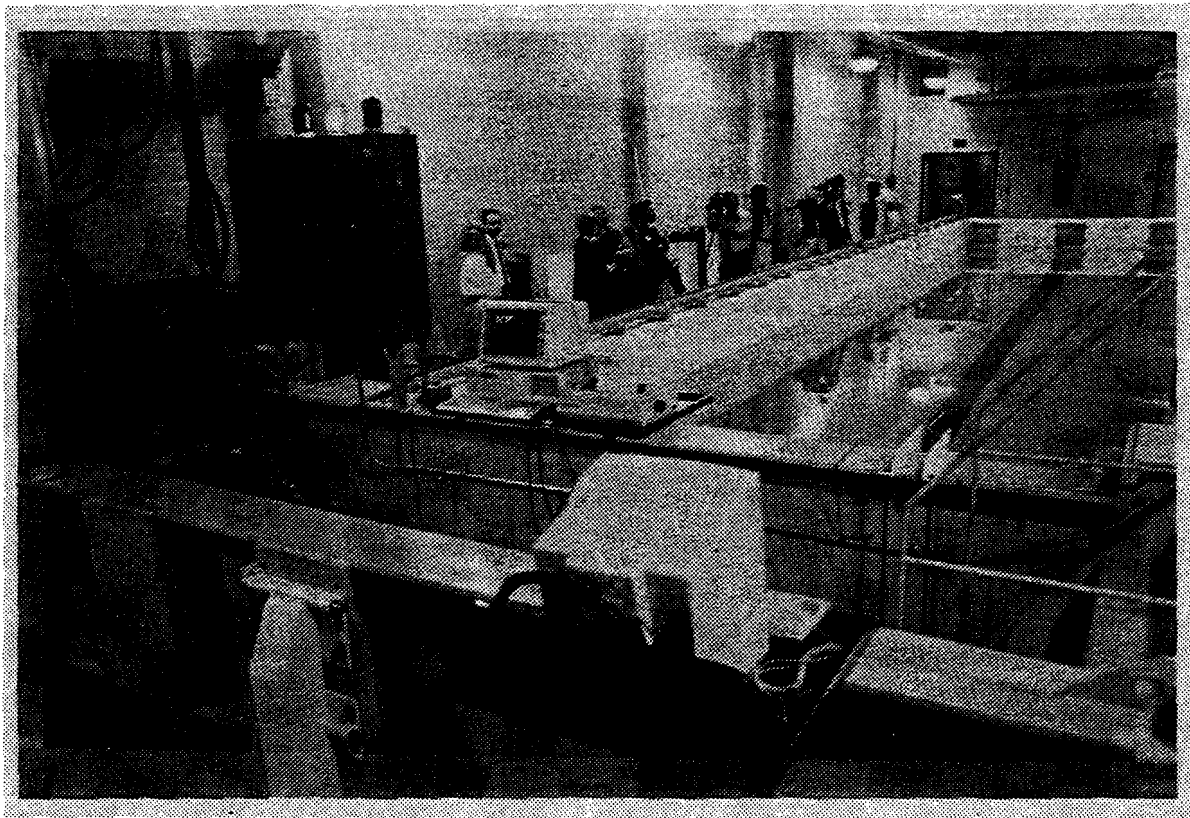
FIGURE 7.1. GENERAL VIEW OF TOW TANK

water allows tests of a specific model to be conducted at 1/16 the speed of an equivalent wind tunnel test at the same Reynolds number. This speed differential is particularly advantageous in flow visualization experiments involving time dependent model motion or transient phenomena. Water based flow visualization experiments are also enhanced through the use of dyes which do not diffuse over the flow field as rapidly as typically occurs with smoke in air. The tow tank is particularly suited to tests involving transient model velocities which are virtually impossible to duplicate in a wind tunnel. The Texas Tech Tow Tank has been successfully applied to research programs concerned with parachute, automotive, and wind turbine aerodynamics as well as the aerodynamic loadings on solar receivers and traffic signal lights.

7.3   Experimental Research Plan

A full-size, three-light traffic signal head was mounted on a 6 5/8 in. (16.8 cm) diameter steel pipe in several configurations. The steel pipe simulated the shape and size of the horizontal cantilever arm which is used to support traffic signals over road intersections. Figure 7.2 depicts the cross-sections of the test configurations viewed from the end of the horizontal arm. Configurations 1 through 4 are traffic signal options mounted without a back plate and configurations 5 through 8 are traffic signal options mounted with a 51 in. x 23 in. (130 x 58 cm) rectangular back plate. The back plate, typically black, is used to provide a contrasting background for the signal lights.

The signals were tested with flow from both the front and back. Hence, the configurations are matched pairs (1&2, 3&4, 5&6, 7&8) where the only difference is in the direction of the relative flow used in the experiment. Furthermore, configurations 1, 2, 5 and 6 are examples of signal heads mounted to hang below the horizontal arm. In configurations 3, 4, 7 and 8, the signal head is mounted in front of the horizontal arm (parallel to the ground) with respect to the arm. Because the blockage ratio of the traffic signal and arm relative to the tow tank was low, the flow field was assumed to be essentially two-dimensional. However, the flow at the ends of the traffic signal was expected to be three-dimensional and this characteristic was investigated during the flow

visualization experiment. No experiments were conducted in which the traffic signals were intentionally configured to experience spanwise flow -- along the axis of the supporting arm.

In addition to the traffic signal lights, the mounting pipe was used to test two other models, a damping plate and a square cylinder, as illustrated as Figure 7.3a and b, respectively . Like the traffic signal, the damping plate was an actual piece of TxDOT equipment. This configuration was used to determine if the damping plate does in fact provide positive aerodynamic damping to a traffic signal and to quantify the magnitude of this effect. The other model was an 8-ft (2.4-m) long sleeve with square cross-section which could be slid over the mounting pipe to present a square cross-section to the flow. This cross-section is known to be susceptible to galloping. It was used as a test geometry to validate the experimental force measurements obtained from the tow tank experiments.

Figure 7.4a depicts the relationship of the pipe-mounted traffic signal to the towing carriage in the tow tank. The traffic signal is shown in Configuration 1. Note that the pipe is mounted to the bridge and extends down into the water. A second mounting configuration used during the flow visualization, Figure 7.4b, used a pipe extension to place the signal underneath the bridge where clear video-tapes could be made through a plexiglass port.

7.3.1 Flow Visualization Tests

To determine the significance of vortex shedding from traffic signal heads and the corresponding Strouhal numbers, dye was injected at up to twenty locations around the mounting pipe and signal head. The dye ports were turned on in various combinations and video-tapes were made of the resulting flow field. Small-scale turbulence features were most apparent when dye was injected close to the pipe and traffic signal. Conversely, the primary vortex frequency was more easily observed when dye was injected approximately two characteristic diameters downstream of the model (characteristic diameter is the largest cross-stream dimension of the model). Furthermore, by placing dye ports in the middle and on the ends of the traffic signal, three-dimensional features of the flow were investigated. Repeated experimental runs and dye port adjustments were made for each of the Configurations 1 through 8 (see Figure 7.2), to obtain the
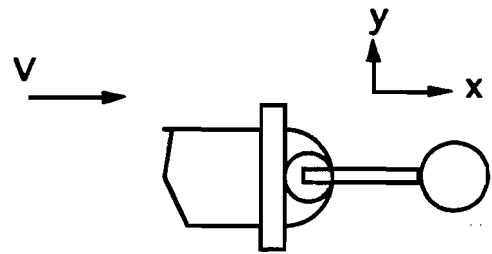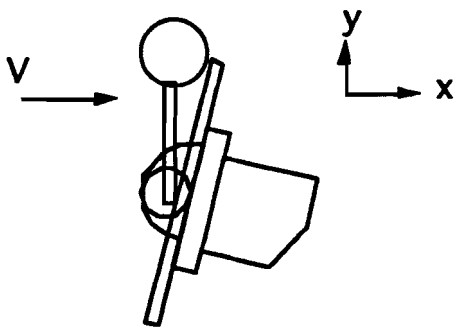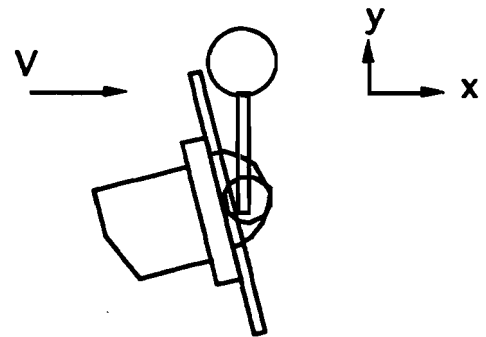
94
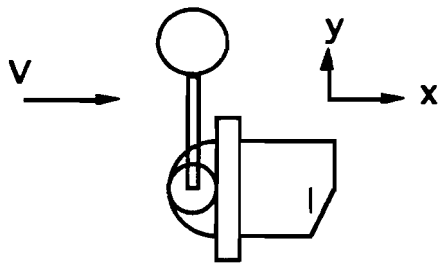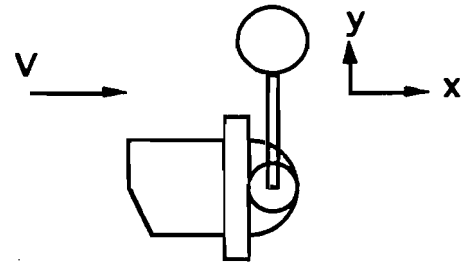
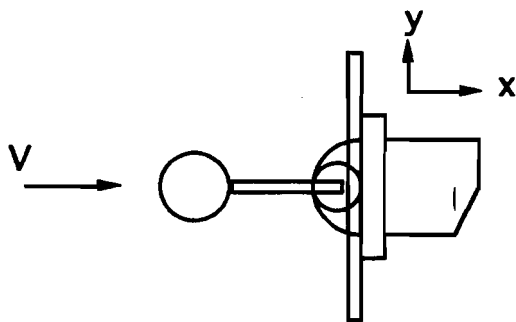(a) Configuration 1   (b) Configuration 2
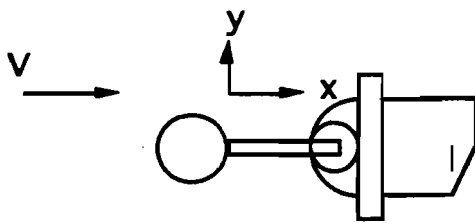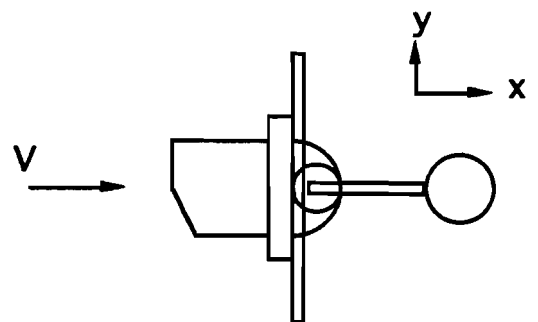
(c) Configuration 3   (d) Configuration 4

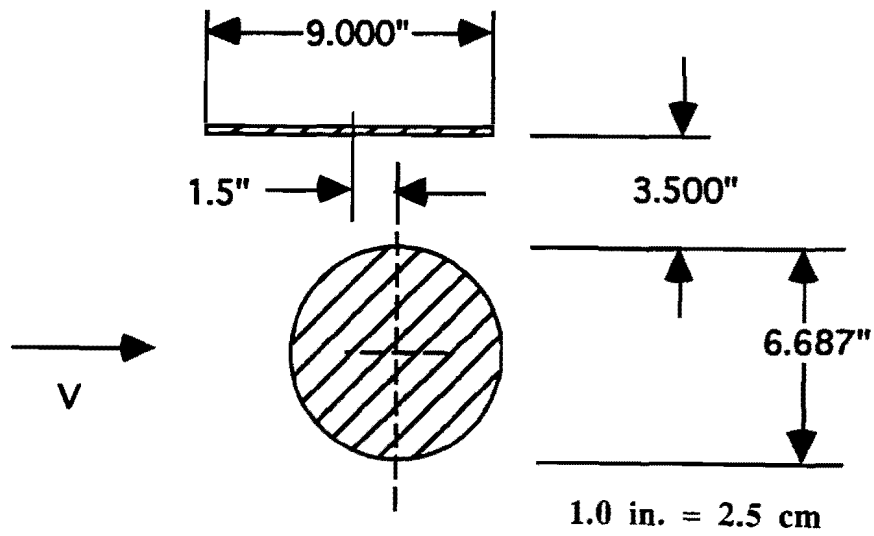(e) Configuration 5   (f) Configuration 6
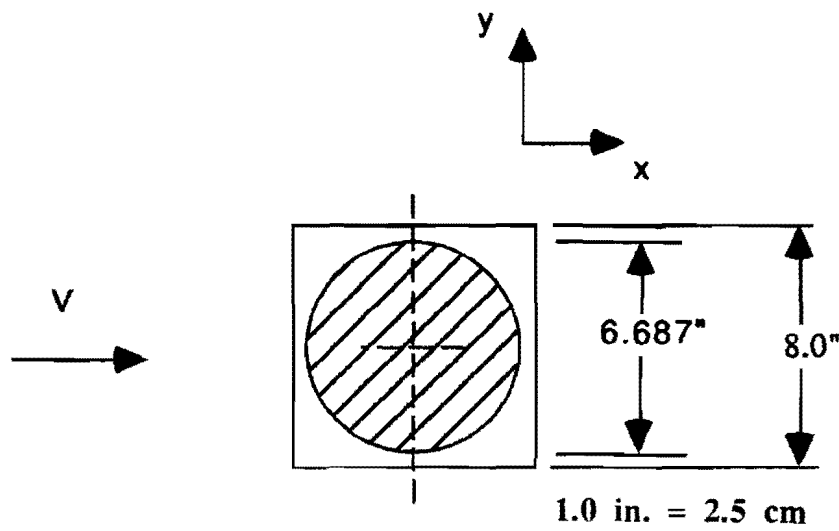
(g) Configuration 7   (h) Configuration 8

FIGURE 7.2. TRAFFIC SIGNAL CONFIGURATIONS FOR TOW TANK EXPERIMENTS
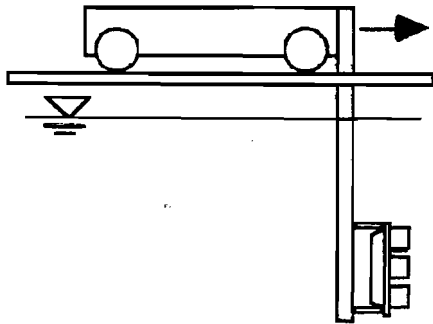
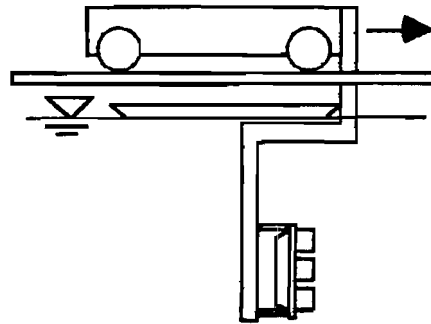(a)   Damping Plate Configuration

(b)   Square Cylinder Configuration

FIGURE 7.3. TWO MODELS TESTED IN TOW TANK

(a) Configuration for
Force Measurements

(b) Configuration for Flow
Visualization Tests

FIGURE 7.4. TOW CARRIAGE MOUNTING CONFIGURATIONS

best visualization of the vortex features. Over three hours of video-tape recordings were made during the flow visualization portion of the experiment. When a dye port location successfully captured periodic flow reversals which could be studied to obtain the vortex shedding frequency, the video-tape of that experimental run was analyzed frame-by-frame on a video editor. The number of video frames between flow reversals is proportional to the period of that flow feature and can be used to compute the Strouhal number. These results generally confirmed values obtained from the water table experiments.

7.3.2 Force Measurements

Force measurements were made by attaching the mounting pipe to a force balance which simultaneously measured the lift, drag, and side forces. For the orientation of the model shown in Figure 7.4, the drag is the force acting on the model in the free stream direction, the lift is an axial force aligned with the mounting pipe, and the side force acts perpendicular to the plane defined by the mounting pipe and the free stream velocity vector. This side force is the driving force of interest for the signal structure vibration study. In a field experiment or during normal operation, this direction would correspond to the vertical or the direction commonly associated with lift.

The traffic signal mounting arm was connected to the balance by a coupler which could vary the angle of attack of free stream flow relative to the traffic signal. Static angles of attack, as depicted in Figure 7.5, simulate the conditions experienced by an object subject to galloping. In Figure 7.5 V_x is analogous to the wind velocity which is aligned with the ground and the x-axis of the traffic signal. The x-y axis is always attached to the model and indicates that in simple galloping, all motion is in the y-direction (pure plunging). Therefore, the angle between the wind and the model is always zero. However, the motion of the model in the y-direction (V_y) results in an induced angle of attack. The relative velocity, V_{rel}, is the vector sum of V_x and V_y. It is also the velocity produced by the tow tank ($V_{rel} = V_{tank}$). The angle of attack, α, is measured between the x-axis and V_{rel}. In other words, when the simulated motion of the model is in the negative y-direction, a positive induced velocity of V_y results in a positive angle of attack.
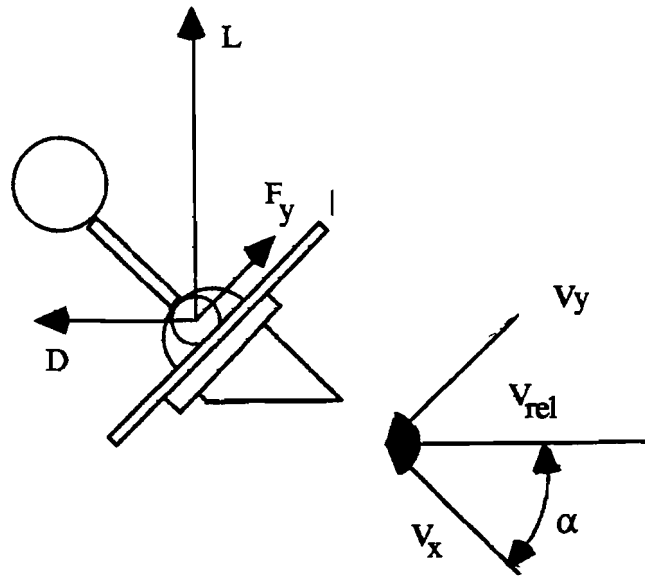
98

FIGURE 7.5. VELOCITY, ANGLE OF ATTACK AND FORCE COMPONENT DEFINITIONS

The force of interest in galloping applications is in the y-direction because this is the force which either dampens or drives the motion of the model. Therefore, the coefficient, C_{Fy}, must be computed. The necessary equations are as follows (refer to Figure 7.5):

$$V_x = V_{rel}\cos\alpha \qquad (7.1)$$

$$F_y = L\cos\alpha + (D-Dtare)\sin\alpha \qquad (7.2)$$

$$C_{Fy} = \frac{F_y}{1/2\rho V_x^2 A} \qquad (7.3)$$

where A is the signal area, and D_{tare} is the drag on the pipe with no traffic signal mounted on it.

The tow tank was operated at 1 fps (2.5 cm/s) for 50 seconds and 2000 data points were collected for each angle of attack tested. The first 4 seconds of data were discarded to avoid acceleration dynamics and the average force was computed for each axis. Finally, the coefficient of force in the y-direction was computed. This procedure was completed for each of the 8 traffic signal configurations, the damping plate and the square cross-section. In addition, several repeatability experiments were conducted to ensure the following: (1) repeatability and accuracy of the measurements over long periods of time and over several duplicate experimental runs, (2) repeatability of the angle of attack measurements when the model was removed and reinstalled, (3) repeatability of the force measurements when the model was removed, disassembled, reassembled and reinstalled, and (4) repeatability of the balance calibration after several experiments.

7.4   Data and Interpretation

7.4.1 Vortex Shedding

Table 7.1 contains the quantitative results of the flow visualization portion of the experiment. The result of $S_t=0.19$ for the circular cylinder closely agrees with that of other researchers (see Figure 1.1). While the periodic vortices shed from the simple cylinder were easy to see, large amounts of video had to be reviewed to find useful data for most of the signal head

TABLE 7.1

STROUHAL NUMBER FOR TRAFFIC SIGNAL CONFIGURATIONS AND A CIRCULAR CYLINDER AT SUBCRITICAL REYNOLDS NUMBER

Configuration *	Average S_t	No. of Runs	Range of S_t	Range of Variances	Reynolds Number
1	0.205	9	0.13-0.26	0.03-0.15	2×10^5
2	0.197	6	0.15-0.28	0.03-0.08	2×10^5
4	0.222	4	0.21-0.24	0.05-0.08	1.1×10^5
Cylinder	0.190	1	0.19	0.04	2.8×10^5

*See Figure 7.2 for configuration details.

configurations. In general, even though the flow velocity was well within the subcritical Reynolds number range, the flow was very disorganized. The variety of edges and corners on the traffic signals produced a complex turbulent flow field in which identification of a dominant shedding frequency was difficult. Overall, the shedding frequencies of Configurations 1, 2, and 4 presented in Table 7.1 are at the high end of those expected from the review of research performed on simple cylinders and squares. However, previous research has shown that increased surface roughness, short aspect ratios and three-dimensionality all tend to produce more random and frequent vortex shedding. Compared to a simple long cylinder or square, traffic signals display all three characteristics and could therefore be expected to have higher Strouhal numbers.

Randomness and high frequency are characteristics that make vortex shedding from traffic signal heads an unlikely candidate to produce significant wind-driven oscillations. First, random and disorganized vortex shedding is less energetic and thus less able to sustain significant oscillations. Second, a relatively high shedding frequency implies that the required lock-in wind velocity for signal heads would be around 5 mph (2.2 m/s). Since the lock-in velocity is relatively low, the driving forces would also be low.

7.4.2 Galloping

The force coefficients for the eight traffic signal configurations, the square cross-section cylinder, and the damping plate are tabulated for various angles of attack in Table 7.2. Plots of the force coefficient data are presented and discussed below.

Figure 7.6 depicts the results for C_{Fy} versus angle of attack for a square cross-section cylinder. A comparison to Figure 1.2 indicates that they are very similar to those obtained by other researchers. This significantly increases the level of confidence in results produced by the force measurement portion of this experiment. Notice in Figure 7.6 that $dC_{Fy}/d\alpha < 0$ for angles of attack less than 10°. This is a classic result for an object that experiences aerodynamic forces aligned with its direction of motion when initially disturbed in a direction perpendicular to the freestream velocity, i.e., for an object exhibiting negative aerodynamic damping. The negative slope for C_{Fy}

TABLE 7.2

C_{Fy} FOR TRAFFIC SIGNAL CONFIGURATIONS
SQUARE CYLINDER AND DAMPING PLATE

| Angle of Attack (degrees)	Traffic Signal Configurations								Square Cylinder	Damping Plate
	1	2	3	4	5	6	7	8		
-45	-0.46	-1.52	-0.75	-0.30	0.58	-0.07	-1.70	0.23	-0.24	-1.70
-40	-0.45	-1.27								
-35	-0.36	-0.91								-1.32
-30	-0.23	-0.67				-0.07		0.12		
-25	-0.10	-0.44			0.58	0.06	0.24	0.15		-0.93
-20	0.08	-0.21	-0.75		0.48	0.13	0.23	0.20		-0.72
-15	0.10	-0.01	-0.51	-0.30	0.36	0.20	0.14	0.21		-0.39
-10	0.18	0.15	-0.33	-0.90	0.28	0.28	0.16	0.19		-0.04
-7.5	0.23	0.14	-0.40	0.17	0.21	0.28	0.05	0.17		
-5.0	0.26	0.21	-0.25	0.23	0.19	0.33	0.07	0.15		0.40
-2.5	0.33	0.23	-0.22	0.40	0.12	0.36	0.01	0.12		
0.0	0.32	0.27	-0.02	0.45	0.10	0.39	0.10	0.10	0.0	0.96
2.5	0.46	0.30	0.24	0.62	0.03	0.37	0.11	0.13	-0.12	
5.0	0.43	0.22	0.38	0.56	-0.05	0.37	0.17	0.13	-0.24	1.40
7.5	0.51	0.26	0.54	0.66	-0.07	0.38	0.22	0.19	-0.42	
10	0.52	0.28	0.50	0.59	-0.10	0.36	0.17	0.14	-0.46	1.68
15	0.53	0.15	0.46		-0.26	0.47	0.07	0.15	-0.26	1.82
20	0.52	0.25	0.64		-0.36	0.45	-0.01	0.23	0.33	1.83
25	0.45	0.57			-0.49	0.57	-0.05	0.24	0.76	1.04
30	0.59	0.72				0.64	-0.14	0.26	1.21	
35	0.45	0.84							1.57	
40	0.35	0.69							1.66	
45	0.19	1.02							2.31	
Figure	3.2	3.3	3.4	3.5	3.6	3.7	3.8	3.9	3.1	3.10
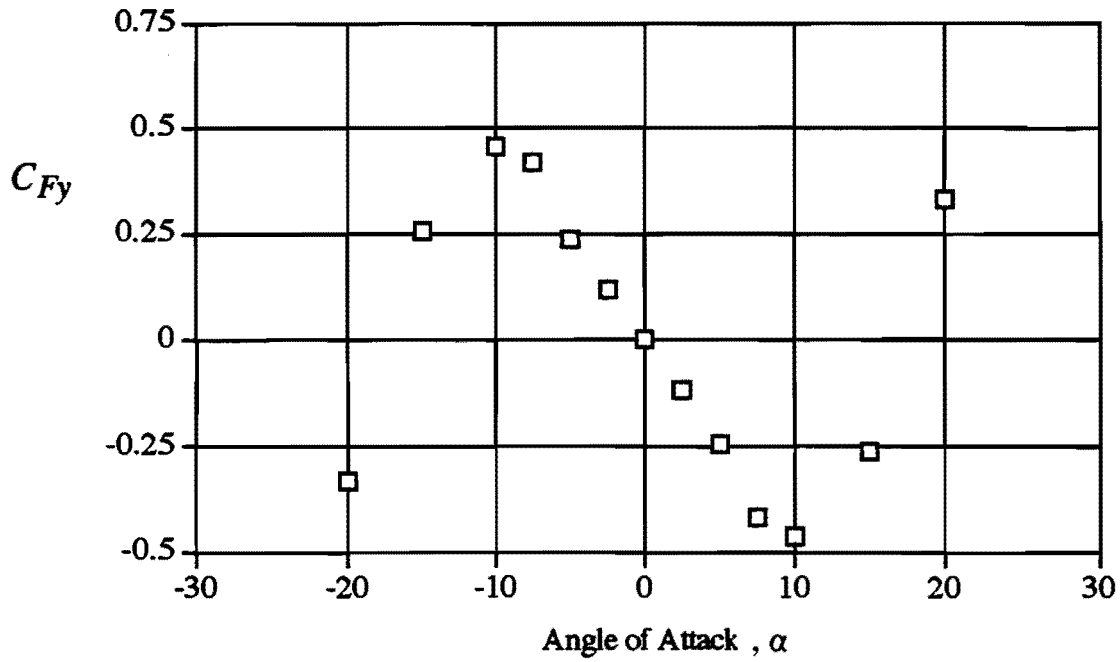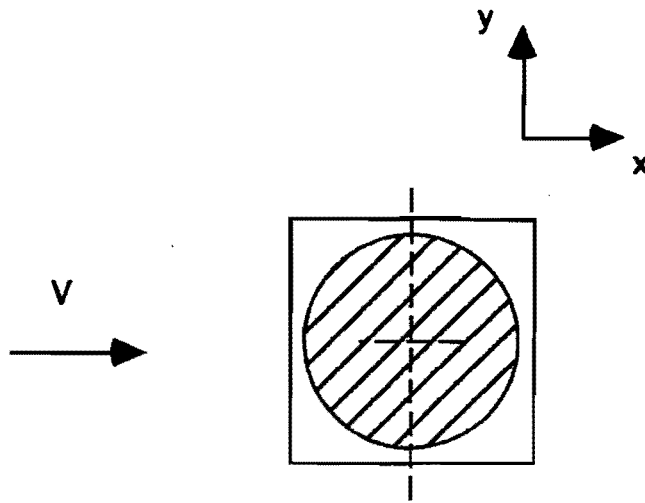
FIGURE 7.6 C_{Fy} **VERSUS ANGLE OF ATTACK FOR A SQUARE CYLINDER**

indicates that the aerodynamic forces are destabilizing and the model is susceptible to galloping oscillations.

Figure 7.7 depicts the results for C_{Fy} versus angle of attack for traffic signal Configuration 1. The slope for $\alpha < 7.5$ is positive which means that for all displacements where the signal head is moving up (positive y and negative α) the forces would be stabilizing and oppose the motion. For $7.5 < \alpha < 30$, the aerodynamic forces are neutrally stable. However, significant motion of the signal head would have to occur before a positive angle of attack of 30° could occur. In addition, when the signal head was rebounding from its deflected position, negative angles of attack would occur and result in damping forces.

Although Configuration 1 possesses positive aerodynamic damping and is not susceptible to galloping, it is, however, prone to buffeting in wind gusts. From Figure 7.7, it may be noted that $C_{Fy} = 0.3$ at zero angle of attack. Thus, a vertical force is generated whenever a wind gust occurs which causes the traffic signal to lift momentarily. After the gust subsides, the traffic signal head goes through a period of essentially free vibrations with a combination of material and aerodynamic damping. The vibratory response will be prolonged if the signal head is tilted downwards by 15° to improve visibility of the signal from the ground. Relative to this initial orientation, the slope of the C_{Fy} is essentially zero giving the signal head neutral aerodynamic stability.

Figure 7.8 depicts the results for C_{Fy} versus angle of attack for traffic signal Configuration 2. The signal head is positively stable ($dC_{Fy}/d\alpha > 0$) in galloping for $\alpha < -10$ and $\alpha > 20$. Also, it is neutrally stable in galloping but gust sensitive for $-10 < \alpha < 20$. In this case, if the signal head were installed at negative 15°, it would be more stable and readily visible from the road. It may be noted, however, that this configuration is the most gust sensitive when the wind is coming from the back of the signal head (i.e., Configuration 1). Therefore, the type of signal head used in Configurations 1 and 2, when located below the support arm could be installed in such a manner to
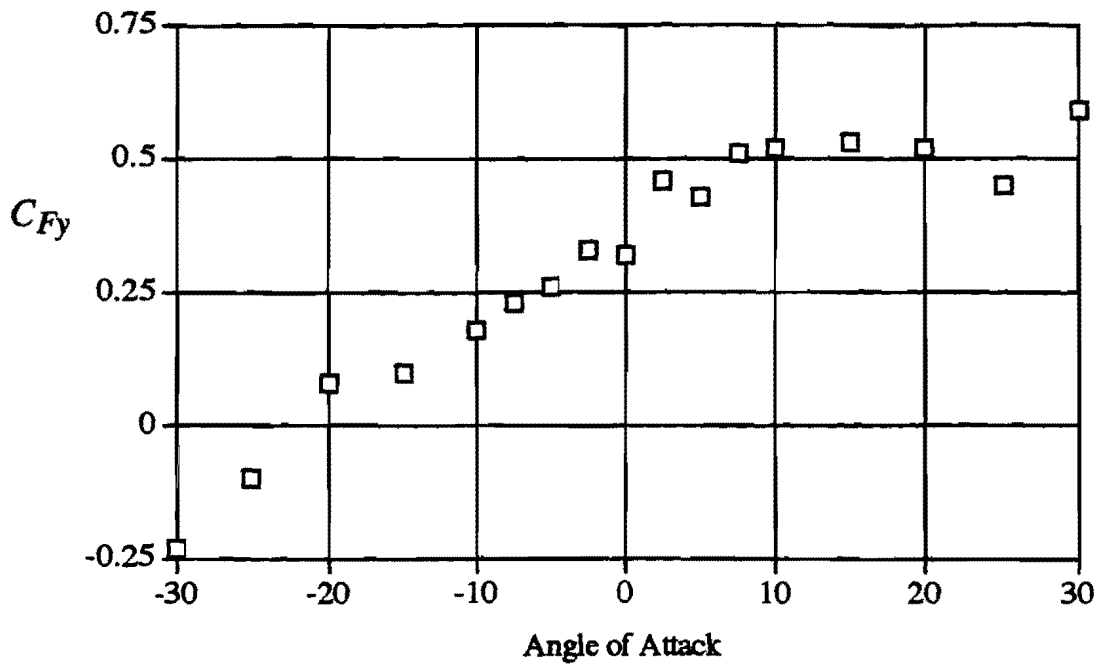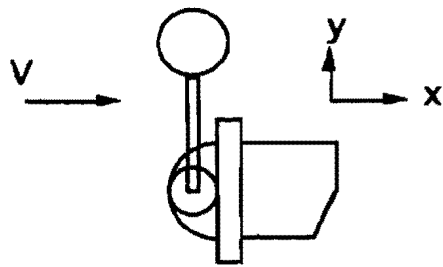
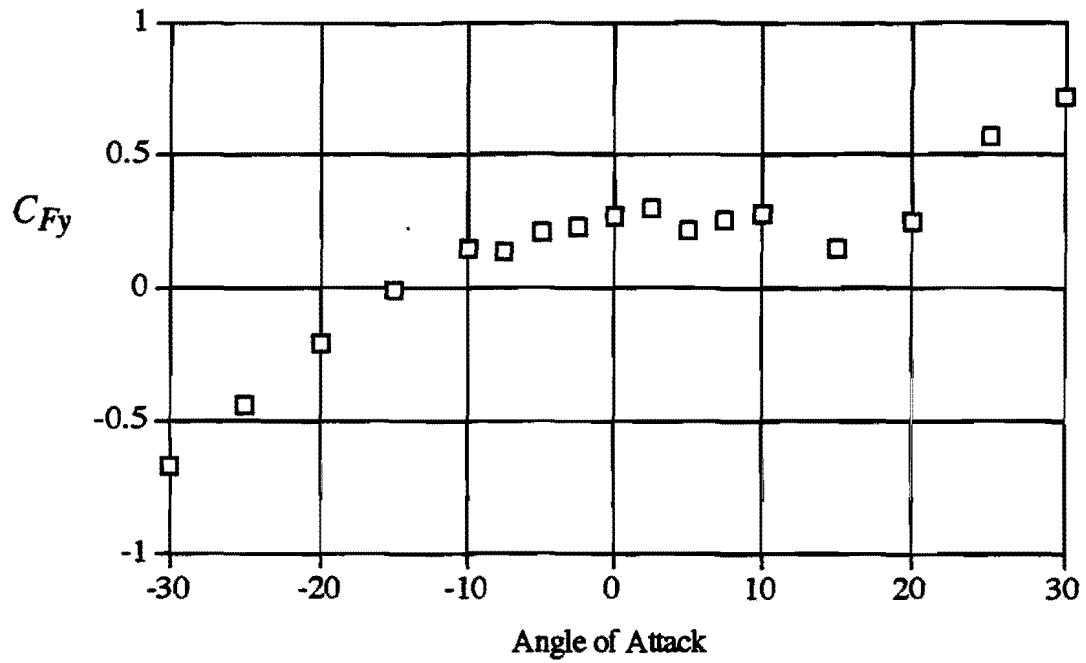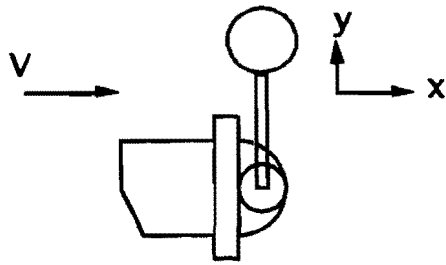FIGURE 7.7. C_{Fy} VERSUS ANGLE OF ATTACK FOR TRAFFIC SIGNAL CONFIGURATION 1

FIGURE 7.8. C_{FY} VERSUS ANGLE OF ATTACK FOR
TRAFFIC SIGNAL CONFIGURATION 2

be stable when the wind is coming from the front of the light (Configure 2) but very gust sensitive when the wind comes from the back of the light (Configure 1).

Figure 7.9 depicts the results for C_{Fy} versus angle of attack for traffic signal Configuration 3. This configuration is very stable. Gust sensitivity is low because $C_{Fy\,(\alpha=0)} = 0$. Galloping susceptibility is low because $dC_{Fy}/d\alpha>0$. However, the region of $7.5<\alpha<15$ is relatively flat. Therefore, if the signal light were mounted at $+12.5°$ angle of attack it would be more gust sensitive and have a very narrow band of galloping potential.

Figure 7.10 depicts the results for C_{Fy} versus angle of attack for traffic signal Configuration 4. This configuration is gust sensitive with $C_{Fy(\alpha=0)} = 0.45$. Also, $dC_{Fy}/d\alpha-= 0$ for $2.5<\alpha<10$ which suggests neutral dynamic stability. Therefore, if Configuration 4 were mounted in the field at a positive angle of attack of 5 to 10 degrees, it would be undamped for gust induced oscillations. A solution would be to mount it at $-10°$ angle of attack which would improve the viewing angle from the street, reduce the gust sensitivity to zero, and add positive dynamic stability. However, this would correspond to a $+10°$ angle of attack installation for Configuration 3, which would shift its curve to the left making its performance very similar to the unadjusted Configuration 4.

Figure 7.11 depicts the results for C_{Fy} versus angle of attack for traffic signal Configuration 5. This configuration is slightly gust sensitive with $C_{Fy}(\alpha=0) = 0.10$. However, $dC_{Fy}/d<0$ for all α which indicates that this configuration is dynamically unstable and would have a definite tendency to gallop. A possible excitation mode for any observed galloping of Configuration 5 could be its slight gust sensitivity. Of all configurations tested, Configuration 5 clearly has the greatest susceptibility to galloping and should be avoided in field applications when possible.

FIGURE 7.9. C_{FY} VERSUS ANGLE OF ATTACK FOR
TRAFFIC SIGNAL CONFIGURATION 3

FIGURE 7.10. C_{FY} VERSUS ANGLE OF ATTACK FOR
TRAFFIC SIGNAL CONFIGURATION 4

The signal was installed with 15 degrees of tilt because of interference between the back plate and the mounting pole.
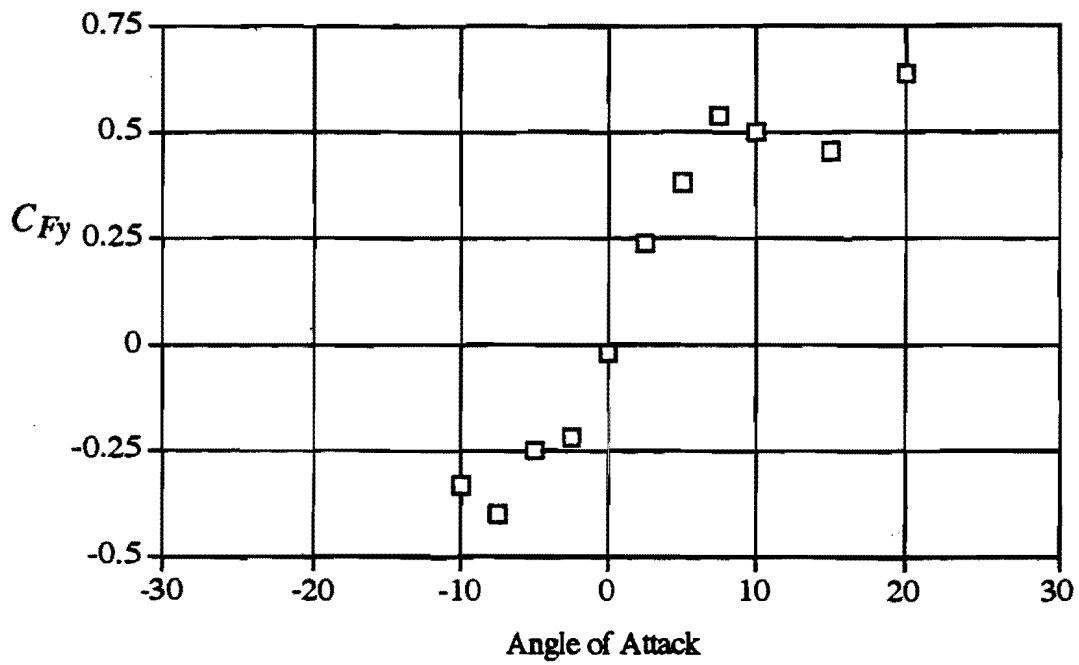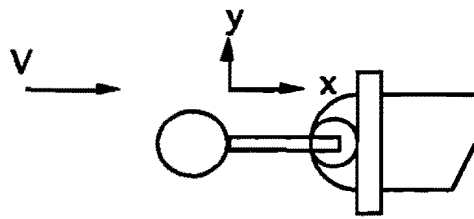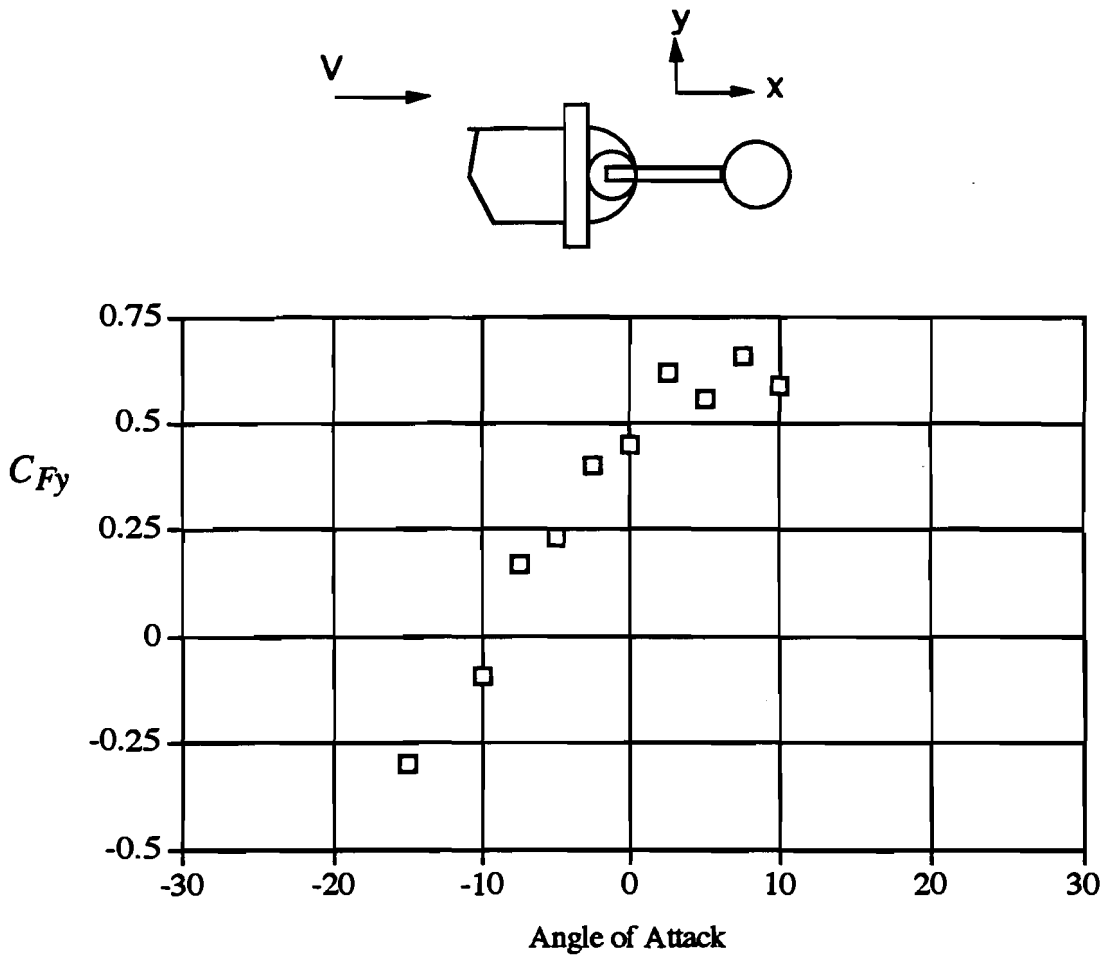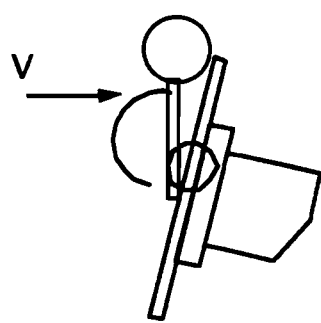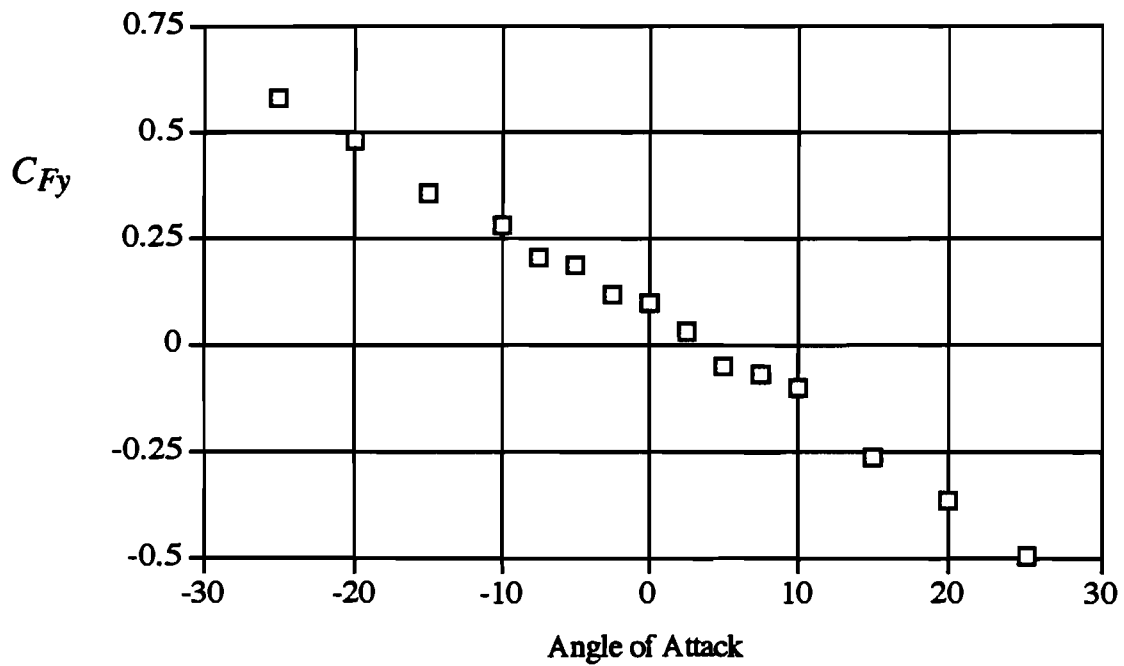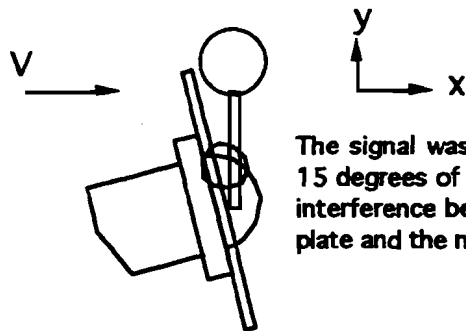
FIGURE 7.11. C_{FY} VERSUS ANGLE OF ATTACK FOR TRAFFIC SIGNAL CONFIGURATION 5

Figure 7.12 depicts the results for C_{Fy} versus angle of attack for traffic signal Configuration 6. This configuration is gust sensitive with $C_{Fy}(\alpha=0) = 0.39$. In addition, $dC_{Fy}/d\alpha>0$ for $0<\alpha<10$ which indicates a region of neutral dynamic stability. Therefore, if Configuration 6 were installed at a positive angle of attack of approximately 5 degrees, gust induced oscillations would not be positively damped. This condition is very likely in the field since the mounting hardware available for this experiment required the researcher to simulate a 15 degree tilt of the signal head towards the street. If field installations had only 10 degrees of tilt towards the street then Configuration 6 would have the maximum possible gust sensitivity and Configuration 5 would still tend to gallop.

The results for C_{Fy} versus angle of attack for traffic signal Configurations 7 and 8 are presented in Figures 7.13 and 7.14, respectively. The dynamic stability for these configurations is essentially neutral with $dC_{Fy}/d\alpha$ approximately equal to zero.

Figure 7.15 depicts the results for C_{Fy} versus angle of attack for a damping plate. This configuration has positive dynamic stability, $dC_{Fy}/d\alpha>o$. Therefore, it is potentially an effective anti-galloping device.

The signal was installed with 15 degrees of tilt because of interference between the back plate and the mounting pole.
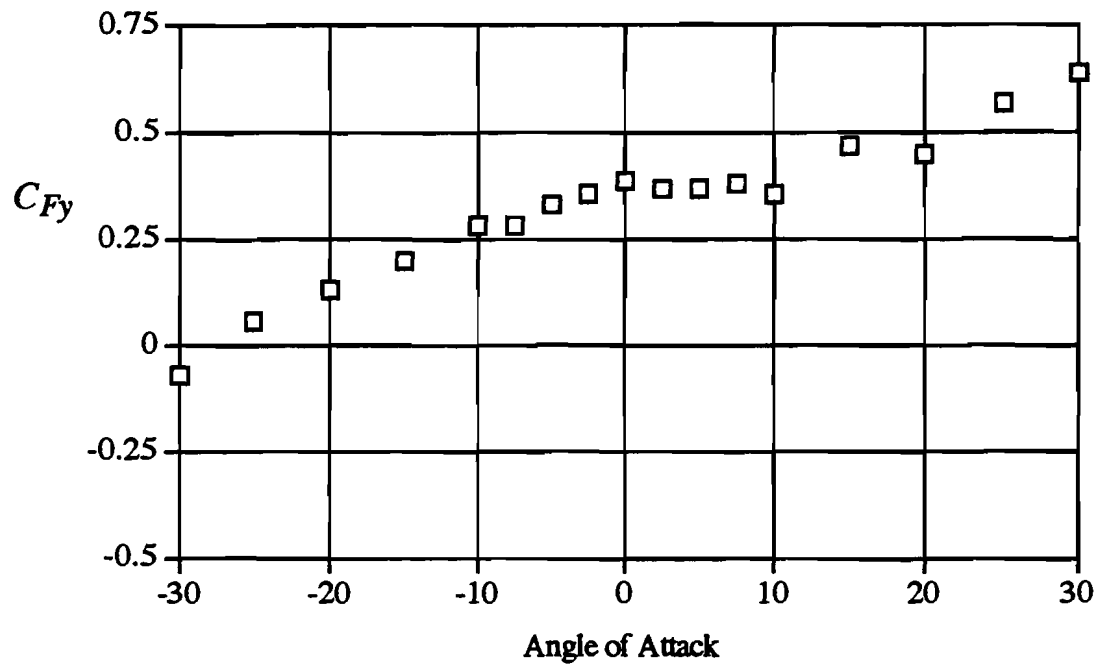
FIGURE 7.12. C_{FY} VERSUS ANGLE OF ATTACK FOR TRAFFIC SIGNAL CONFIGURATION 6
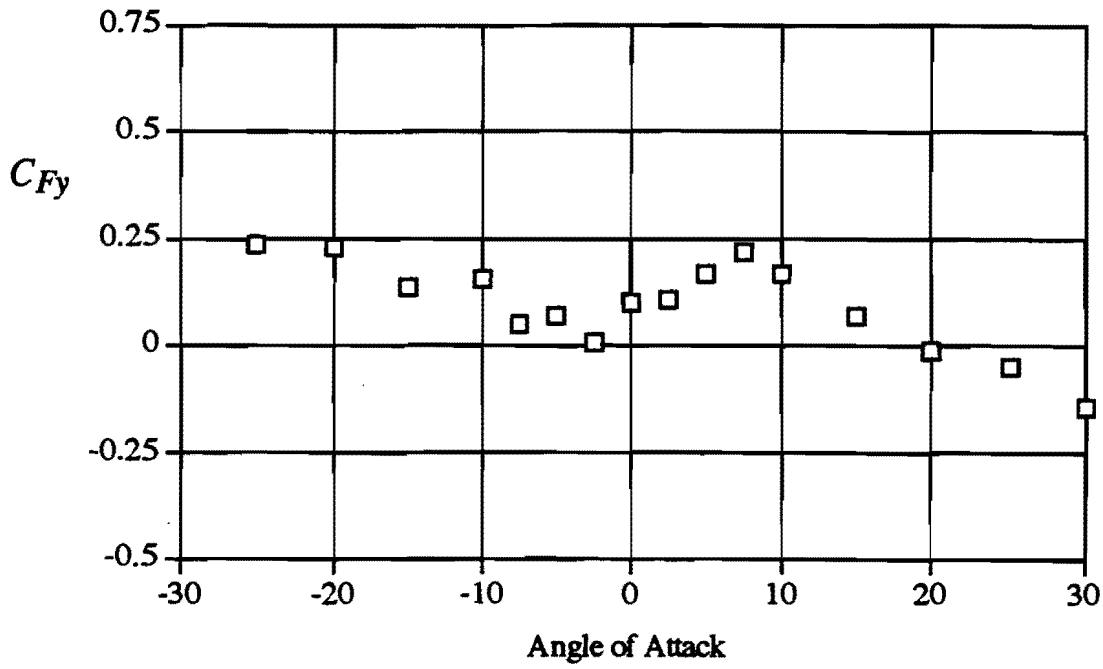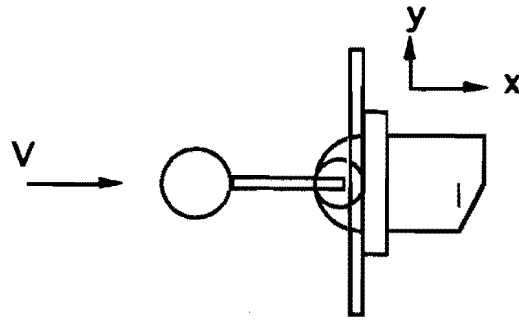
FIGURE 7.13. C_{FY} VERSUS ANGLE OF ATTACK FOR
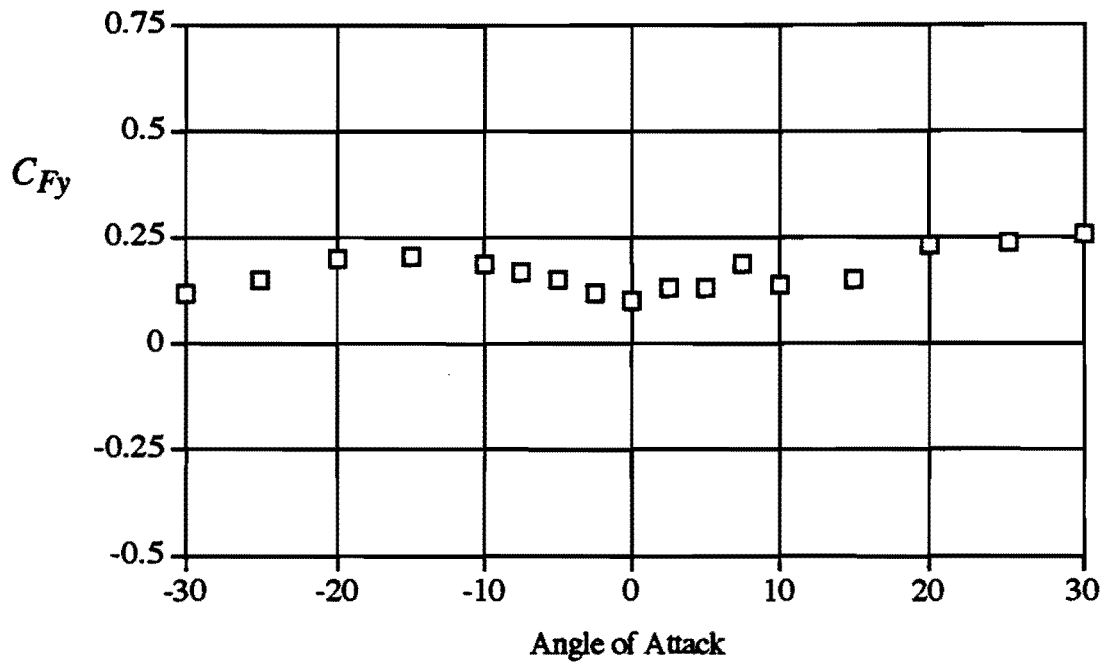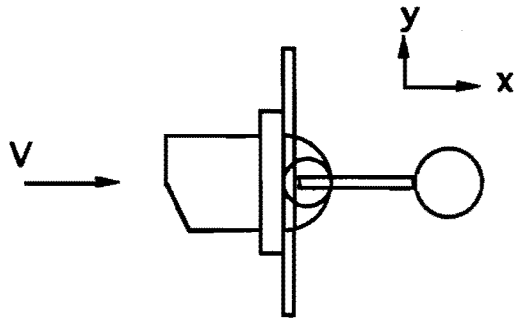TRAFFIC SIGNAL CONFIGURATION 7

FIGURE 7.14. C_{Fy} VERSUS ANGLE OF ATTACK FOR
TRAFFIC SIGNAL CONFIGURATION 8

115
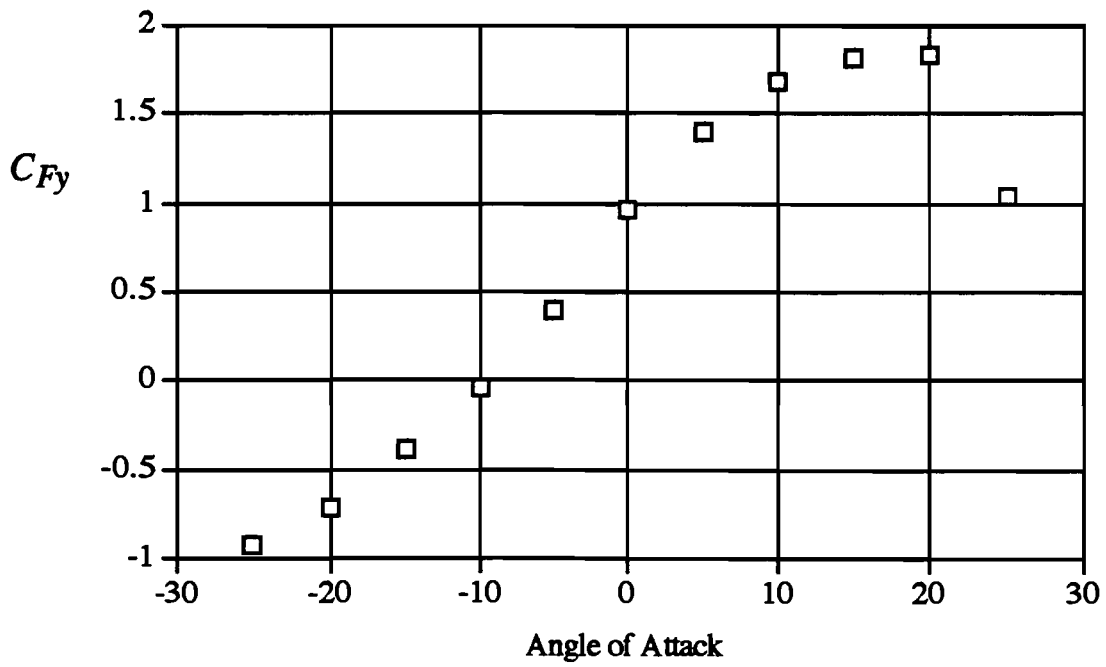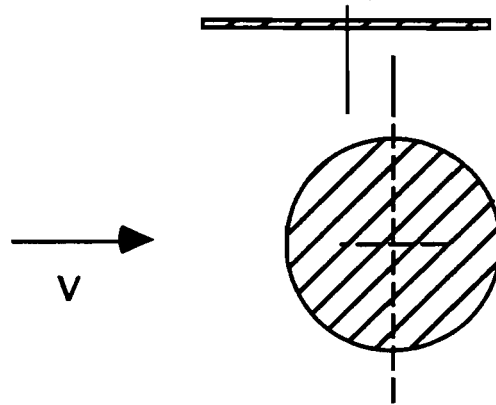
FIGURE 7.15. C_{Fy} VERSUS ANGLE OF ATTACK
FOR A DAMPING PLATE

8. FIELD EXPERIMENTS

Full-scale field experiments provide an opportunity to deal with behavior of the actual structure without the problems of modeling and scaling errors. Fundamental frequency and damping can be measured directly. The wind conditions are "real," rather than simulated. The flow conditions are three-dimensional representing the actual situation.

Field experiments are not without a few disadvantages. Some field conditions are difficult to control. The wind does not always blow and rarely at the speed and direction required by the experiment. Experiments cannot always be repeated under the exact same conditions. Individual parameters cannot always be isolated by holding all other parameters constant. Instrumentation is more difficult to control under the field conditions than in the laboratory. Despite these disadvantages field experiments provide the best information on the behavior structures subjected to wind loads.

8.1 Objectives

The objectives of the field experiments were as follows:

(1) Determine the structural characteristics, fundamental frequency and damping, of traffic signal structures.

(2) Reproduce the large amplitude vibrations observed under conditions of a steady wind.

(3) Test the effectiveness of measures designed to mitigate vibrations.

The structural characteristics of the two signal structures tested were needed to evaluate the galloping phenomena and to verify results of finite element method (FEM) analyses of the structures. In order to mitigate the large amplitude vibrations, it was necessary to be able to initiate them. Once we were able to initiate the vibrations, the circumstances under which the vibrations are sustained could be identified.

A number of mitigation measures were identified and tested. The full-scale field tests either verified their effectiveness or demonstrated that the concepts did not work.

8.2 Field Research Plan

Results of the tow tank experiments were used to develop the field research plan. From observations of operational signal structures and the tow tank experiments, it was clear that the galloping phenomena takes place under a rather narrow set of conditions. The angle of attack of the wind was the most critical condition. Thus, the need to control the angle of attack, was one of the first field conditions addressed. We needed the ability to rotate the signal arm to a predetermined angle of attack of the wind. Otherwise, we would have to wait for the wind to blow from the required direction. On the other hand, the stiffness of the anchor bolts under service conditions also needed to be reproduced. The design of the turn-table foundation had to meet these two critical criteria.

Instrumentation was needed to measure the characteristics of the wind and the structural response of the signal structure to wind effects. The research plan included an evaluation of various transducers such as linear variable displacement transducers (LVDTs), electrical resistance strain gages, and a tilt meter. The existing meteorological tower at the WERFL provided the needed data on wind characteristics.

Two different traffic signal structures were erected and tested at the field site. The first structure had a 40-ft (12.2-m) cantilever arm. It was available early in the project and was used primarily as a shake down test for the instrumentation and to verify results of the FEM analyses. The second signal structure was purchased specifically for this study. With a 48-ft (14.6-m) cantilever arm, it met the TxDOT standards for SMA-80. The size and flexibility of this structure suggested it would be susceptible to galloping. A series of individual tests were designed for each of the two signal light structures in order to achieve the stated objectives of the project. These tests are described in detail in subsequent sections of this report.

8.3 Facilities and Instrumentation

The field experiments were conducted on the two signal light structures with either one or two signal light configurations. The tests were conducted at the Texas Tech University Wind Engineering Research Field Laboratory (WERFL). Wind characteristics were determined from

instrumentation on the 160-ft (49-m) meteorological tower. Structural response was measured with transducers mounted on the signal structure and the WERFL data acquisition system.

8.3.1 Texas Tech Field Site

The WERFL is located on the Texas Tech University campus in a large open field with very few obstructions within a one-mile radius of the site. Facilities at the WERFL include a 30 x 45 ft pre-engineered metal building mounted on a circular track so the building can be rotated. Inside the rotatable building is an 8 x 8 ft (2.4 x 2.4 m) concrete block building that does not rotate. This building contains the data acquisition system for monitoring wind instrumentation and various transducers.

The 160-ft (49-m) meteorological tower supports anemometers at the 13, 33, 70 and 160 ft (4, 10, 21 and 49 m) levels. The instruments provide data for determining wind speed profile and turbulence intensity. Other weather instruments include temperature, barometric pressure and relative humidity sensors that are mounted at the 33 ft (10 m) level.

8.3.2 Test Signal Structures

Two signal structures were selected for testing. The first one, hereafter referred to as the 40-ft (12.2-m) signal structure, was an old structure that had been taken out of service. The dimensions do not match current TxDOT standard specifications. All weights and dimensions had to be measured in the field. The structure was selected for testing because it was readily available when testing began. Details of the 40-ft (12.2-m) signal structure are shown in Figure 8.1.

The second signal structure tested had a 48-ft (14.6-m) cantilever arm, hereafter referred to as the 48-ft (14.6-m) signal structure. It was purchased directly from a manufacturer and meets current TxDOT specifications for an SMA-80 structure. The characteristics of this structure make it particularly susceptible to galloping under the right conditions of signal head arrangement, wind direction and wind speed. Figure 8.2 shows details of the 48-ft (14.6-m) signal structure.

Both signal structures have base plates to accommodate four anchor bolts that are normally set in a concrete pier foundation. The signal structure foundation used in the tests had provision

8.74 in.

9.55 in.

7.32 in.

3.94 in.

17.75 ft

22.4 ft

40 ft.

16 ft.

11.1 in.

1.0 in. = 2.5 cm
1.0 ft = 0.30 m
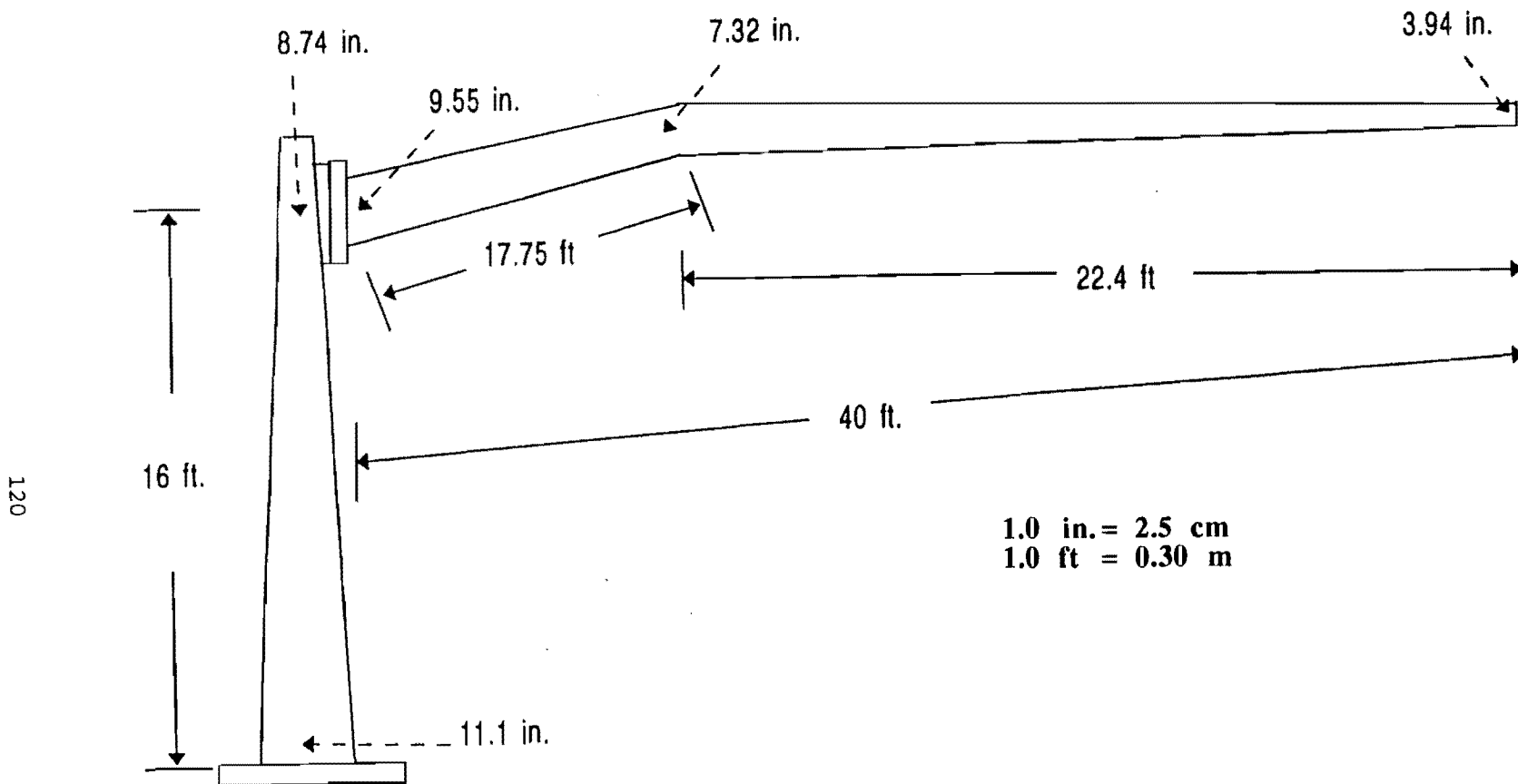
FIGURE 8.1.   DIMENSIONS OF THE 40-FT (12.2-m) SIGNAL STRUCTURE

10.5 in.

10.5 in.

4.1 in.

48 ft.

18 ft.

1.0 in.= 2.5 cm
1.0 ft = 0.30 m

13.0 in.
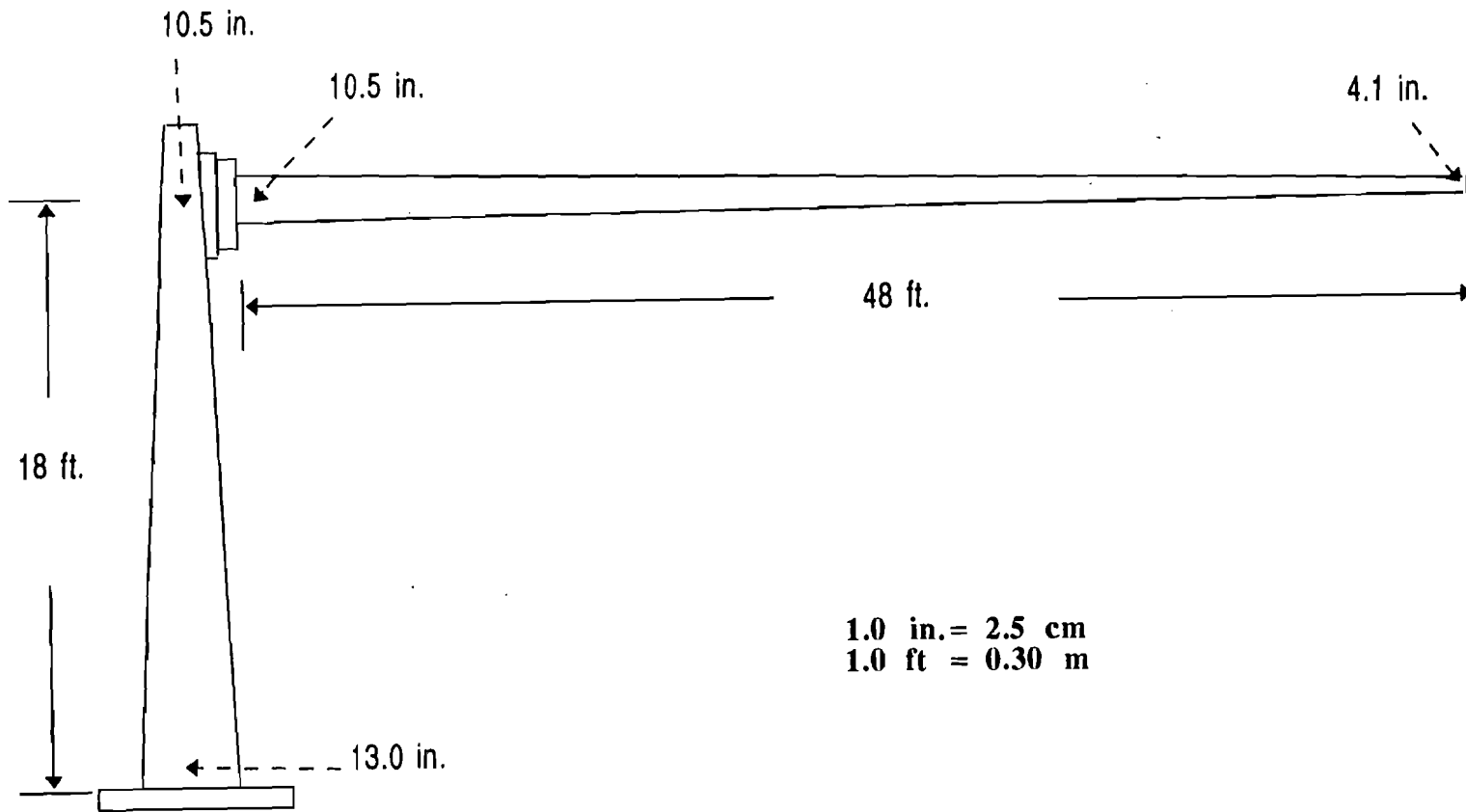
FIGURE 8.2.   DIMENSIONS OF THE 48-FT (14.6-m) SIGNAL STRUCTURE

for four anchor bolts, except they were attached to a rotatable steel plate that could be rigidly clamped at any desired wind angle. The base plate is held in a secure position with the anchor bolts by providing nuts on top and underneath the base plate (See Fig. 8.3).

8.3.3 Foundation

Because of the need to rotate the signal arm to any wind angle of attack the rotatable foundation had to meet the following criteria:

(1) Capability to easily rotate signal structure to any desired orientation in 15° increments.

(2) Exhibit the same foundation rigidity, when clamped, as a structure under service conditions.

Except for the rotatable turret bearing, the foundation was constructed to the same specifications as one being used for actual service conditions.

The rotatable foundation consists of the following parts, as shown in Figure 8.4:

(1) Concrete pier foundation

(2) Steel bottom plate (fixed)

(3) Rotatable turret bearing

(4) Steel top plate (rotates)

(5) Clamping bolts (secures top plate)

(6) Signal structure anchor bolts

(7) Signal structure base plate

(8) Signal structure, pole

The following procedure was followed in rotating the signal structure to some desired orientation relative to the wind direction.

(1) The wind direction was monitored for at least five minutes to obtain an average value.

(2) The four clamping bolts were removed, which allowed the structure to rotate freely.

(3) The structure was rotated to desired angle in 15° increments. The clamping bolts were reinstalled in the threaded holes provided in the steel base plate and tightened.

Figure 8.5 shows the possible orientations of the signal structure arm. To achieve vibrations due to galloping the cantilever arm needed to be very nearly perpendicular to the mean wind direction.

FIGURE 8.3.   SIGNAL STRUCTURE FOUNDATION

Signal Structure Pole (8)

Signal Structure
Base plate (7)

Signal Strucuture
Anchor Bolts (6)

Clamping
Bolts (5)

Top Plate (4)
(Rotates)

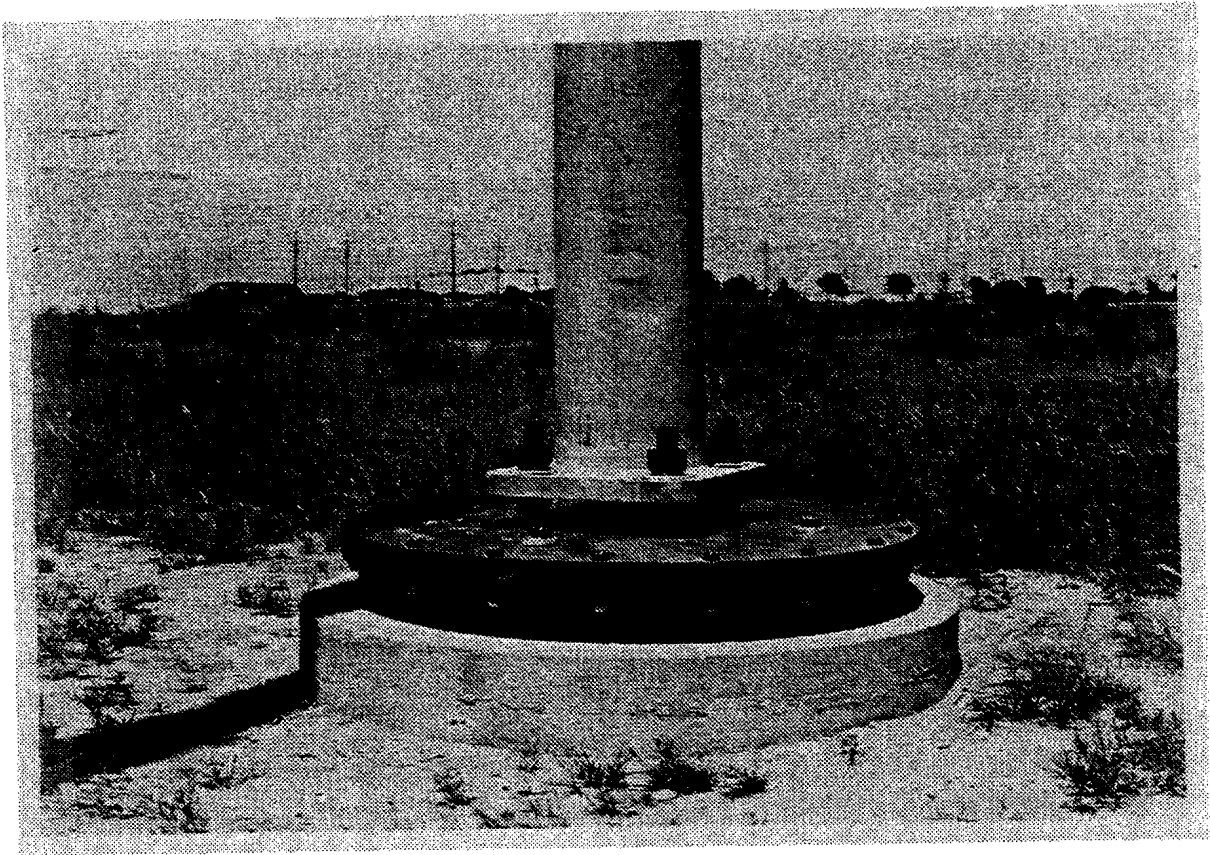Turret Bearing (3)
(Rotates)

Bottom Plate (2)
(Fixed)

Ground Level
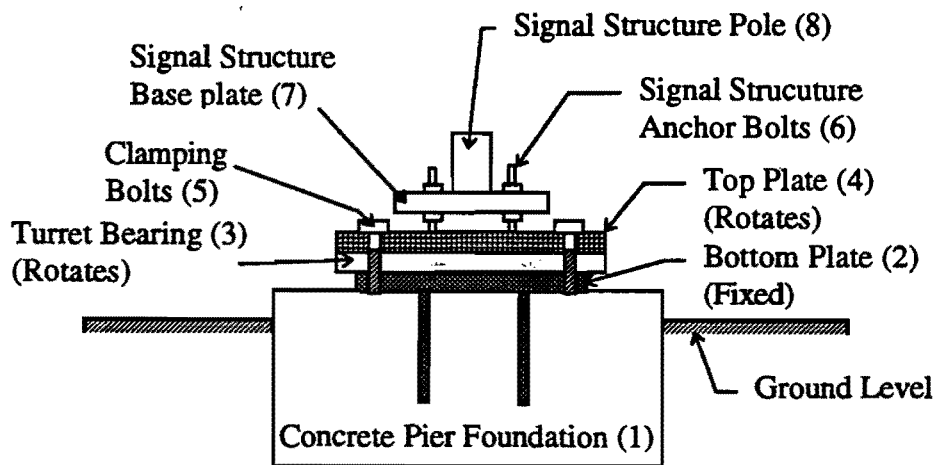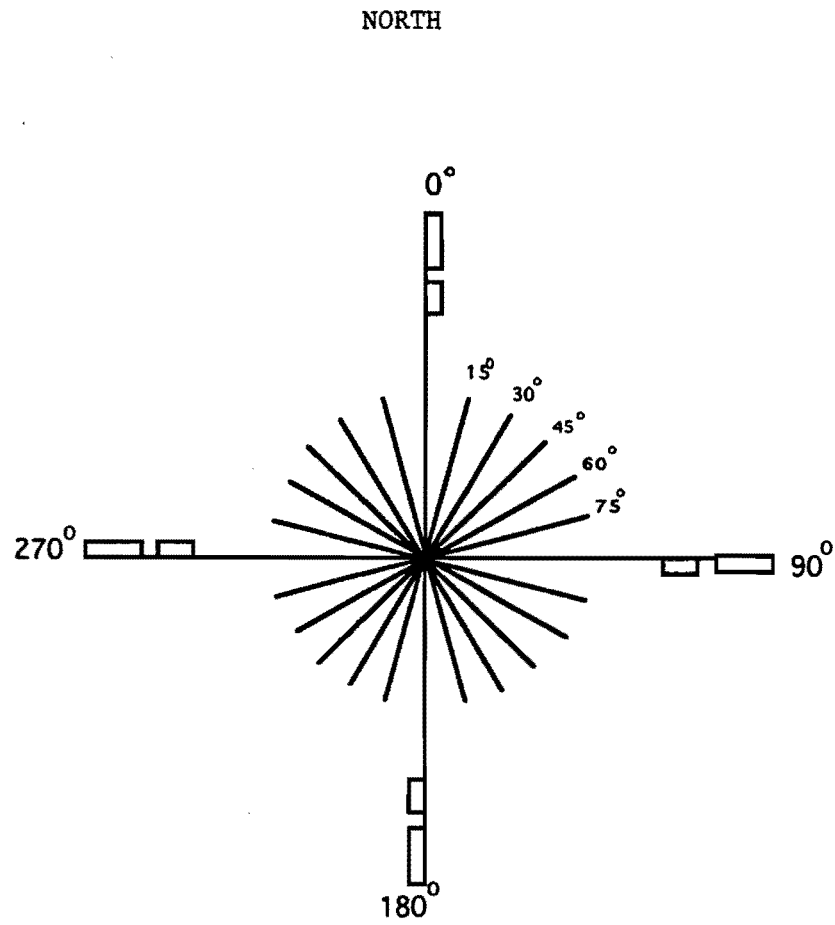
Concrete Pier Foundation (1)

**FIGURE 8.4   ROTATABLE FOUNDATION FOR
TRAFFIC SIGNAL STRUCTURE**

FIGURE 8.5. POSSIBLE ORIENTATIONS OF
SIGNAL STRUCTURE ARM

8.3.4 Instrumentation

Instrumentation was needed to measure wind characteristics and structural response.

Wind Instruments

Anemometers mounted on the 160-ft (49-m) meteorological tower and on a 9-ft (6-m) portable tower were used to measure characteristics of the natural wind. The instruments on the meteorological tower provided data for determining wind speed profile and turbulence intensity. Figure 8.6 is a plot of wind profile and turbulence intensity for a wind blowing from the Southwest. These profiles, which are typical for most other directions, are typical of open country terrain (Exposure Category 3, according to the revised standard).

A three-cup anemometer and wind direction vane were mounted on a 19-ft (6-m) pole that was placed near the signal structure installation. These instruments measured the wind speed and direction needed to set the proper orientation of the signal structure relative to wind direction.

Data runs requiring a continuous measurement of wind speed and direction were taken continuously for 15-minute periods. The quality assurance program determines if the wind speed and direction time histories are stationary or not. Stationarity of the time series is determined by both the Run Test and the Reverse Arrangement Test (Bendat and Piersol, 1986). Only these records that are stationary are used in subsequent analyses.

Transducers

Three transducers were tested in the field for their effectiveness in measuring response of the signal structure to the wind effects. They were (1) electrical resistance strain gages, (2) a linear variable differential transducer and (3) a tilt meter. Figure 8.7 shows locations where the transducers were mounted.

One set of strain gages were installed on the 40-ft (12.2-m) signal structure. Two gages were mounted on opposite sides of the vertical pole, in line with the cantilevered arm of the signal structure 13 in. (33 cm) above the base of the pole. As the pole bends downwind, the gage on the outside measures the tension strains while the one on the inside measures compression. The gages
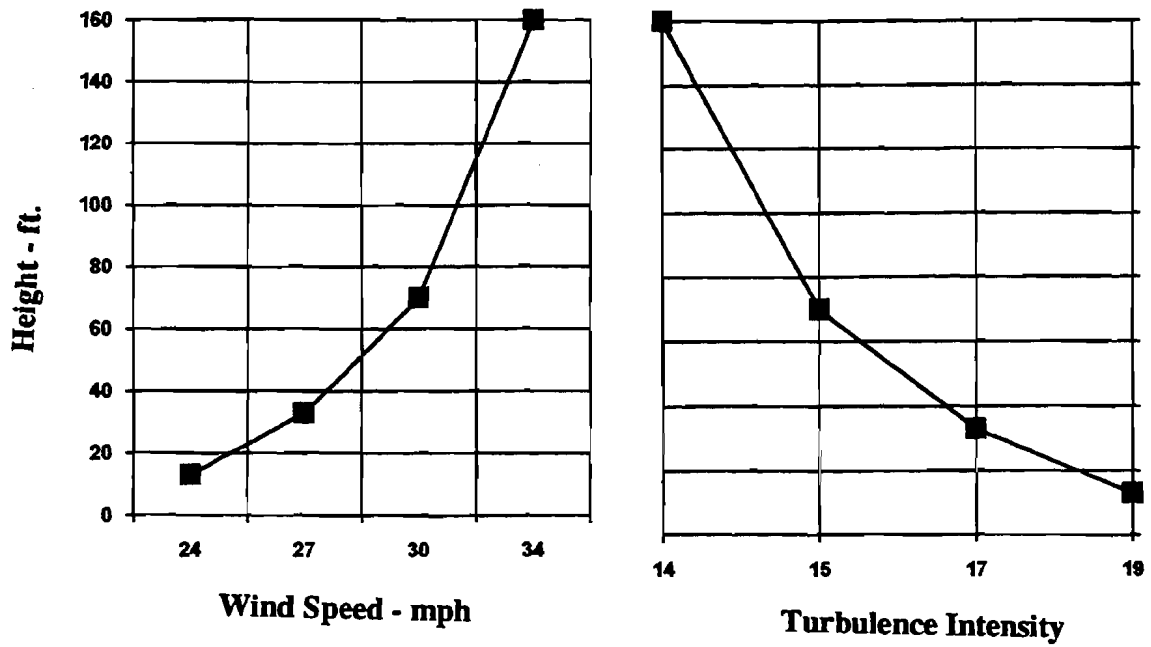
1.0 ft   = 0.30 m
1.0 mph = 0.45 m/s

FIGURE 8.6.   WIND PROFILE AND TURUBLENCE
INTENSITY FOR WERFL
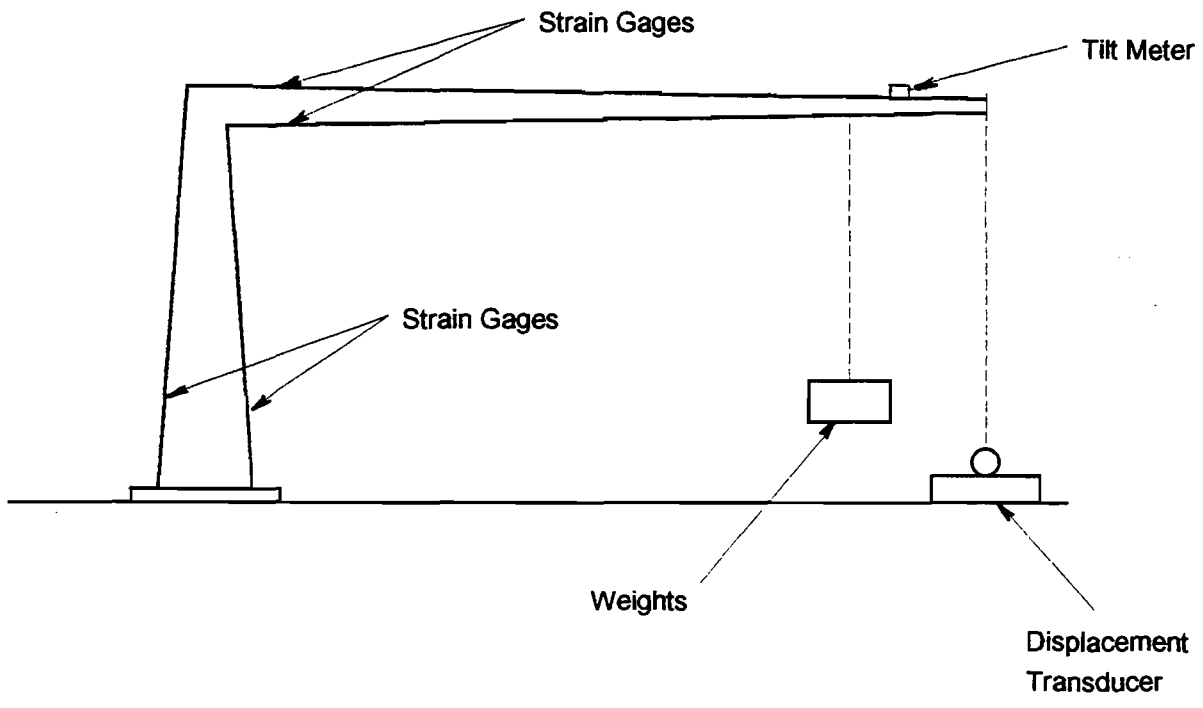
FIGURE 8.7. LOCATIONS OF SENSORS ON SIGNAL STRUCTURE

were connected into a Wheatstone half-bridge circuit as shown in Figure 8.8. This arrangement measured the bending strain and compensated for axial strains and temperature strains.

Two sets of strain gages were installed on the 48-ft (14.6-m) signal structure. One set was located 13-in. above the base of the vertical pole and the other set was located on the cantilever arm a distance of 11 in. (28 cm) from the connection plate of the arm. In order to obtain a higher voltage output, a full Wheatstone bridge was configured with four active gages. Two gages were mounted on the tension side of the structure, as well as two on the compression side. The full-bridge Wheatstone circuit is shown in Figure 8.9.

Temperature changes during a data run will give erroneous strains readings, if provisions have not been made for temperature compensation. Under harsh field conditions, temperature compensation is especially important. Temperature fluctuations affect the bridge circuit in two ways:

(1)   The bridge will output an erroneous strain reading, if there are no provisions for temperature compensation.

(2)   Temperature fluctuation may also affect the resistance of lead wires in the circuit.

Temperature compensation can be achieved in a Wheatstone bridge, if gages in opposite legs of the bridge experience the same temperature changes. Lead wires should be kept as short as possible. For this reason, the amplifier circuit boards are installed very near the location of the gages, rather than in the instrumentation room near the data acquisition equipment.

In the field, voltages from nearby electrical or magnetic fields can create noise that affects the voltage output of the bridge. The bridge output due to strain is small and can easily be overshadowed by noise voltage. The noise effects can be eliminated by one of two well-known techniques:

(1)   By amplifying the signal close to the gage. The technique is known as pre-amplification because the signal is amplified before running through a long signal cable. By amplifying the signal before it is affected by noise, the signal voltage is much higher than the noise voltage.

(2)   By using a current signal instead of a voltage signal to measure strain. The inductive nature of the noise voltage does not significantly affect the current carried by the electrical conduit.
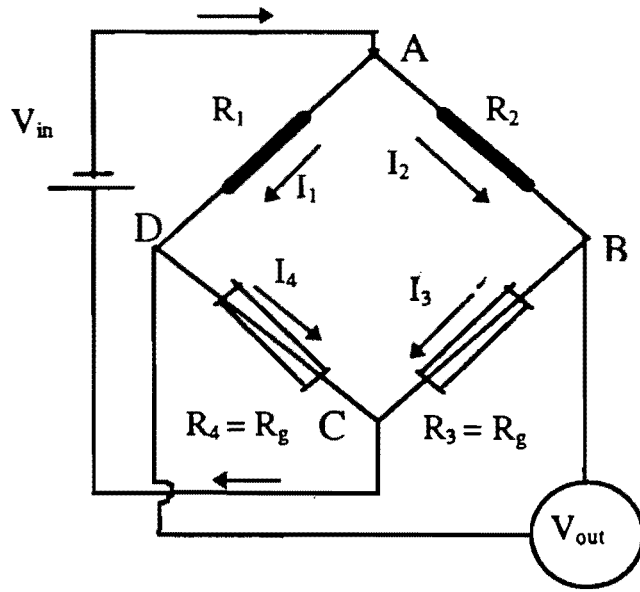
FIGURE 8.8. WHEATSTONE HALF-BRIDGE CIRCUIT
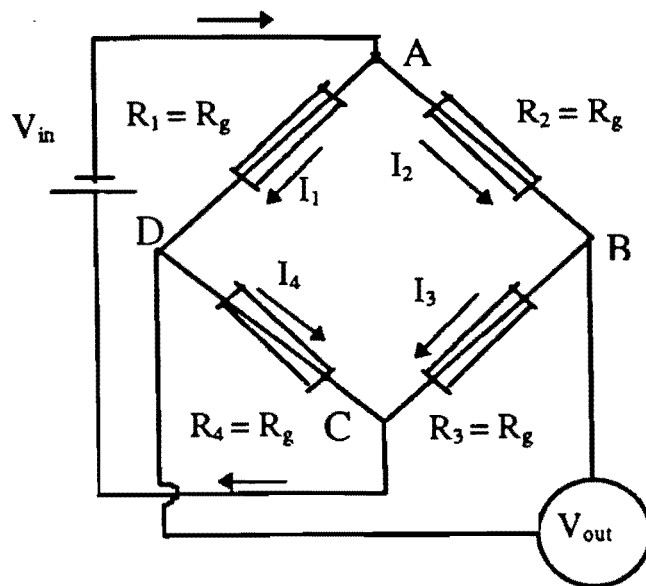
FIGURE 8.9. WHEATSTONE FULL-BRIDGE CIRCUIT

The pre-amplification technique was used in the study.

In order to relate strain to the loading on a structure, the strain gage bridge must be balanced so there is zero output voltage prior to applying the load. The balance is achieved by adjusting the resistance of one of the gages in the Wheatstone bridge. The balance is accomplished by connecting a very high variable resistance in parallel with one of the strain gages. The variable resistance is adjusted until the voltage output from the bridge is zero.

Calibrating the strain gage bridge means establishing a relationship between voltage output and strain in the specimen. Bridge calibration is done by simulating a known strain, i.e., imposing a known change in resistance of one of the gages and measuring the voltage output. The method is known as shunt calibration.

Displacement Transducers

A method was needed to measure the large amplitude deflection at the tip of the cantilever arm. An instrument that seemed to hold promise was an LVDT with a thin wire that unrolled off of a shaft as the displacement took place, similar to a fishing reel. A voltage proportional to the amount of wire rolled off the shaft is the output signal. The instrument has a linear response over a relatively large displacement of the order of 24 in. (61 cm). However, since the arm tip was moving up and down, a tension was needed in the wire to keep it taut. Even though the tension was less than 2 lbs (8.9 N), this was enough to dampen the vibration due to galloping. The sensor worked okay for the free vibration tests, but could not be used for galloping tests.

Tilt Meter

The tilt meter is a small sensor that provides a voltage output signal proportional to the angle of tilt of the surface on which the instrument is mounted. The angle of tilt of the cantilever arm can be measured by mounting the tilt meter at the arm tip as shown in Figure 8.7. The tilt meter gives an indication of deflection and vibration frequency.

131

8.4 Field Studies

The field studies involved three distinct sets of experiments:

(1) Determine structural characteristics of the two full-size signal structures.

(2) Examine the specific conditions under which galloping takes place.

(3) Test the various mitigation concepts.

Each of these experiments is discussed below.

8.4.1 Structural Characteristics

The three structural characteristics of interest were stiffness (expressed as a load versus direction relationship), natural frequencies and damping coefficient.

Stiffness

The two signal structures were tested for stiffness characteristics on calm wind days. The structures were instrumented with strain gages, a tilt meter, and a reel-type LVDT, as described in Section 8.3.4.

Zero load readings were taken on the three transducers. Static concentrated loads were applied at a point near the free end of the cantilever arm of the signal structure. The instruments were read as each load increment was added to obtain relationships between load and strain, tilt angle and displacement, respectively. Results of these tests are summarized in Table 8.1 for both the 40-ft (12.2-m) and the 48-ft (14.6-m) structures. Because of small fluctuations in the transducer outputs, even on a calm day, the data were recorded as five minute means.

Figure 8.10 shows load versus strain relationships for the 40-ft (12.2-m) and 48-ft (14.6-m) signal structures. Note that the curves are essentially linear. It is apparent that the 48-ft (14.6-m) signal structure experiences slightly lower strains than the 40-ft (12.2-m) signal structure at the same loading.

Natural Frequencies

Tests were conducted to obtain the natural frequencies of vibration of the two signal structures. A concentrated load was suspended by a wire connected about three-ft from the free

132

TABLE 8.1

MEASURED STRAINS, TILT AND DISPLACEMENT
OF 40-FT (12.2-m) AND 48-FT (14.60-m) SIGNAL STRUCTURES[1]

Static Load (lbs)	Pole Strain, μstrain		Arm Strain, μstrain	Arm Tip Tilt (degrees)		Arm Tip Displacement (in.)	
	40-ft Arm	48-ft Arm	48-ft Arm	40-ft Arm	48-ft Arm	40-ft Arm	48-ft Arm
0	0	0	0	0	0	0	0
50	56	41	43	1.00	0.91	3.19	3.14
60	66	50	53	1.23	1.08	3.82	3.76
70	77	56	60	1.43	1.23	4.45	4.37
80	89	64	70	1.62	1.40	5.01	5.00
90	98	73	82	1.80	1.61	5.50	5.75

[1]See Figure 3.8 for location of transducers.

1.0 ft = 0.30 m
1.0 lb = 0.45 kg
1.0 in.= 2.5 cm
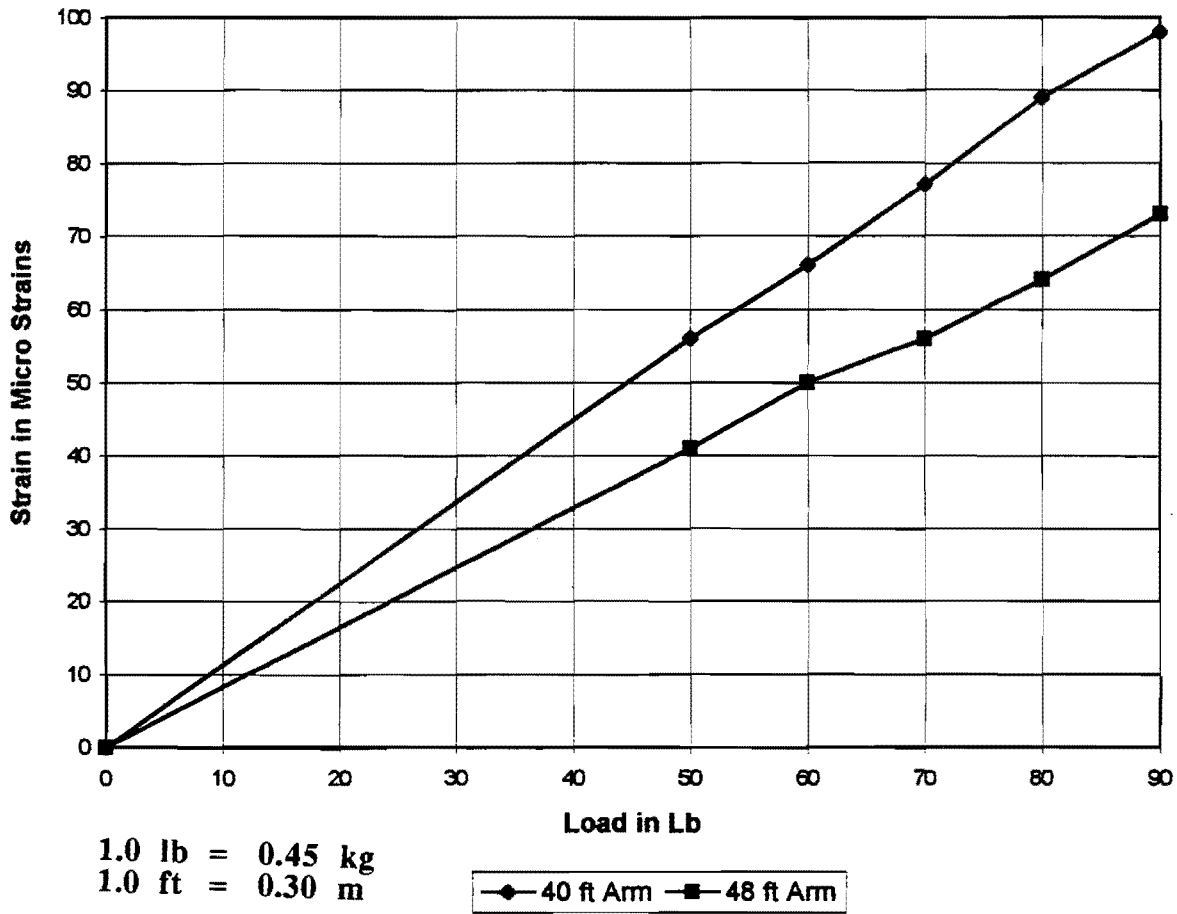
133

1.0 lb = 0.45 kg
1.0 ft = 0.30 m

FIGURE 8.10. **LOAD VERSUS STRAIN IN VERTICAL POLE OF 40-FT (12.2-m) AND 48-FT (14.6-m) SIGNAL STRUCTURES**

end of the cantilever arm (See Figure 8.7). The wire was cut to quickly release the weight and allow the arm to under go free vibration. The three sensors were monitored to obtain time histories of strain, tilt and displacement. The strain records were selected for the frequency analysis because the results appeared to be the most reliable of the three instruments. The analog signal from the transducers were converted to digital form. A spectral analysis was then performed to identify the fundamental frequencies of vibration.

The experiment was first performed on the bare arm without signal lights attached. Figure 8.11 and 8.12 show time history of strain for the two bare signal structures. The two spectral analyses are shown in Figure 8.13 and 8.14 for the 40-ft (12.2-m) and 48-ft (14.6-m) signal arms, respectfully.

Both spectral analyses show that the second modes make a negligible contribution to the energy content of the spectrum. Clearly the fundamental mode is dominant in this case. The significance is that the structures are vibrating in the fundamental mode at the fundamental frequency with negligible contribution to response from the higher modes.

The fundamental frequencies change when traffic signal lights are mounted on the signal structure. The change depends on the mass of the signal lights and their location relative to the free end of the arm. Table 8.2 compares fundamental frequencies of the bare structures and a configuration of two signal lights on the structure. The presence of the signal lights on the structure reduced the fundamental frequency by about 30%.

Mounting the signal lights on the structure does not change the fact that they are vibrating at the fundamental frequency with no contributions from the higher modes. This fact allows the use of a direct, linear relationship between strain and arm tip displacement in subsequent analyses.

Damping

The only practical way to determine percent critical damping is to measure it in the field. Damping of the structures is needed in dynamic analysis of the signal light structures using FEM. The strain versus time histories of free vibration given in Figure 8.11 and 8.12 were used to obtain damping values. The log decrement approach (Clough and Pienzen, 1980) was used to obtain the
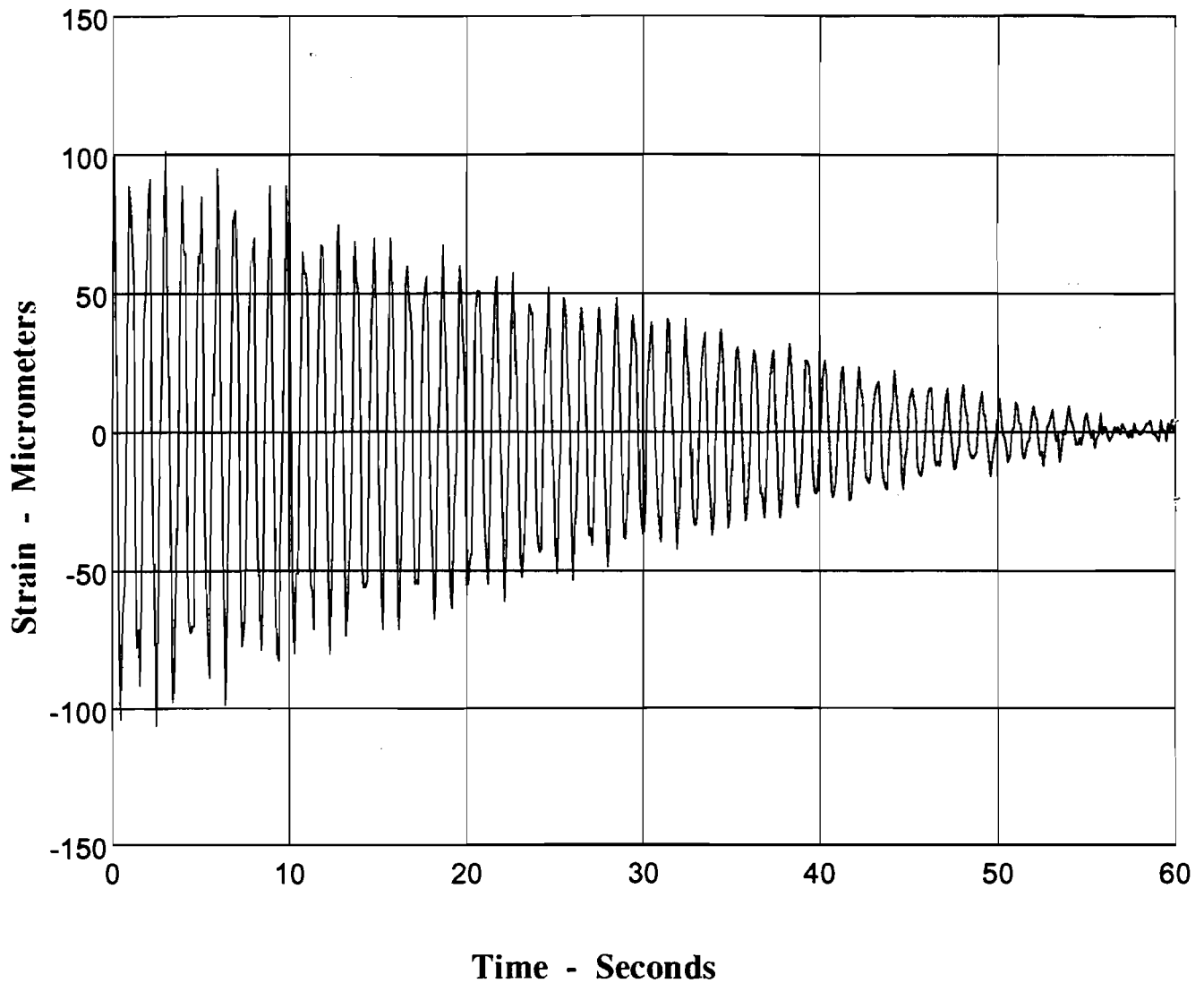
FIGURE 8.11. FREE VIBRATION RESPONSE OF 40-FT (12.2 m) SIGNAL STRUCTURE WITHOUT TRAFFIC LIGHTS; STRAIN IN VERTICAL POLE VERSUS TIME
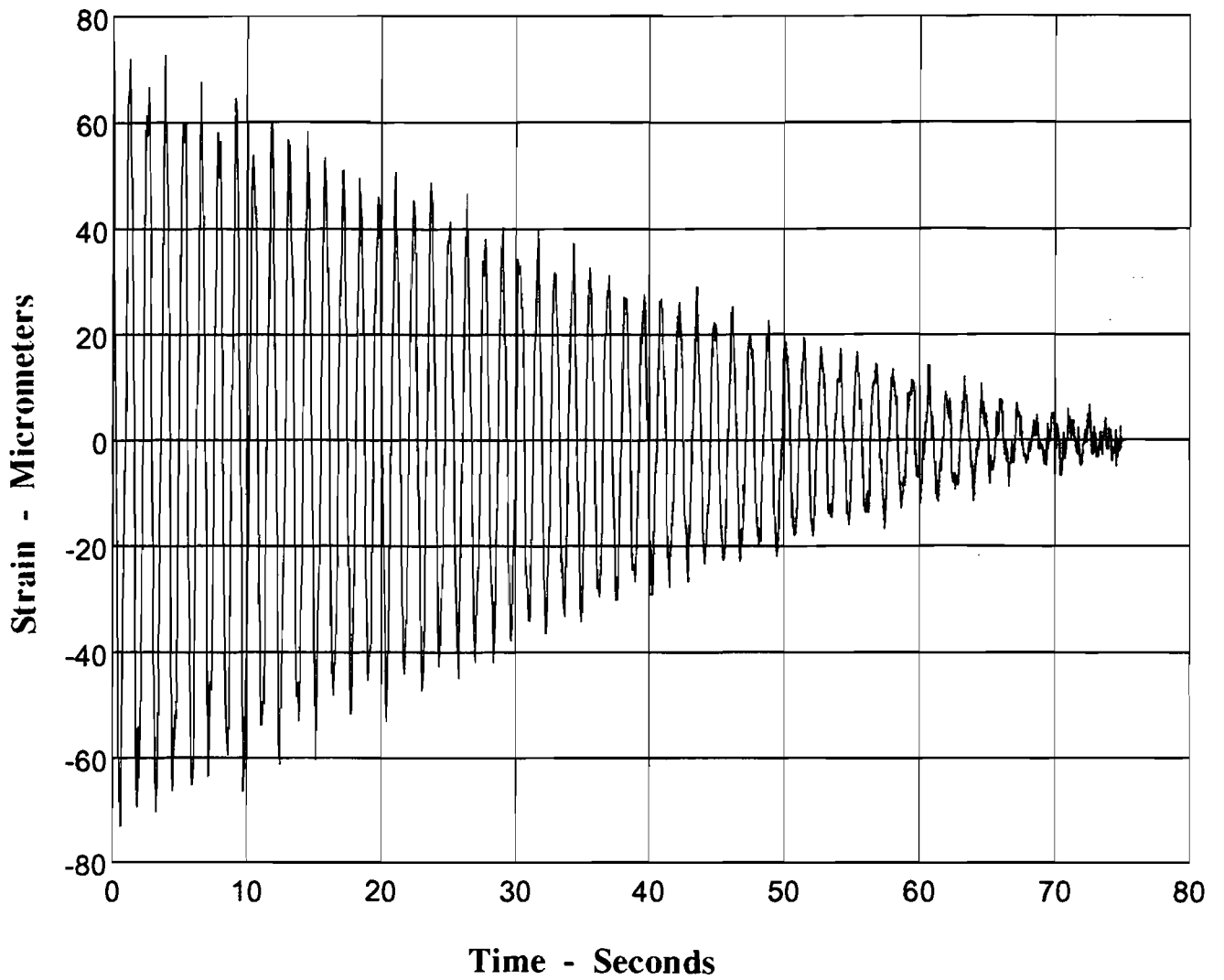
FIGURE 8.12. FREE VIBRATION RESPONSE OF 48-FT
(14.6 m) SIGNAL STRUCTURE WITHOUT
TRAFFIC LIGHTS; STRAIN IN VERTICAL
POLE VERSUS TIME

40-ft Signal Structure - Without Lights

1st Mode	1.02 Hz
2nd Mode	3.28 Hz
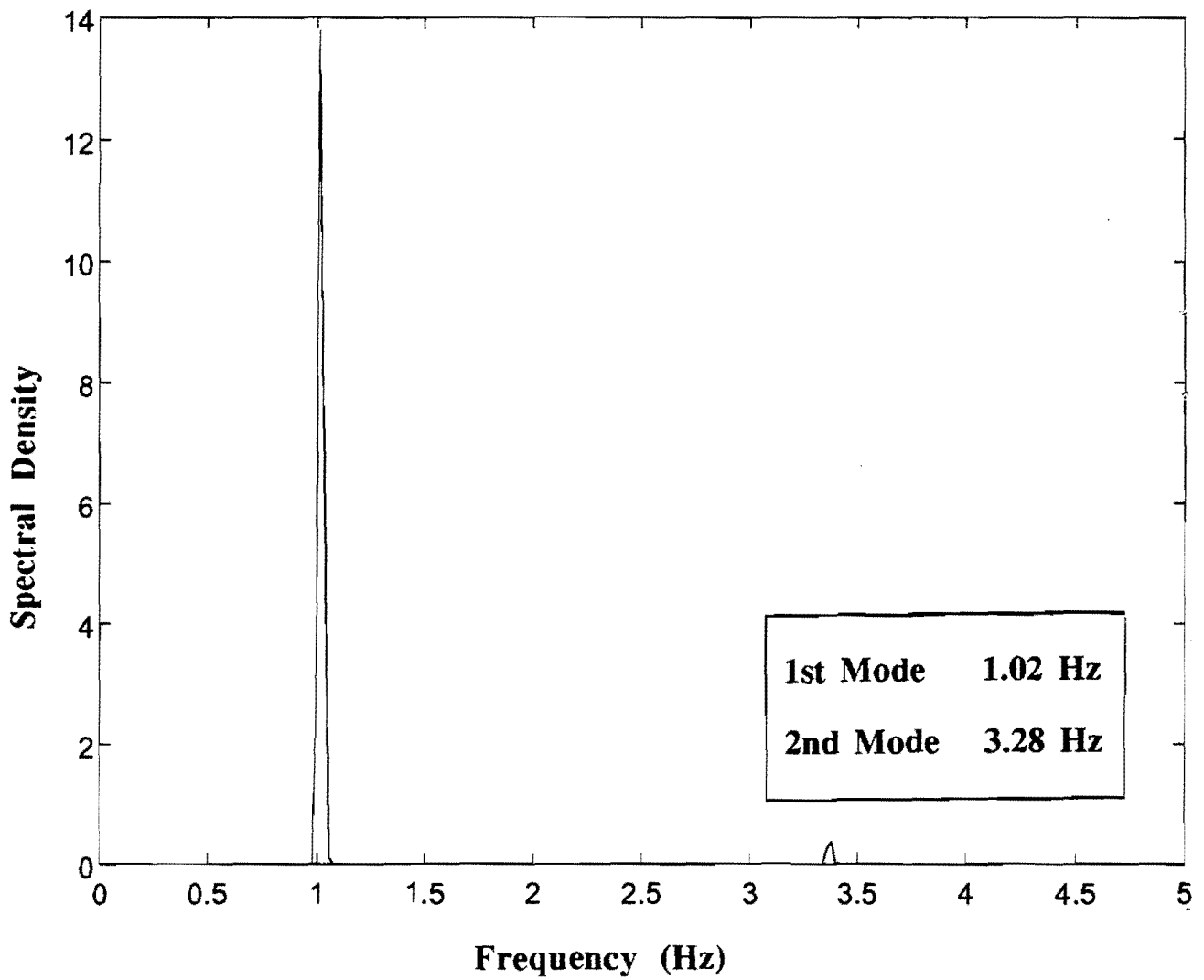
FIGURE 8.13. SPECTRAL ANALYSIS OF 40-FT (12.2-m) SIGNAL STRUCTURE WITHOUT TRAFFIC LIGHTS

48-ft Signal Structure - Without Lights

1st Mode	0.98 Hz
2nd Mode	3.24 Hz
3rd Mode	5.62 Hz
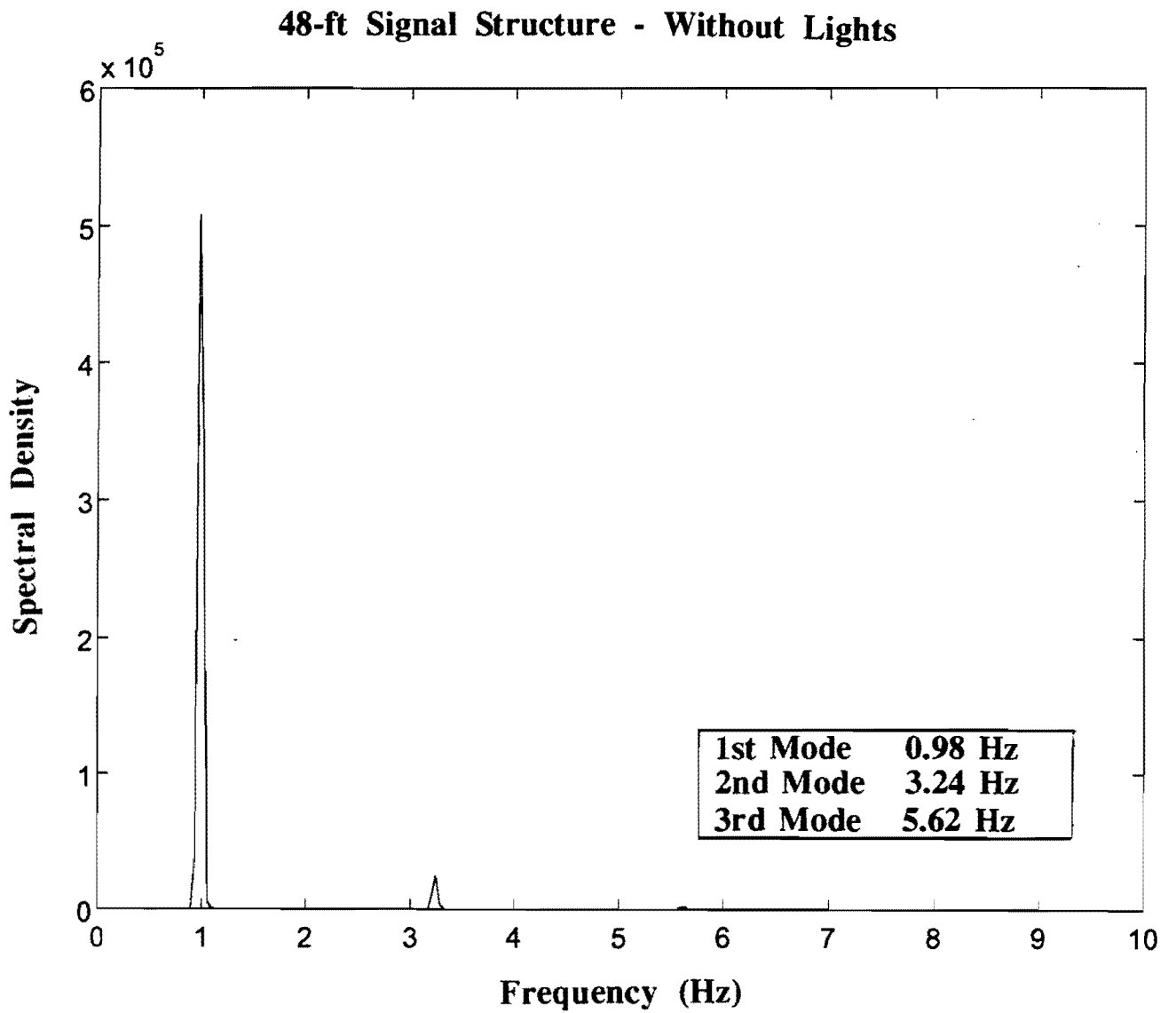
FIGURE 8.14. SPECTRAL ANALYSIS OF 48-FT (14.6-m) SIGNAL STRUCTURE WITHOUT TRAFFIC LIGHTS

TABLE 8.2

MEASURED FUNDAMENTAL FREQUENCIES
OF 40-FT (12.2-m) AND 48-FT (14.6-m) SIGNAL STRUCTURES

Structure	Fundamental Frequency, Hz	
	Without Lights	With Lights
40-ft (12.2-m) Arm	1.02	0.78
48-ft (14.6-m) Arm	0.98	0.74

TABLE 8.3

MEASURED DAMPING COEFFICIENT FOR
40-FT (12.2-m) AND 48-FT (14.6-m) SIGNAL STRUCTURES

Structure	Damping Ratio, %	
	Without Lights	With Lights
40-ft (12.2-m) Arm	0.52	0.78
48-ft (14.6-m) Arm	0.38	0.62

damping ratios for the two signal structures. Values with signal lights and without signal lights are tabulated in Table 8.3. Clearly the presence of the signal lights affect the damping as well as the fundamental frequencies.

8.4.2 Galloping of the Structure

This second series of tests in the field was designed to reproduce galloping in the two test structures and to carefully identify the parameters that contribute to the galloping 40-ft (12.2-m) sign structure.

The structure with the 40-ft (12.2-m) cantilever arm was installed in the field first. The primary purpose was to shake down the instrumentation and obtain qualitative information about the galloping phenomenon in the field. In particular, we wanted to verify results observed in the two tank with those observed in the field.

From the tow tank experiments (See Figure 7.2) signal light Configurations 3 and 4 were found to be very stable, i.e., galloping was not expected to take place, because of the positive slope of the C_{Fy} versus angle of the attack curve over a wide range of attack angles. These same two configurations were set up on the structure in the field. The cantilever arm was rotated to be within $\pm 7.5°$ of the five-minute mean wind direction under several wind speeds. The test was set up several different times, but galloping was not observed in any case. The tow tank and field tests were in complete agreement for these two configurations.

Configurations 7 and 8 from Figure 7.2 also were not expected to exhibit galloping. They were set up in the field and produced results similar to Configurations 3 and 4. Galloping was not observed in any of the field tests where the tow tank studies suggested there should be none.

According to the tow tank studies, Configuration 5 in Figure 7.2 should exhibit galloping, because of the negative slope of the C_{Fy} versus angle of attack curve. With Configuration 5 mounted on the 40-ft (12.2) signal structure, galloping was observed on several occasions with free end displacement amplitudes of 12-16 in. (30-40 cm). From these tests, the data indicate that the only light configuration likely to gallop is Configuration 5.

142

48-ft (14.6-m) Signal Structure

According to tow tank test results, the signal light configuration that produced galloping with the largest amplitude displacements of the free end of the cantilever arm was Configuration 5. Hence, this configuration was used in all subsequent tests on the 48-ft (14.6-m) signal structure. The three primary factors required for the structure to exhibit galloping were:

(1)   Wind direction angle of attack

(2)   Wind speed

(3)   Signal light Configuration 5.

All field tests that involved galloping essentially followed the same procedure. The wind vane on the 19-ft (6-m) portable pole near the structure was monitored to obtain one-minute mean wind direction. The signal structure arm was rotated so the wind direction was normal to the cantilever arm within ±7.5° from the back side of the signal light.

In Configuration 5, the signal light is suspended below the signal arm and has a back plate. Flow is from the back side toward the front side of the signal light. After adjusting the signal structure to the most favorable wind direction, the structure would achieve a state of steady galloping through the following sequence of events: The free end of the cantilever arm was held steady by means of a thin wire. We released the wire and allowed the signal structure to vibrate at will. Initially, small displacements normal to the wind flow took place. The small vibrations were attributed to vortex shedding. The signal structure was allowed to continue vibrating. Gradually the amplitudes of vibration increased. If the wind speed and direction held steady, vibrations would continue to increase in amplitude until some limiting value was achieved. The vibration took place at a frequency very near the fundamental frequency of the sign structure..

A change in wind speed or wind direction would alter the vibration characteristics. With significant change in wind direction, the vibration amplitudes would decrease and galloping would cease. A change in wind speed resulted in a change in displacement amplitude, if wind direction held steady.

Ideally, we would have measured displacements of the free end if the cantilever arm with the reel-type LVDT. However, because the driving force associated with galloping are so small, the tension in the wind caused significant damping of the vibrations.

To demonstrate the problem with using the LVDT, the following experiment was conducted. The signal structure was set up to gallop as described above. After a period of time, the displacement amplitude reached a steady state and clear evidence of galloping. The wire to the fishing reel LVDT was carefully hooked to the free end of the arm without stopping the vibration. The wire has no more than a two-pound (0.9 kg) tension. Suddenly the displacement amplitude was reduced and did not regain the original displacement amplitude. The wire was then unhooked, after a few minutes the galloping resumed and retained its original steady state amplitude.

From these experiments, we concluded that the fishing reel LVDT could not be used for measuring displacements during galloping. All remaining tests relied on the strain gage readings either in the arm and/or the vertical pole from which displacement could be derived. The strain gage readings proved to be reliable and accurate.

8.5 Mitigation Measures

Galloping has been identified as the mechanism for large amplitude displacements in traffic signal structures under certain conditions of wind direction, speed and structure characteristics, as discussed above. When galloping occurs, over the useful life of the structure, failure may occur at some point in time due to the formation of fatigue cracks. This situation occurred in the signal structure that failed in Dalhart, Texas in April, 1991. In addition to the potential of failure, the large amplitude vibrations are a distraction to passing motorists.

Galloping appears to be a problem when the displacement amplitude exceeds $\pm$ 8 in. ($\pm$20 cm). Several mitigation measures were tested in the field to reduce the amplitude of the vibration. These included a damping plate (wing) attached to the cantilever arm, tuned mass dampers, and water slosh damper. The damping plate was by far the most effective mitigation measure.

144

8.5.1 Tuned Mass Damper

This technique is frequently used in tall buildings to suppress vibrations from wind and earthquake forces. The concept of a tuned mass damper, sometimes called a dynamic absorber, could be applied to the traffic signal structure.

Considering the cantilever signal structure as a single degree of freedom system, the dynamic absorber is obtained by attaching an additional mass m_2 to the signal structure by means of an equivalent spring with stiffness k. The dynamic structure can be represented as shown in Figure 8.15, the galloping creates a force on the signal structure $F \sin \omega t$. Let the mass and stiffness of the signal structure be m_1 and k_1, respectively. Because galloping takes place at the fundamental frequency, it follows that

$$\omega = \omega_1 = \sqrt{k_1/m_1} \tag{8.1}$$

where ω_1 is fundamental frequency of the signal structure.

To be effective, values of m_2 and k must be selected to make the displacement of the signal structure $y_1 = 0$. To accomplish this, the absorber must be designed so that

$$k/m_2 = k_1/m_1 \tag{8.2}$$

Thus

$$k = m_2(k_1/m_1) \tag{8.3}$$

In the field, we measured the fundamental frequency of the 48-ft (14.6-m) signal structure f_1. Then

$$
\begin{aligned}
\omega_1 &= f_1/2\Pi = \sqrt{k_1/m_1} \\
&= 4.65 \text{ rad/sec}
\end{aligned}
\tag{8.4}
$$

Then, from Eq. 8.3

$$
\begin{aligned}
k &= m_2\omega_1{}^2 \\
&= m_2(4.65)^2 \\
&= 21.60 \; m_2
\end{aligned}
\tag{8.5}
$$

F sinωt

$k_1/2$ $k_1/2$

m_1

k

m_2

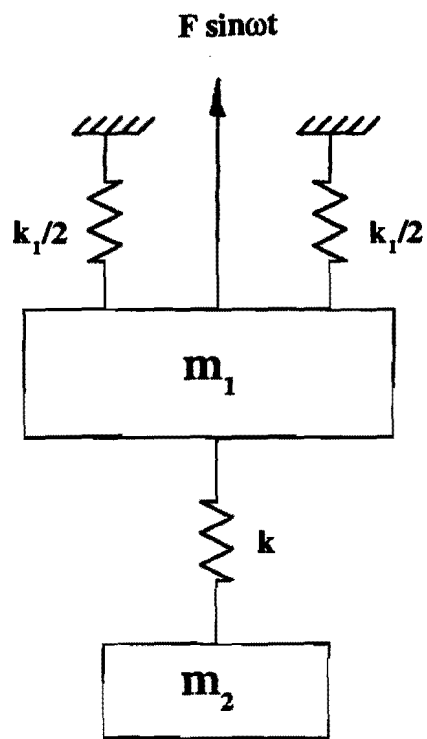**FIGURE 8.15.   MODEL OF DYNAMIC ABSORBER**

Let w_2 =   weight of absorber, lbs
                                       = $m_2 g$

Then,

$$k = 21.6 \, (w_2/386.4)$$
$$= 0.056 \, w_2 \; (\text{lb/in.}) \tag{8.6}$$

If we assume $w_2 = 10$ lbs (4.5 kg), then $k = 0.56$ lb/in. (98 N/m).

While these numbers seem reasonable [10 lb (4.5 kg) weight on a spring with 0.5 lb/in. (98 N/m) stiffness], the practical application to a real traffic signal structure is difficult. A 10 lb (4.5 kg) weight on a spring with a stiffness of 0.5 lb/in. (98 N/m) would deflect 20 in. (50 cm).

The vibrating absorber mass may be a distraction to motorists. Using a cantilever beam to achieve the 0.5 lb/in. (98 N/m) stiffness and to support a 10 lb (4.5 kg) weight is also not practical. For these reasons, this mitigation technique is not recommended.

8.5.2 Liquid Tuned Damper

Liquid tuned dampers have been used successfully in Japan to mitigate wind-induced vibrations in tall buildings. Energy dissipated by sloshing water (or other liquid) tends to dampen the response of a structure to wind-induced vibrations.

A three-ft long piece of PVC pipe was partially filled with water and inserted into the free end of the cantilever arm of the 48-ft signal structure. The concept was ineffective in mitigating vibrations owing to galloping. The sloshing apparently did not dissipate sufficient energy to be effective. In some tests, the vibration amplitudes were increased. The idea was abandoned after a few tries in the field.

8.5.3 Damping Plate (Wing)

Various damping plate configurations have been used by TxDOT maintenance personnel to mitigate wind-induced vibrations with marginal success. The typical installation consists of a plate 9 in. x 36 in. (23 cm x 91 cm) mounted on a section of the bare arm away from the signal light. This configuration was tried in field tests on both the 40-ft (12.2-m) and the 48-ft (14.6-m) signal

arms with no success in mitigating vibration amplitudes; the reason being, the plate must be mounted directly above the signal light to be effective. In addition, a much larger plate is required. An experiment was designed to demonstrate the effectiveness of a large damping plate. The 16 in. x 66 in. (41 cm x 168 cm) plate was mounted above the traffic lights in Configuration 5 (see Figure 7.2), as shown in Figure 8.16.

On a day when the wind speed was between 10-15 mph (4.5 - 7 m/s), the signal arm was rotated to be normal to the 5-minute mean wind direction. The wind was essentially from the south (180°) so the signal arm was rotated 270° and pointed toward the west. Initially, the damping plate was mounted on the structure. A continuous set of records was obtained consisting of 217 5-minute records. After validation the data, plots of 5-minute mean wind direction, 5-minute mean wind speed and RMS of strain on the vertical pole of the 48-ft (14.6-m) signal structure were made as shown in Figures 8.17, 8.18 and 8.19, respectively. These are essentially time-histories of the three parameters.

The RMS, which is the root mean square of the fluctuating strain component for each five-minute record, is a measure of the amount of fluctuation of the strain about a zero mean. A large value of RMS implies large fluctuation (displacements) of the signal structure.

The signal structure would not be expected to gallop unless the wind direction was within ±7.5° of due south (180°). Thus, from Figure 8.17 galloping is expected from record 27 to 91 when the wind direction is favorable for galloping. Little or no galloping is indicated for records from 27 to 75, as shown by the relatively small values of RMS during that time period.

At about record 73, the plate was quickly removed from the signal structure. Values of RMS in Figure 8.19 indicate a very strong galloping from record 75 to 91. At record 91 the wind direction has shifted more than 10°, so it is no longer normal to the back side of the signal structure. Thereafter, galloping is not observed in Figure 8.19. The absence of galloping is further verified by observing the variations of wind speed between records 115 and 172. Yet, the RMS remained essentially constant.

16 in.

Wing is
(16 x 66) in.

5.25 in.

Arm

22 in.

Backplate

1.0 in. = 2.5 cm
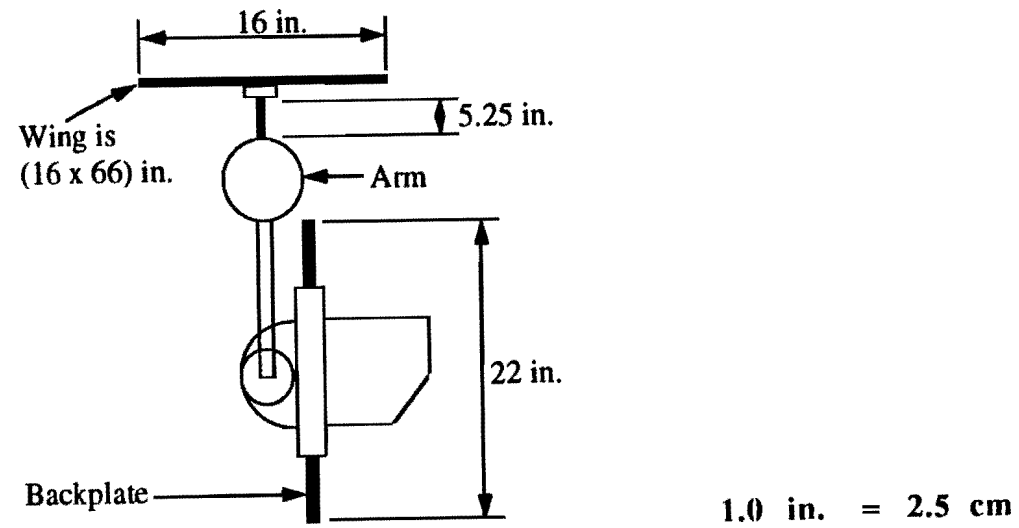
FIGURE 8.16 **MOUNTING ARRANGEMENT FOR
LARGE DAMPING PLATE (WING)**
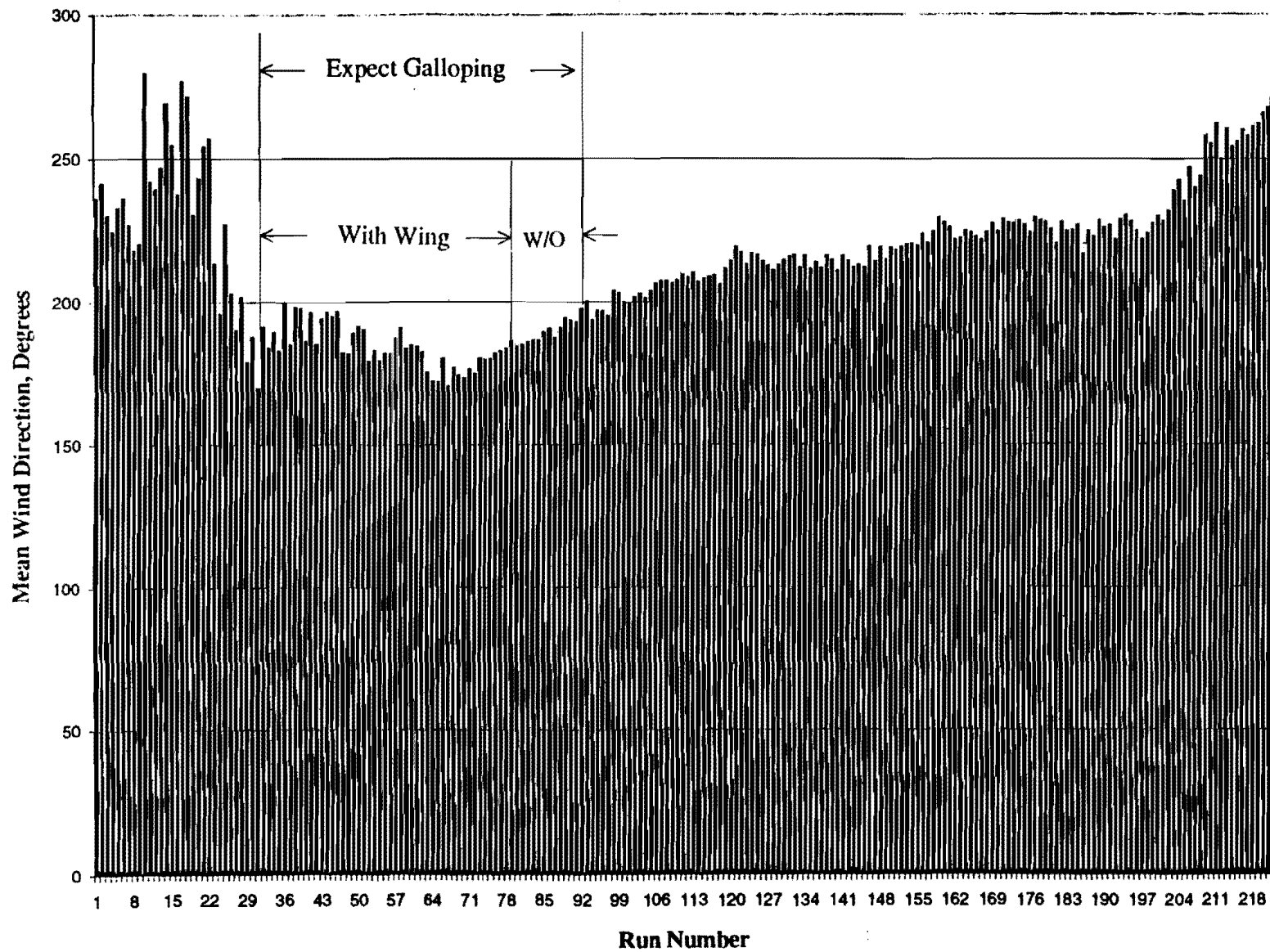
FIGURE 8.17. MEAN WIND DIRECTION VERSUS RUN NUMBER
FOR 48-FT (14.6-m) SIGNAL STRUCTURE (TIME)

150
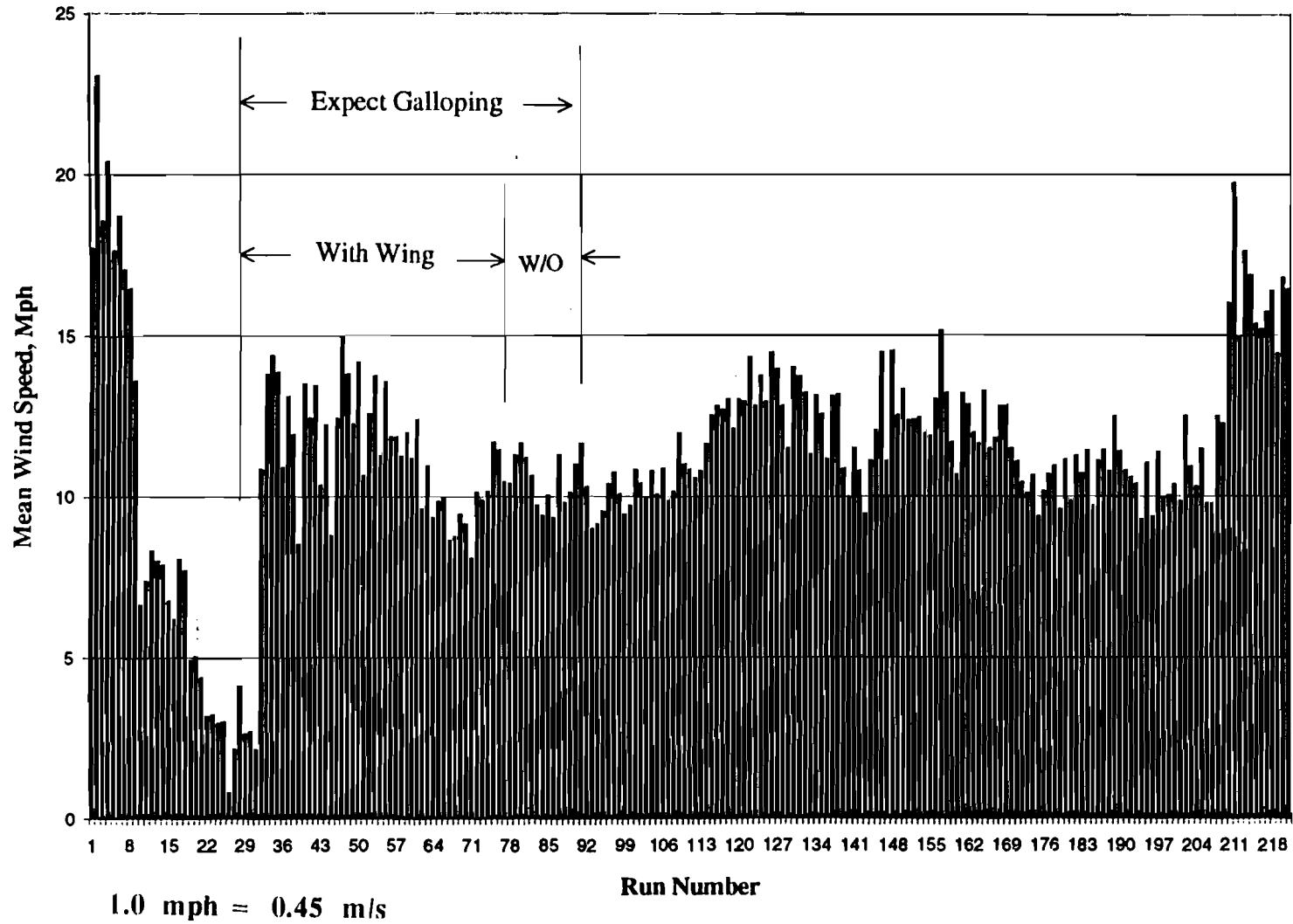
FIGURE 8.18. MEAN WIND SPEED VERSUS RUN NUMBER
FOR 48-FT (14.6-m) SIGNAL STRUCTURE (TIME)

1.0 mph = 0.45 m/s
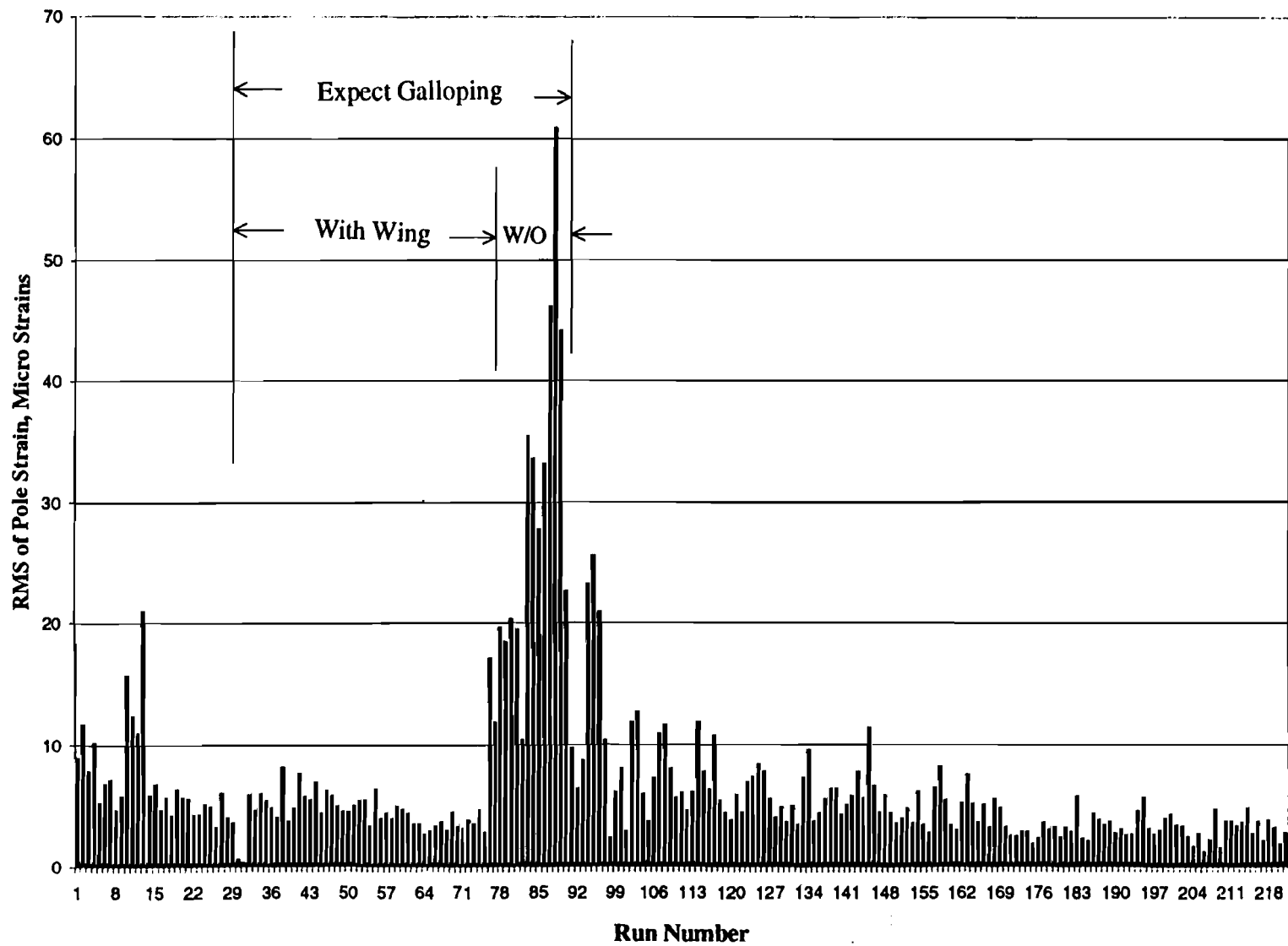
FIGURE 8.19. RMS OF VERTICAL POLE STRAIN VERSUS RUN
NUMBER FOR 48-FT (14.6-m) SIGNAL STRUCTURE

The experiment clearly demonstrates the effectiveness of the large damping plate. To be effective, the plate must be mounted above the signal light with at least a 3-in. (8-cm) separation between the damping plate and top of the signal light backing plate. The large wing, which is a standard sign blank, is essential for effective mitigation of the vibration.

Use of the large damping plate was clearly the most effective method for mitigating vibration due to galloping. When galloping is observed in an existing signal structure, a large damping plate (wing) can be installed over the signal light to effectively reduce the vibration.

The advantages of this mitigation strategy are:

(1)   It is a relatively easy "fix," requiring no knowledge of the dynamic characteristics of the existing structure.

(2)   Materials are readily available and easy to install by TxDOT maintenance personnel.

(3)   The wing is not a distraction to motorists.

9. COALESCENCE OF RESULTS

The sequence of experimental tests involving the water table, the tow tank and the field site demonstrated that large amplitude vibrations of traffic signal structures are caused by galloping, not by pure vortex shedding. Field testing indicated that galloping takes place under a very narrow range of conditions. Galloping is most likely to take place under the following conditions:

(1)   Wind blowing from back side of a traffic signal structure where traffic light has a back plate (Configuration 5, Figure 7.2)

(2)   Wind direction within ±7.5° of normal to cantilever signal arm

(3)   Steady wind speed in range of 10-30 mph (4.5-13.4 m/s).

It is possible that some configuration of cantilever signal arm and light without back plate can cause galloping since an exhaustive number of configurations were not tested. Both theory and experiments show that galloping vibration frequency is the same as the fundamental structure frequency. The amplitude of galloping vibration varies somewhat over a duration of steady wind speed and direction. It should be mentioned that we did not directly measure galloping displacements of the signal arm because of instrument limitations and continuing variations in displacements; however, the galloping displacements are in the ±8 to 18 in. (±20 to 45 cm) range for the 48-ft (14.6-m) signal structure.

When the cantilever arm vibrates in steady wind in the range of ±4 to ±6 in. (±10 to ±15 cm), it is possibly due to vortex shedding. When the vibration amplitude reaches about ±8 in. (±20 cm) or more, the cause is likely galloping and measures should be taken to suppress the vibration. In the 48-ft (14.6-m) signal structure, the measured stresses are 3.0 ksi (21 MPa) near the base of the vertical pole and 4.71 ksi (32 MPa) at cantilever arm connection at deflection amplitudes of 9.3 in. (23.6 cm) (see Table 8.1). Since stresses and displacement are assumed to be linear in the elastic range, larger displacements result in proportionately larger stresses.

The question of how many cycles of vibration a signal structure is likely to undergo over a lifetime is considered. For galloping to occur, the wind must blow from a narrow range of directions, typically ±7.5° normal to back side of traffic light. The percent of time the wind blows

from a specific direction is defined by a wind rose that is site dependent. The radial plots of a wind rose indicate the percent of time the wind blows in a given direction. Vibration owing to galloping takes place at the fundamental frequency of the signal structure. With traffic lights installed, the 48-ft (14.6-m) signal structure vibrated at 0.74 Hz at the field site. Suppose the wind blows from the critical direction 2% of the time in wind speed range of 10-30 mph (4.5-13.4 m/s). The number of cycles of potentially large amplitude vibration in one year would be

$$N = 0.74 \text{ cycles/sec} \times 31{,}536{,}000 \text{ sec/year} \times 0.02$$

$$= 467{,}000 \text{ cycles/year} \tag{11.1}$$

Over, say, a 10-year life of this signal structure it would, on average, experience 4.7×10^6 cycles. With ± 18-in. (± 4.6 cm) deflection, the calculated stress at cantilever arm connection will vary between 5.4 and 23.7 ksi (37.2 and 163.4 MPa) with mean value of 14.6 ksi (100 MPa) (extrapolated from Table 4.3). This stress range and the number of cycles can cause fatigue problems if there is stress concentration at the connection. Since, galloping is unpredictable and depends on the local wind environment at a site, fatigue may not be a problem. However, large amplitude vibrations are a distraction to motorists and should be mitigated when the amplitude exceeds ± 8 in. (± 20 cm). This restriction provides a sufficient margin of safety against fatigue failures in the field.

Because galloping depends on the configuration of traffic signal, fundamental frequency and damping of the signal structure, as well as the wind environment at the site, it is not possible to predict with a degree of certainty that a particular signal structure will be susceptible to galloping. For this reason we believe the best approach is to continue to use current design criteria (including the proposed new wind load provisions) to design signal structures. TxDOT maintenance personnel should observe the vibration of a new structure after it is installed in 10-20 mph (4.5-9 m/s) winds. If the maximum amplitude of the arm tip exceeds ± 8 in. (± 20 cm), then mitigation measures should be instituted. Mitigation measures to eliminate galloping are as follows:

(1)   Remove the back plate, if feasible

(2)   Change the arm/traffic light arrangement from an unstable condition to a stable one as demonstrated in Figures 7.7 to 7.10.

(3)   Install a large damping plate (wing) over the traffic light nearest the free end, as shown in Figure 8.16.

Any one of the mitigation measures should eliminate galloping vibrations. In an unusual situation it is possible that a combination of mitigation measures will have to be employed to eliminate galloping vibrations.

10. RECOMMENDATIONS

As a result of this extensive study of the behavior of traffic signal structures when subjected to persistent wind in the 10-30 mph (4.5-13.5 m/s) range, the following recommendations are proposed:

(1) Make the signal structure as stiff as economically feasible to reduce vibration and minimize the potential for galloping.

(2) Avoid design installations that result in arm/traffic light/back plate arrangements that are likely to be susceptible to galloping.

(3) Employ mitigation measures to eliminate galloping vibrations when tip displacements of ± 8 in. (± 20 cm) or more in a persistent wind speed range of 10-30 mph (4.5-13.5 m/s) are observed.

(4) Have additional tow tank tests performed in which active vibration at approximately one Hz is induced to envelope arm/traffic light configurations causing galloping vibrations.

(5) Have wind tunnel tests or field tests performed to determine the increase in the drag and lift due to the large wing under high wind conditions.

11. IMPLEMENTATION OF RESEARCH RESULTS

11.1 Revised Standard

The proposed revised wind load standard for signs, luminaires and traffic signal structures can be implemented for immediate use in the State of Texas. The approach utilizes current state-of-the-art techniques in determining wind loads on highway structures. Not only are the wind loads more realistic, in some cases they are justifiably less conservative than those obtained from existing standard. The potential for cost savings in the signal structure fabrication exists without negatively affecting the factor of safety or reliability of the structure.

11.2 Traffic Signal Structure

The study indicates that fatigue failures resulting from galloping of the signal structure is a possibility, though not a major threat. Good serviceability criteria suggests that when deflection amplitudes of the cantilever arm exceeds $\pm$ 8-in., mitigation measures to eliminate galloping should be implemented. The simplest solution may be to change the signal arm and traffic light configuration to one that is not susceptible to galloping (see Figures 7.7 to 7.10). Those configurations exhibiting a positive slope of the force coefficient C_{Fy} versus angle of attack α are stable and are not susceptible to galloping. If galloping is problematic and conditions at an intersection for traffic control do not permit changing the signal arm/traffic light arrangement, then a 16 in. x 66 in. (41 cm x 168 cm) damping plate (wing) should be installed as shown in Figure 8.16. The recommended plate is a standard sign plate that is readily available. The plate must be installed directly above the traffic light located nearest the free end. Installing the wing of dimensions 9 in. x 36 in. (23 cm x 91 cm) between lights, as is the current practice, is not effective.

161

12. CONCLUSION

This project had two objectives:

(1)   Revise the wind load provisions of the design standard specifications for signs, luminaires and traffic signal structures, and

(2)   Investigate large amplitude vibrations [displacement exceeding ± 8 in. (± 20 cm)] in traffic signal structures and devise a means to mitigate them.

The proposed revisions to the design standard specifications incorporate state-of-the-art technology in defining appropriate wind loads, including a new wind speed map for the State of Texas. The procedure is based on the provisions of ASCE 7-88, *Minimum Design Loads for Buildings and other Structures* (ASCE, 1990). The procedure introduces the use of a gust response factor, accounts for different terrain roughnesses and utilizes an updated wind speed map for the State of Texas. In some cases, the revised standard specifications will specify smaller loads than the current standard specifications, leading to more economical structures. The reduced loads are possible without sacrificing safety or reliability.

The large amplitude vibration of traffic signal structures have been thoroughly studied through a literature search, theoretical analysis, and experimental testing. The vibrations are caused by a galloping phenomena which occurs when a specific set of structural and environmental wind conditions are met.

The problem becomes serious when deflection amplitudes of the free end of the cantilever arm exceeds ± 8 in. (± 20 cm). At that point, mitigation measures should be instituted. If a simple rearrangement of the traffic light and signal arm configuration is not feasible, then a damping plate (wing) should be installed. Field tests conducted during the course of this project demonstrated the effectiveness of the plate in mitigating the galloping vibration.

Because one cannot predict with a high degree of certainty if a signal structure will gallop at the time it is designed, the best approach is to have maintenance personnel check on it at regular intervals after it is erected to determine if galloping takes place under the field conditions.

Implementation of the revised design standard specifications and the measures to mitigate galloping vibration fulfill the objectives of this research project.

REFERENCES

AASHTO, 1985: *Standard Specifications for Structural Supports for Highway Signs, Lumuinaires and Traffic Signals*, American Association of State Highway and Transportation Officials.

Achenbach, E. and Heinecke, E., 1981: "On Vortex Shedding from Smooth and Rough Cylinders in the Range of Reynolds Numbers 6×10^3 to 5×10^6," *Journal of Fluid Mechanics*, Vol. 109, pp. 239-251.

ANSI, 1982: *Minimum Design Loads for Buildings and Other Structures*, American National Standards Institute, New York, New York.

ASCE, 1990: *Hurricane Hugo One Year Later*, American Society of Civil Engineers, New York, New York.

Baird, R. C., 1955: "Wind-Induced Vibrations of a Pipe-line Suspension Bridge and Its Cure," *Transactions, American Society of Mechanical Engineers*, Vol. 77, No. 6.

Batts, E., Cordes, M. R., Russel, L. R., Shaver, J. R. and Simiu, E., 1980: *Hurricane Wind Speeds in the United States*, NBS Building Science Series 124, National Bureau of Standards, Washington, DC.

Bearman, P. W., and Obasaju, E. D., 1982: "An Experimental Study of Pressure Fluctuations on Fixed and Oscillating Square-Section Cylinders," *Journal of Fluid Mechanics*, Vol. 119, pp. 297-321.

Bendat and Piersol, 1986: *Random Data, Analysis and Measurement Procedures*, 2nd Ed., Wiley Intrascience, John Wiley and Sons, New York, New York.

Changery, Michael J., 1978: *National Wind Data Final Report*, HCO/T1041, National Climatic Center, Asherville, NC, pp. 265.

Clough, R.W. and Pienzen, J., 1980, *Dynamics of Structures*, McGraw-Hill Book Company, New York, NY.

Den Hartog, J. P., 1932: "Transmission Line Vibration Due to Sleet," *Transactions, AIEE*, Vol. 51, pp. 1074-1076.

Den Hartog, J. P., 1956: *Mechanical Vibrations*, 4th Ed., McGraw-Hill, New York, New York.

Dryden, H. L. and Hill, G. C., 1930: "Wind Pressure on Circular Cylinders and Chimneys," *Bureau of Standards, J. Res.*, Washington, DC, Vol. 5, pp. 653-693.

Durst, C.S., 1960: "Wind Speeds Over Short Periods of Time," *The Meteorological Magazine*, No. 608, pp. 181-186.

Jones, G.W., Cincotta, J. J. and Walker, R. W., 1969: *Aerodynamic Forces on a Stationary and Oscillating Circular Cylinder at High Reynolds Numbers*, NASA Technical Report 300, National Aeronautics and Space Administration, Houston, TX.

REFERENCES (continued)

Levitan, M.L. and Mehta, K.C., 1992: "Texas Tech Field Experiments for Wind Loads, Part II, Meteorological Instrumentation and Terrain Parameters," *Journal of Wind Engineering and Industrial Aerodynamics*, Vol.41-44, Elsevier Science Publishers, pp. 1577-1588.

Mehta, K.C., 1988: National Emergency Training Center, Gaithersburg, Maryland, *Multiprotection Design Science Institute.*

Novak, M., 1969: "Aeroelastic Galloping of Prismatic Bodies," *Journal of the Engineering Mechanical Division*, ASCE, Vol. 95, No. EM1, pp. 115-142.

Novak, M., 1972: "Galloping Oscillations of Prismatic Structures," *Journal of the Engineering Mechanics Division*, ASCE, Vol. 98, No. EM1, pp.27-46.

Obasaju, E. D., 1983: "Forced-Vibration Study of the Aeroelastic Instability of a Square-Section Cylinder Near Vortex Resonance," *Journal of Wind Engineering and Industrial Aerodynamics*, Vol. 12, pp. 313-327.

Okajima, A., 1982: "Strouhal Numbers of Rectangular Cylinders," *Journal of Fluid Mechanics*, Vol. 123, pp. 379-398.

Parkinson, G. V. and Brooks, N. P. H., 1961: "On the Aeroelastic Instability of Bluff Cylinders," *Transactions ASME, Journal of Applied Mechanics*, Vol. 83 , pp. 252-258.

Parkinson, G. V. and Smith, J. D., 1962: "An Aeroelastic Oscillator with Two Stable Limit Cycles," *Transactions ASME, Journal of Applied Mechanics*, Vol. 84, pp 444-445.

Parkinson, G. V. and Wawzonek, M. A., 1981: "Some Considerations of Combined Effects of Galloping and Vortex Resonance," *Journal of Wind Engineering*, Vol. 8, pp. 135-143.

Peterka, 1993: "Extreme Gust Wind Speeds," *Proceedings*, 7th U.S. National Conference on Wind Engineering, UCLA, Los Angeles, California.

Price, P., 1956:"Suppression of the Fluid-Induced Vibration of Circular Cylinders," *Journal of the Engineering Mechanical Division*, Vol. 82, pp.1030.

Pulipaka, N., McDonald, J.R. and Mehta, K.C., "Wind Effects on Cantilevered Traffic Signal Structures," *Proceedings*, Ninth International Conference on Wind Engineering, January 1995, New Delhi, India, Vol. IV, pp. 2043-2050.

Roshko, A., 1955; "Experiments on the Flow Past a Circular Cylinder at Very High Reynolds Number," *Journal of Fluid Mechanics*, Vol. 10, pp. 345-356.

Sachs, P., 1977: *Wind Forces in Engineering*, Pergamon Press, New York.

Scruton, C., 1963; *On the Wind-Excited Oscillations of Stacks, Towers and Masts*, Paper 16, Britain National Physical Laboratory.

Scruton, C. and Walshe, D.E.J., 1957: "A Means for Avoiding Wind-Excited Oscillations of Structures of Circular or Nearly Circular Cross-Section," unpublished report NPL/Aero/335. (Also: *British Patent No. 907,851*.)

REFERENCES (continued)

Simiu, E., Changery, M., and Filliben, J., 1979: *Extreme Wind Speeds of 129 Stations in the Contiguous United States,* NBS Building Science Services 118, National Bureau of Standards, Washington, DC, p. 314.

Simiu, E. and Scanlan, R.H., *Wind Effects on Structures*, Second Ed., John Wiley and Sons, New York, NY.

Singh, A.K., *Gust Response Factor for Flexible Pole Structures*, a Masters Report in Civil Engineering, Texas Tech University, Lubbock, TX, July 1993.

Szepessy, S. and Bearman, P. W., 1992: "Aspect Ratio and End Plate Effects on Vortex Shedding from a Circular Cylinder," *Journal of Fluid Mechanics*, Vol. 234, pp. 191-217.

Titan Corporation, 1993: *Stardyne,* 4.0, Charsworth, California 91311.

Vierck, R. K., 1967: *Vibration Analysis,* International Textbook Company, Scranton, PA, p.59.

Walshe, D. E. and Wootton, L. R., 1970: "Preventing Wind-Induced Oscillations of Structures," *Proceedings,* Institute of Civil Engineers, Vol. 47, pp. 1-24.

Woodgate, L. and Maybrey, J.F.M., 1959; "Further Experiments on the Use of Helical Strakes for Avoiding Wind-Excited Oscillations of Structures of Circular or Nearly Circular Section," Unpublished Report NPL/Aero/381.

APPENDIX A

Proposed Revisions to
Standard Specifications for Structural Supports
for Highway Signs, Luminaries and Traffic Signals
(AASHTO, 1985) for Use in Texas
1993

PROPOSED REVISIONS
TO
STANDARD SPECIFICATIONS FOR STRUCTURAL SUPPORTS
FOR HIGHWAY SIGNS, LUMINAIRES AND TRAFFIC SIGNALS
(AASHTO 1985)
FOR USE IN TEXAS
1993

SECTION--LOADS

1.2.4--Wind Load

Wind load shall be the horizontal pressure of the wind on the support structure, signs, luminaires and traffic signals, and will be determined by the Wind Pressure Formula in Article 1.2.5(A). The appropriate wind speed will be determined from Figure 1.2.4. Adjustment of the indicated wind speed to account for the importance of the structure and the associated mean recurrence interval is through the use of an importance factor, I. This factor is discussed in Article 1.2.5(B).

The basic wind speed map does not show isolated high wind areas; therefore, sound judgment must be used in selecting wind speeds for the location in which the structure is to be installed.

1.2.5--Application of Wind Load

Application of wind load (acting horizontally):

(A) Wind Pressure --
Wind pressure shall be computed by the following formula:

$$P = 0.00256 \ (I * V)^2 C_h C_g C_d \quad \text{or}$$

$$(P = 0.0473 \ (I * V)^2 C_h C_g C_d)$$

where:

P = Wind pressure in pounds per square foot (Pa)
V = Basic wind speed from Figure 1.2.4, miles per hour (km/h)
I = Importance factor from Table 1.2.5B, Article 1.2.5(B)
C_h = Coefficient for height above ground and exposure category from Table 1.2.5C; exposure category is given in Article 1.2.5(C).
C_d = Drag coefficient from Table 1.2.5D
C_g = Gust response factor from Table 1.2.5E.

(B) Importance Factor --

The importance factor, I, shall be selected from Table 1.2.5B based on the importance of the structure, the length of expected life of the structure and the probability of wind speed
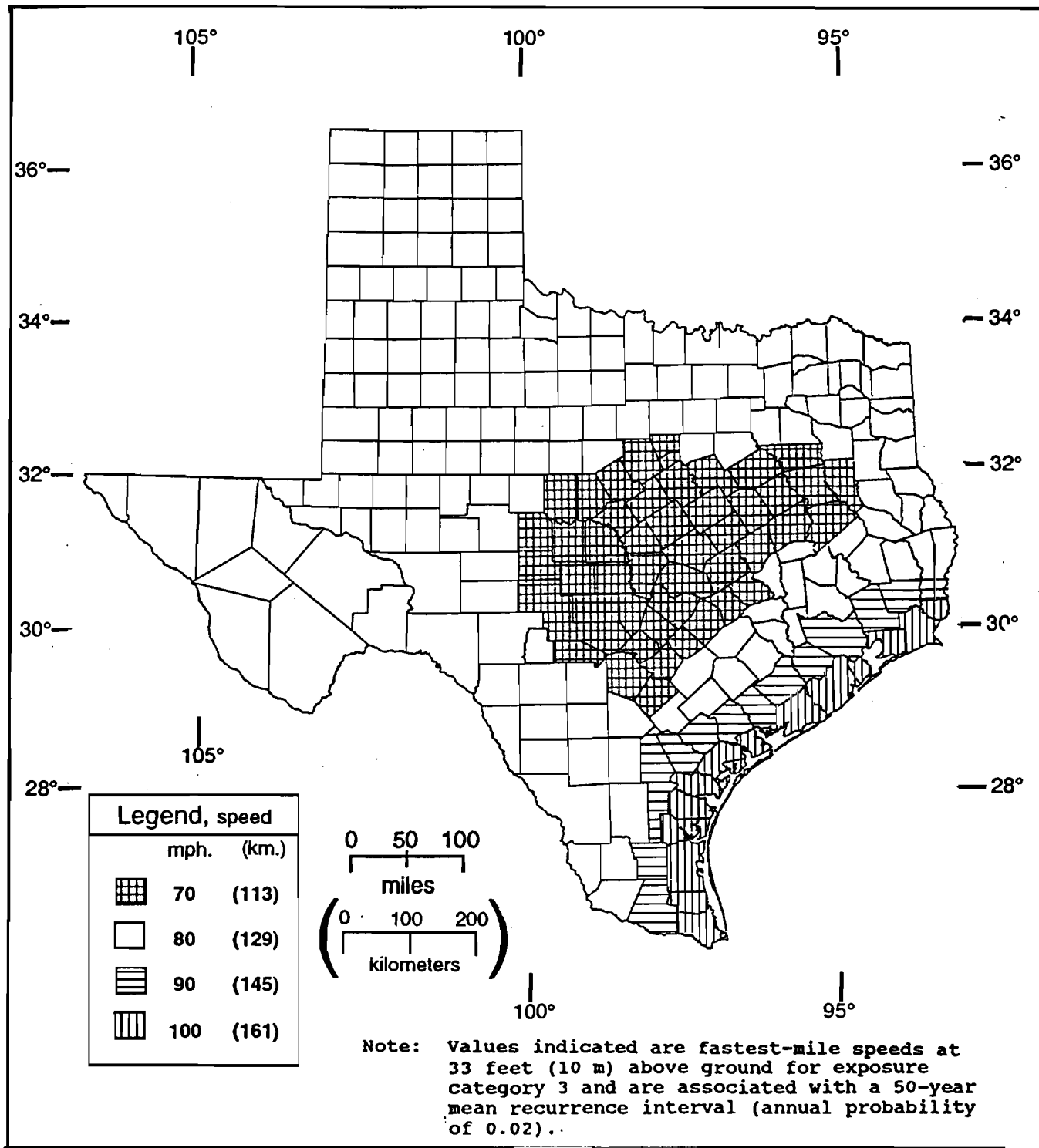
171

Figure 1.2.4. Basic Wind Speed, miles per hour, for Counties in Texas.

172

occurrence (mean recurrence interval). The mean recurrence interval will be selected from Table 1.2.5A depending upon the type of structure under consideration and its location. Engineering judgment should be used in selecting the value from this table. Selection of a larger interval will be more conservative.

Table 1.2.5A
Recommended Mean Recurrence Interval for Various Structures

Structure	Mean Recurrence Interval (Years)
Luminaire Support Over 50 feet (15.24 m) Height,	50
Structure Supporting Sign(s) Over Roadway	50
Luminaire Support Less Than 50 feet (15.24 m) Height	25
Traffic Signal Support Structures	25
Structure Supporting Sign(s) Not Over Roadway	25
Traffic Signs (breakaway)	10

Table 1.2.5B
Importance Factor, I

Mean Recurrence Interval (Years)	I	I*
5	0.82	0.82
10	0.88	0.88
25	0.95	1.00
50	1.00	1.05
100	1.07	1.11

* For hurricane zones where basic wind speed is 90 mph (145 km/h) or greater and within 100 miles (161 km) of oceanline.

(C)   Exposure Category --

An exposure category that reflects the characteristics of the ground surface irregularities at the site where the structure is to be constructed shall be determined. Based on the site condition within 1500 feet (457 m) of the structure, the appropriate exposure category should be selected taking into consideration the major variations in ground surface roughness that arise from vegetation and constructed features. In case of doubt as to the category to be used, the higher category should be selected. The exposure in which a specific structure is sited shall be assessed as being one of the following categories:

Exposure Category 1. Towns, suburbs and cities, dense forest country.

Exposure Category 2. Countryside or outskirts of towns and villages with scattered buildings or clumps of trees and large bushes. This category also includes areas with grass and crops more than 3-feet (0.91 m) tall.

Table 1.2.5C
Velocity Pressure Exposure Coefficient, C_h

Height Above Ground (ft)	(m)	Exp 1	Exp 2	Exp 3	Exp 4
0-15	(0-4.57)	0.37	0.55	0.80	1.20
20	(6.10)	0.42	0.61	0.87	1.27
25	(7.62)	0.46	0.66	0.93	1.32
30	(9.14)	0.50	0.71	0.98	1.37
33	(10.06)	0.52	0.73	1.00	1.40
40	(12.19)	0.57	0.79	1.06	1.46
50	(15.24)	0.63	0.85	1.13	1.52
60	(18.28)	0.68	0.91	1.19	1.58
70	(21.34)	0.73	0.96	1.24	1.63
80	(24.38)	0.77	1.01	1.29	1.67
90	(27.43)	0.82	1.06	1.34	1.71
100	(30.38)	0.86	1.10	1.38	1.75
120	(36.58)	0.93	1.17	1.45	1.81

Notes:

1. Linear interpolation for intermediate values is acceptable.

2. Exposure categories are defined in Article 1.2.5C.

Change current Table 1.2.5C designation to Table 1.2.5D.

Table 1.2.5E
Gust Response Factor C_g

Structure Height (ft)	(m)	Exp 1	Exp 2	Exp 3	Exp 4
0-15	(0-4.57)	1.67	1.51	1.33	1.16
20	(6.10)	1.61	1.46	1.30	1.14
25	(7.62)	1.56	1.43	1.28	1.13
30	(9.14)	1.53	1.41	1.26	1.12
33	(10.06)	1.51	1.39	1.26	1.12
40	(12.19)	1.47	1.37	1.24	1.11
50	(15.24)	1.43	1.34	1.22	1.10
60	(18.28)	1.40	1.32	1.21	1.09
70	(21.34)	1.38	1.30	1.19	1.09
80	(24.38)	1.35	1.28	1.18	1.08
90	(27.43)	1.34	1.27	1.18	1.07
100	(30.38)	1.32	1.26	1.17	1.07
120	(36.58)	1.29	1.24	1.15	1.06

Notes:

1. Linear interpolation for intermediate values of height is acceptable.

2. Values of gust response factor shall be not less than 1.0.

3. Gust response factor for total structure shall be determined using the maximum height of the structure.

Exposure Category 3. Open terrain with few trees and hedges; grass plains with vegetation less than 3-feet (0.91 m) in height; areas such as airports.

Exposure Category 4. Unobstructed areas exposed to wind flowing over large bodies of water. Flat desert or arid areas with limited ground cover.

The exposure category and the height above the ground are used in Table 1.2.5C to determine the velocity pressure exposure coefficient C_h. The height used for horizontal members will be the height to the centroid of the component being loaded by the wind. For vertical members, the velocity pressure coefficient shall vary with height.

For site conditions elevated considerably above the surrounding terrain, where the influence of the ground on the wind is small, consideration must be given to using higher velocity pressure coefficient based on the surrounding terrain as ground level.

(D) Wind Drag Coefficients --

Wind drag coefficients are tabulated in Table 1.2.5D for various shapes of structural components.

(E) Gust Response Factor --

Gust response factors are tabulated in Table 1.2.5E for various exposure categories and height above the ground surface. For a structure one gust response factor based on the total height of the structure is selected.

(F) Notation for Wind Loads --

{no changes from existing AASHTO Standard Specifications for Structural Supports for Highway Signs, Luminaires and Traffic Signals except to renumber figures 1.2.5D(1), (2), (3), (4) to 1.2.5F(1), etc }

APPENDIX B

Proposed Revisions to Commentary on
Standard Specifications for Structural Supports
for Highway Signs, Luminaires and Traffic Signals
(AASHTO 1985) for Use in Texas
1993

PROPOSED REVISIONS
TO
COMMENTARY ON STANDARD SPECIFICATIONS FOR
STRUCTURAL SUPPORTS FOR HIGHWAY SIGNS, LUMINAIRES
AND TRAFFIC SIGNALS
(AASHTO 1985)
FOR USE IN TEXAS
1993

1.2.4--Wind Load

The basic wind speed for a particular location will be selected based on the wind speed map shown in Fig. 1.2.4 of the standard. This map is developed using data up to 1991 from 26 locations within the State of Texas and 7 locations from surrounding states. This data was standardized as to height (33 feet) (10.06 m) and exposure using the same methods and probability distributions as used in ASCE 7-88. Data from ASCE 7-88 have been incorporated where needed along the Gulf Coast to include the effect of hurricane winds. The wind speed data is used to indicate wind speeds by county rather than by plotted contours. The effect of the importance of the structure are considered through an importance factor. A discussion of this factor is provided in Article 1.2.5(B) of this commentary.

Basic wind speed should be increased where records or experience indicate that values higher than those reflected by Figure 1.2.4 of the standard are experienced. The authority having jurisdiction shall, if necessary, adjust the basic wind speeds to account for higher local winds. Such adjustments should be based on meteorological advice and the values standardized for height and exposure.

1.2.5(A) Wind Pressure --

The wind pressure formula is derived from fundamental fluid-flow theory. The rise in pressure on an immersed body, caused by bringing the air to rest, is the dynamic pressure of the air on the body. Therefore, $p = wv^2/2g$. If w is taken as the density of "standard air," 0.0761 lb/cu ft (1.22 kg/m^3)(at 15°C and 760 mm of mercury) and v is converted to V in mph (km/h), then the wind pressure is 0.00256V^2 (0.0473V^2). The importance factor adjusts the basic wind speed to account for the life of the structure and its importance. The velocity pressure exposure coefficient, C_h, adjusts the wind pressure for the effect of height above ground level and the surrounding terrain roughness. C_d, the drag coefficient, is a dimensionless coefficient that varies with the shape of the object receiving the wind loading. C_g, the gust response factor, accounts for the loading effect caused by the additional velocity of the wind gust over the fastest-mile speed. The pressure on the structural component is

then determined by multiplying the wind dynamic pressure by C_h, the velocity pressure exposure coefficient, C_d, the drag coefficient, and C_g, the gust response factor.

1.2.5(B)   Importance Factor --

The importance factor, I, converts the basic wind speed to a speed associated with various mean recurrence intervals. The mean recurrence interval is selected on the basis of the anticipated length of structure life and the importance of the structure. Table 1.2.5A of the standard provides recommended values of the mean recurrence interval for various types of structures. This table reflects the life expectancy, endangerment of life in case of failure and value of the structure. Table 1.2.5B of the standard provides the values of the importance factor for various mean recurrence intervals. The use of other than recommended mean recurrence interval is, of course, at the discretion of the Engineer and their use should be based on desired life expectancy, safety considerations, ease of replacement, etc.

Values of the importance factor shown in Table 1.2.5B of the standard show two sets of values because the probability distribution of hurricane winds is different than for other winds. The values for the hurricane zone should be used when the basic wind speed is 90 miles per hour (145 km/h) or greater and the location is within 100 miles (161 km) of the oceanline.

1.2.5(C)   Exposure Categories --

Friction due to ground roughness reduces wind speed. The influence of ground roughness on wind speed diminishes with increasing height above the ground. At and above the gradient height (700 to 1200 feet above ground) (213 to 366 m) the effect of ground roughness is negligible. However, in the lowest 300 feet (91 m), the ground roughness has a significant effect on wind speed and hence wind pressure.

The effects of ground roughness is accounted for through identifying a site as being one of four exposure categories, namely exposure category 1, 2, 3, or 4. A circular area within 1500 feet (457 m) of the structure should be investigated. A exposure category is selected for each direction that has consistent ground characteristics. If the design wind is expected to come from only one direction, the selected exposure category for that direction is used for the design of the structure. If the direction of the design wind is unknown, the largest exposure category of any direction which causes critical wind loading is used for the design of the structure.

Exposure category 1 represents normal urban and suburban development, both residential and commercial, with only a few undeveloped lots. A heavy, solid forest of tall trees would also be in this category. If the terrain has scattered buildings, isolated trees, or large clumps of tall bushes, exposure category 2 should be used. Flat, open terrain with short grass such as at an airport or a highway right of way, where the wind speed is little affected by the friction of the ground, will qualify as exposure category 3. Exposure category 4 is used only when the

wind is flowing over water or flat arid area with limited ground cover. It is not possible to describe all of the various terrain types that may be encountered; engineering judgment is essential in selecting the appropriate exposure category. In case of doubt, the choice of a higher exposure category will give a conservative result.

If the site is on a bluff or a hill, where the immediately surrounding ground cannot influence the wind, the height of the structure should be based on the ground elevation at the bottom of the bluff or hill. In this situation, a reasonable upper limit of C_h, velocity pressure exposure coefficient, is 1.7 times the C_h value for the height above the immediately surrounding ground.

The velocity pressure exposure coefficients shown in Table 1.2.5C of the standard can be obtained using the equation:

$$C_h = 2.58 \ (\ z/z_g \ )^{2/\alpha}$$

where

    z is the height above ground
    z_g is the gradient height above ground
    α is the power law coefficient.

The minimum value of z is 15 feet (4.57 m). The values of z_g and α are given in Table 1.2.5G.

Table 1.2.5G
Constants for Exposure Categories

Exposure Category	α	z_g ft. (m)		Surface Drag Coefficient D_o	ASCE 7-88 Category
1	4.5	1200	(366)	0.01	B
2	5.5	1050	(320)	0.0075	-
3	7.0	900	(274)	0.0050	C
4	10.0	700	(213)	0.0030	D

The relation between the exposure category used in this specification and that used in ASCE 7-88 is indicated in the last column of Table 1.2.5G. To take into account ground roughness intermediate between exposures B and C (ASCE 7-88), a new exposure category, 2, was developed using the terrain description of ESDU International, volume 1b (wind speeds and turbulence) as a reference. The roughness length of this category is about 0.33 feet (0.1 m) (used in log-log profile) and it covers the outskirts of towns and villages, countryside with scattered buildings or clumps of trees and larger bushes, and areas with grass and crops more than three feet (0.91 m) tall. Other parameter values for exposure category 2 in the table have been interpolated between exposure category B and C of ASCE 7-88.

1.2.5(D) Wind Drag Coefficients --

Table 1.2.5D of the standard provides values for the wind drag coefficient, C_d, for various shapes that are frequently used

for sign structures.
{ use existing AASHTO commentary pp. 54-55 on drag coef. }

1.2.5(E) Gust Response Factor --

The gust response factor (GRF) depends primarily on the gusti-
ness in the wind and on the structure's size, and accounts for
the additional loading effects due to wind turbulence over the
fastest-mile wind speed. Since gusts are localized, small struc-
tures are more susceptible to being totally enveloped by a gust,
and thus, have a larger GRF than larger structures. Also, gusti-
ness in the wind depends on ground roughness and height above
ground; this variation is reflected in the equation for tur-
bulence intensity T_z.
The values listed in Table 1.2.5E of the standard are calcu-
lated from the following equation:

$$C_g = 0.65 + 3.65 \, T_z$$

where

$$T_z = \frac{2.35 \, (D_o)^{0.5}}{(z / 33)^{(1/\alpha)}}$$

where   z is the height of the structure in feet
{Use z/10 in the equation for T_z when z is measured
in meters}
α is the power law coefficient
D_o is the surface drag coefficient.
The values of α and D_o are listed in Table 1.2.5G of the commen-
tary for various exposure categories.
A single GRF is selected for a structure since the entire
structure responds as a unit. It is based on the height of the
structure to reflect smaller values of GRF for increased height.
This factor does not include allowances for the effects of cross-
wind deflection, vortex shedding, instability due to galloping or
flutter, or loading due to dynamic resonance amplification for
flexible buildings.
This approach to defining GRF is different than the gust
factor approach previously used in the AASHTO standard. A gust
factor of 1.3 in effect is equivalent to a GRF of 1.69 irrespec-
tive of the ground roughness and the size of the structure. Use
of the GRF leads to a more consistent safety for structures
located in various terrain and, in most cases, smaller loads.

1.2.5(F) Notation for Wind Loads --

{ use existing AASHTO Commentary pp. 55 to 57 }